3-1999

Three Dimensional Hydrodynamic-Sedimentation Modeling Study : Hampton Roads Crossing, Lower James River, Virginia

John D. Boon
Virginia Institute of Marine Science

Harry V. Wang
Virginia Institute of Marine Science

S. C. Kim
Virginia Institute of Marine Science

Albert Y. Kuo
Virginia Institute of Marine Science

G. M. Sisson
Virginia Institute of Marine Science

Three Dimensional Hydrodynamic-Sedimentation Modeling Study

Hampton Roads Crossing, Lower James River, Virginia

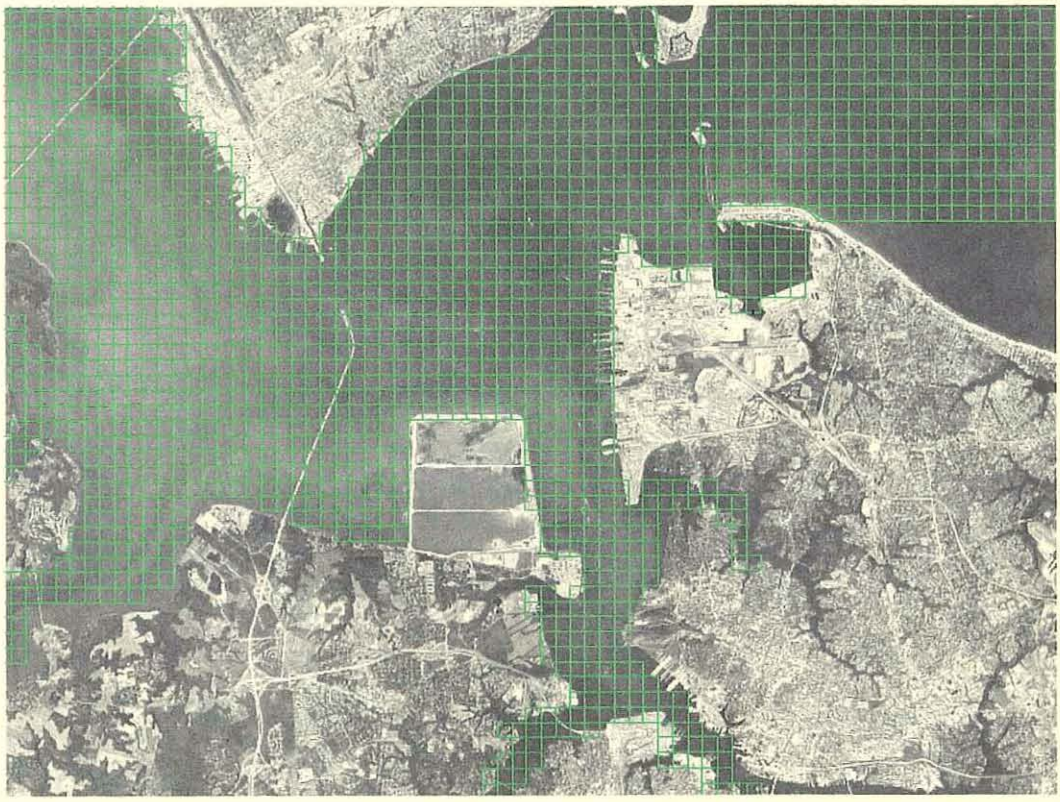

John D. Boon, Harry V. Wang, S. C. Kim, A.Y. Kuo and G. M. Sisson

A Report to the

Virginia Department of Transportation

Special Report No. 354
in Applied Marine Science and Ocean Engineering

Virginia Institute of Marine Science
Department of Physical Sciences
Gloucester Point, Virginia 23062

March 1999

Three Dimensional Hydrodynamic-Sedimentation Modeling Study

Hampton Roads Crossing, Lower James River, Virginia

by

John D. Boon, Harry V. Wang, S. C. Kim, A.Y. Kuo and G. M. Sisson

A Report to the

Virginia Department of Transportation

Special Report No. 354
in Applied Marine Science and Ocean Engineering

Virginia Institute of Marine Science
Department of Physical Sciences
Gloucester Point, Virginia 23062

March 1999

EXECUTIVE SUMMARY

A three-dimensional hydrodynamic-sedimentation computer model, HYSED-3D, was used to evaluate the effect of bridge-tunnel infrastructure for a proposed highway crossing of Hampton Roads on the physical characteristics (tides, currents, circulation, salinity, and sedimentation) of the James River estuary in Virginia. Model-represented infrastructure included tunnel islands and bridges on pilings connecting the islands to interstate highways in Newport News, Hampton, Norfolk, and Portsmouth, Virginia. Combinations of these elements occur in each of three proposed crossing routes designated **Alternative 1** (Hampton-Norfolk), **Alternative 2** (Hampton-Norfolk, Norfolk-Portsmouth), and **Alternative 9** (Newport News-Portsmouth-Norfolk).

Simulation comparisons were made between the existing waterways and infrastructure in Hampton Roads (Base Case) and the proposed construction in a series of model test runs representing both normal and extreme hydrologic conditions. Variations in tidal range were simulated using a three-constituent tide model. Three levels of freshwater inflow into the headwaters of the James River were represented using historical stream gauge data. The simulation of sedimentation was designed based on the existence of a 'turbidity maximum' upstream from the area of concern.

Based on the hydrodynamic characteristics and the layout of the proposed crossings, nine and seven stations, respectively, were selected for examination of potential changes in tidal height and current velocity. No changes in tidal height were observed at any of the nine stations in response to the three alternatives over the range of conditions tested. Small changes were observed in time histories of surface and bottom current at three of the seven representative locations. The three locations of observed change are proximal to tunnel islands associated with Alternatives 2 and 9. An examination of the spatial (plan-view) distribution of the instantaneous current field revealed that most of the changes were caused by local deviations in the direction and phase, not the magnitude, of the current. Further examination of instantaneous and time-averaged (residual) current data shows that some aspects and features of the general circulation may also be altered by Alternatives 2 and 9. A recurring tidal front near Newport News Point showed a minor phase change in response to Alternative 9. A residual current 'eddy' in the Elizabeth River entrance diminished in response to Alternatives 2 and 9. Unlike the tidal front near Newport News Point, the existence of the eddy at the entrance to the Elizabeth River has not been confirmed by field observation.

Salinity changes were observed in the vicinity of bridges on pilings, especially those for Alternative 9. This was primarily a response to piling-induced turbulence, increased vertical mixing and the elimination of surface-to-bottom salinity gradients immediately downstream. No changes were observed in the longitudinal salinity distribution along the channel axis of the James River in response to any of the alternatives under any of the conditions tested.

Sedimentation was simulated in terms of both the sedimentation potential and the simulated accumulation of suspended material from a designated source upstream. Similar to bottom salinity, a small decrease in sedimentation occurred in the vicinity of bridge pilings for Alternatives 2 and 9 in response to turbulence-induced vertical mixing caused by these structures. A small increase in sedimentation potential was observed at the northeast end of Hampton Flats in response to structures added by Alternative 1. Conditions of high river inflow greatly increased the amount of fine-grained sediment reaching the lower James River from upstream.

TABLE OF CONTENTS

List of Tables

List of Figures

List of Appendices

ACKNOWLEDGEMENTS

This study was funded by the Virginia Department of Transportation under a contract with Baker Environmental, Inc., a unit of the Michael Baker Corporation, Coraopolis, Pennsylvania. We are indebted to Mr. Thomas Biksey of Baker Environmental for his valuable assistance in providing information on infrastructure for the proposed Hampton Roads crossing and for providing helpful comments on the draft report. Special thanks are given to Miss Katie Farnsworth, Department of Physical Sciences, Virginia Institute of Marine Science, for her aid in developing the ArcView® GIS database of model information used in this project.

The views expressed herein are those of the authors and do not necessarily reflect the views of the Virginia Department of Transportation or Baker Environmental, Inc.

I. Introduction

a. Purpose - The purpose of this study is to conduct tests using a numerical model to determine whether the planned construction of highway infrastructure for the Third Crossing of Hampton Roads will impact the primary physical characteristics of the lower James River, a sub-estuary of the lower Chesapeake Bay (Figure 1). Primary physical characteristics include the tidal and non-tidal circulation of water within the lower James River and one of its principal tributaries, the Elizabeth River. They include as well the distribution of salt (salinity) and suspended matter (sediment) within these waterways and the transfer of sediment from the water column to the sea bed through the process of sedimentation.

The aim of model testing is to examine the changes likely to occur for a given structural design and weigh its effects, if any, in comparison to existing conditions. Changes in circulation, for example, may be indicated by an increase or decrease in current speed and/or a change in current direction at a particular point or region within the model domain. Infrastructure under consideration is limited to tunnel islands and bridge pilings, features required for the crossing that are designed to be in contact with the water column along a pre-determined route. Testing for the planned Third Crossing presently focuses on three separate engineering designs, each involving one or more routes crossing Hampton Roads.

b. Test Cases – The four test cases considered in this study are as follows:

1. Base Case – The present configuration of the lower James including the existing tunnel islands of Interstate Route I-64 and I-664, and their connecting bridges.

2. Alternative 1 – The Base Case with the addition of a third tunnel, two tunnel islands, and two bridges on pilings connecting Hampton to Norfolk across the entrance to the James River. Basically, this is an expansion of the I-64 crossing.

3. Alternative 2 – The Base Case and Alternative 1 with the further addition of a new tunnel at the entrance to the Elizabeth River, a single tunnel island west of the river channel, and a single bridge on pilings leading south to a roadway along the eastern edge of Craney Island continuing to Portsmouth.

4. Alternative 9 – The Base Case with the addition of a second tunnel along I-664 leading south from the city of Newport News, and a new east-west bridge connecting I-664 with the Elizabeth River tunnel island and bridge described for Alternative 2. None of the structure for Alternative 1 is included in Alternative 9.

The location of the highway routes incorporated in the Base Case and alternative crossings is shown in plan view in Figures 2, 3, 4 and 5, respectively. Figure 6 shows the HYSED-3D model grid with 370 m x 370 m grid spacing as it appears in the lower James River.

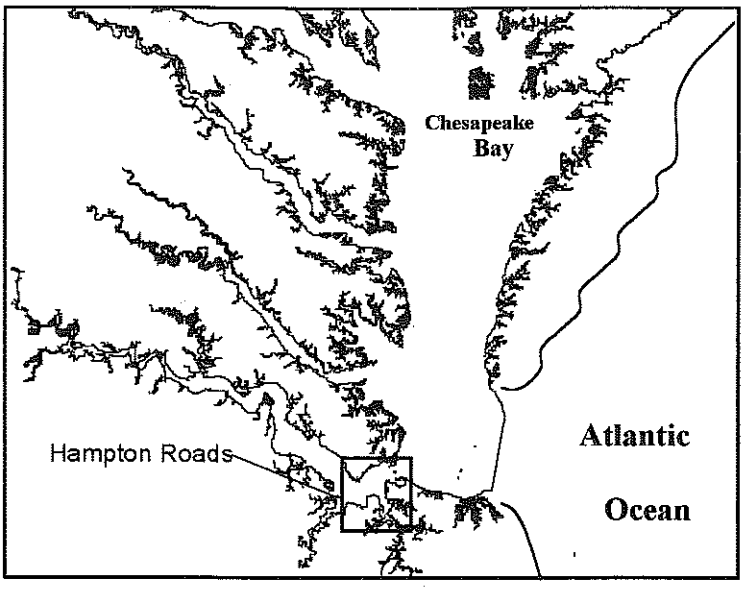

Figure 1. Map showing location of Hampton Roads.

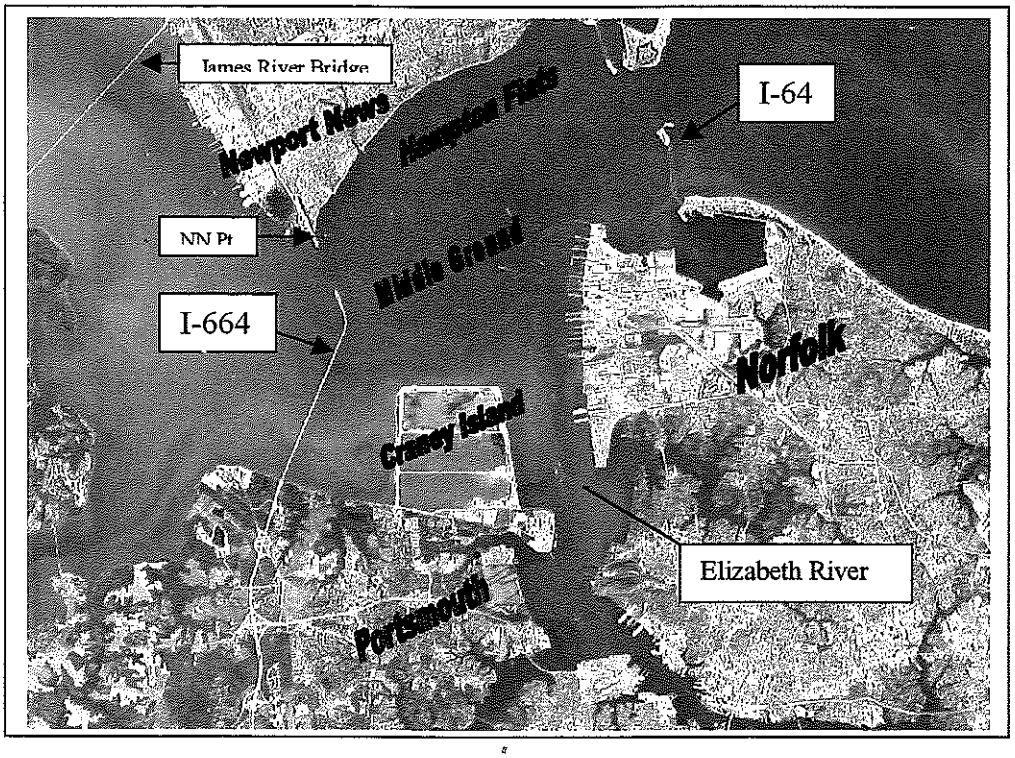

Figure 2. Base Case, Hampton Roads, Virginia.

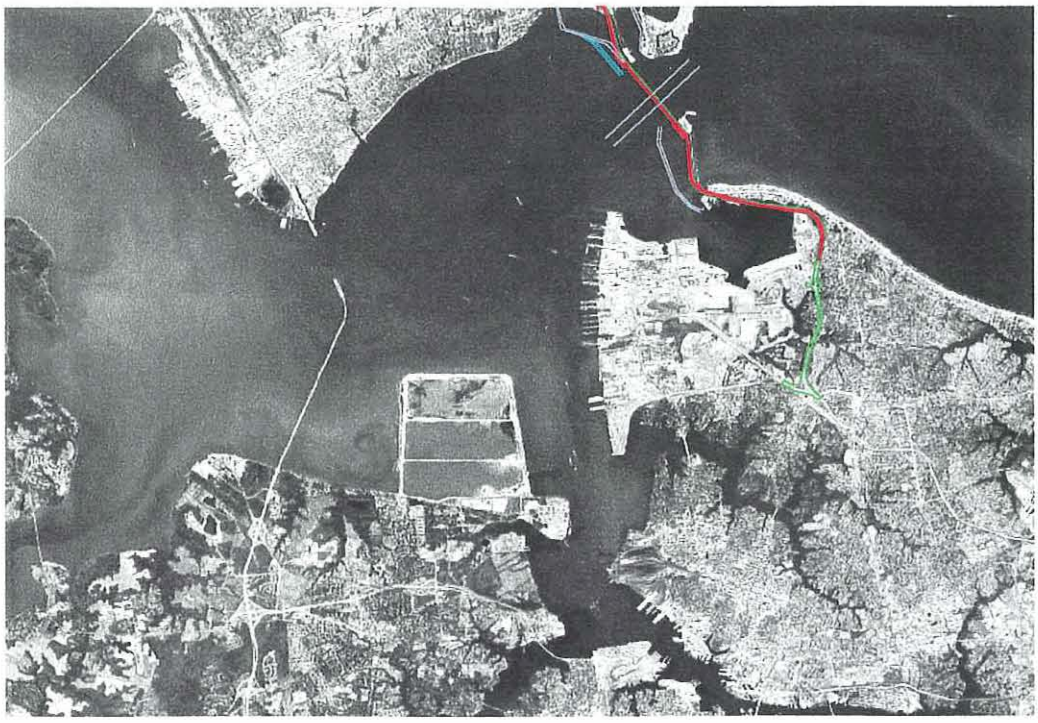

Figure 3. Alternative 1, Hampton Roads, Virginia.

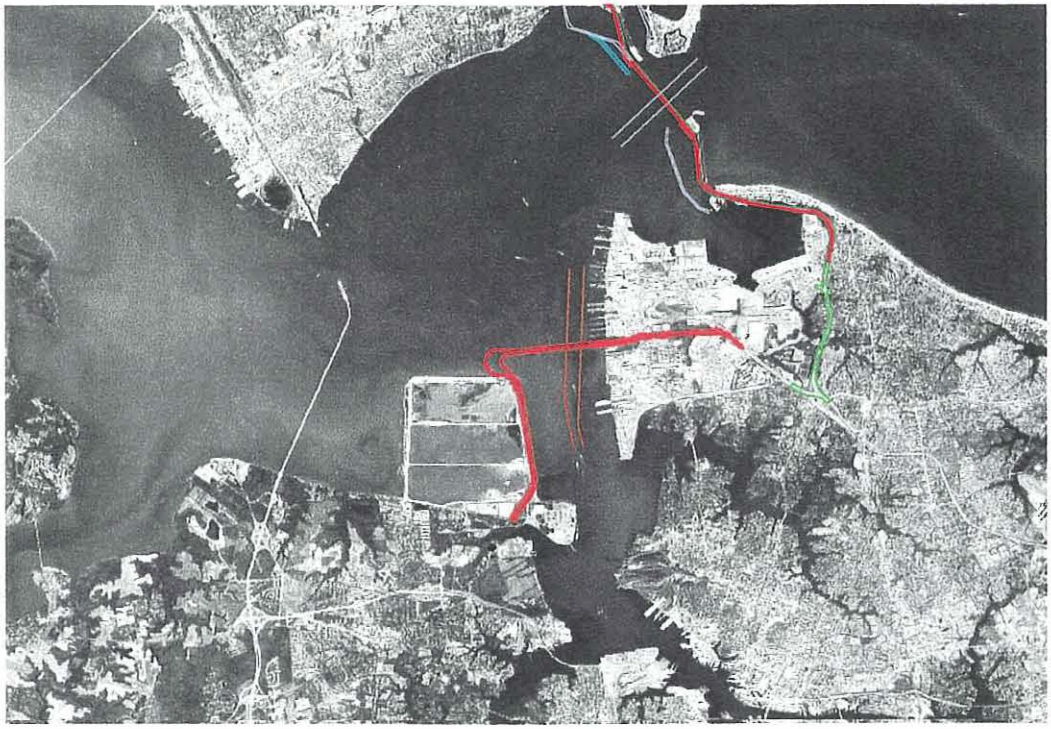

Figure 4. Alternative 2, Hampton Roads, Virginia.

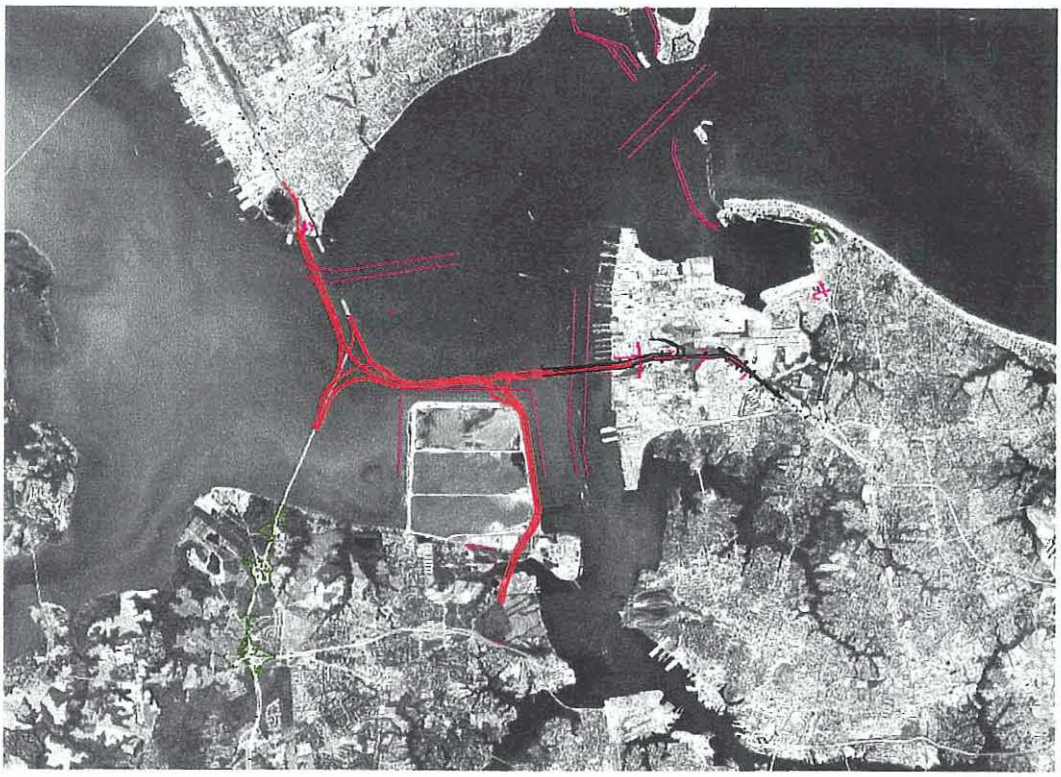

Figure 5. Alternative 9, Hampton Roads, Virginia.

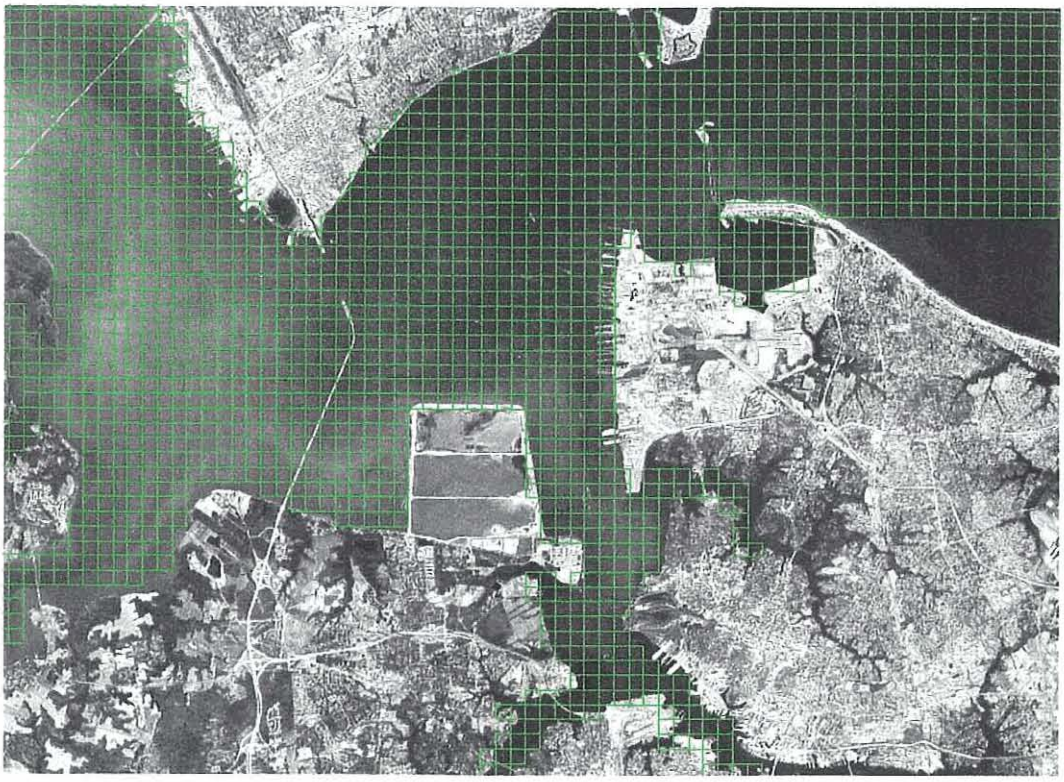

Figure 6. HYSED-3D Model Grid in Hampton Roads (grid interval: 370 m).

II. VIMS Hydrodynamic-Sedimentation Model (HYSED-3D)

a. General Description - The three-dimensional Hydrodynamic-Sedimentation Model (HYSED-3D) used in this study is one of a family of special purpose numerical models developed at the Virginia Institute of Marine Science (VIMS) from an innovative parent program, the Environmental Fluid Dynamics Computer Code (EFDC).The reader is referred to Hamrick (1996) for a detailed description of the EFDC. The hydrodynamic equations and the computational scheme used in this finite difference model are similar to the Blumberg-Mellor model (Blumberg and Mellor, 1987) and the U.S. Army Corps of Engineers Chesapeake Bay model (Johnson et al., 1993). In basic form, these models simulate the hydrodynamic behavior of the estuary by predicting change in surface elevation (including tides), horizontal and vertical water movement (including both tidal and non-tidal currents), and the three-dimensional distribution of conservative water properties such as the salt content (salinity). In addition, the HYSED-3D model incorporates a sedimentation component that allows the user to examine the deposition sites of "tagged" sediment particles with a specified settling velocity and known point of release. The sedimentation component is described in more detail in Section II.c.

The domain of the HYSED-3D model includes the entire length of the James River from its entrance in lower Chesapeake Bay to the fall line near Richmond, Virginia. It includes most of the Elizabeth River, a tributary to the James, with the exception of the Eastern and Southern Branches just beyond the city of Norfolk waterfront area. The entire model grid consists of 4608 active "cells", a portion of which covers the Hampton Roads area as shown in Figure 6.

As implemented in Chesapeake Bay, the EFDC and its derivative programs differ from the Corps of Engineers Chesapeake Bay model in that EFDC uses stretched (sigma) coordinates in place of fixed coordinates to locate points in the vertical dimension. Either rectangular or orthogonal curvi-linear coordinates may be used for the horizontal dimensions. The HYSED-3D model for the James River uses State Plane Coordinates in meters and the 1983 North American Datum (NAD83) to reference all geographic positions, including intersections of the model grid with 370 meter spacing in both the east-west and north-south directions (Figure 6). Each cell formed by the intersecting grid lines is broken vertically into six layers of equal thickness, the thickness varying locally as a function of tide and water depth.

b. Model Initialization, Boundary Conditions – To develop the salinity field in the James River, each separate model run requires a "start-up" period simulating the equivalent of 35 days in real time. During this interval, each grid cell is assigned an initial salinity and computation of new salinity values proceeds until all of the active cells reach equilibrium. The start-up is then followed by an additional 33-day simulation period in which various forms of model output are recorded. Concomitant with initialization, boundary conditions are imposed at the upstream and downstream ends of the model domain. For the downstream boundary, these include bay salinity and tide; for the upstream boundary, freshwater (river) inflow is specified.

As part of the testing design for the model cases discussed in section I, three sets of boundary conditions were devised to represent characteristic variations in tidal range and freshwater

inflow. The required variations in tidal range were appropriately simulated within each standard model run through the use of a three-constituent tide model as discussed below. Three separate runs were required, however, to simulate the characteristic variations in freshwater inflow.

1. Fresh Water Inflow - Historical data from the U.S. Geological Survey stream gauge station at Richmond, Virginia, indicate that freshwater inflow may be characterized by **low inflow** at 20.4 m^3/s, **mean inflow** at 226 m^3/s, and **high inflow** at 650 m^3/s. The data have not been analyzed to determine the percentage of total time that each condition prevails on average. However, the low inflow condition is indicative of drought periods that show considerable inter-annual variability while the high inflow condition is consistent with storm-generated runoff that occurs once a year on average with only a few days duration. Corresponding surface and bottom salinity values used for the downstream boundary, based on VIMS field measurement data, are presented in Table 1.

Table 1. Salinity values in parts per thousand (ppt) used for the downstream boundary condition, James River Entrance.

Salinity at:	Low Inflow	Mean Inflow	High Inflow
Surface	28.5 ppt	19.8 ppt	15.9 ppt
Bottom	29.5 ppt	25.7 ppt	24.0 ppt

2. Tidal Forcing – Tidal forcing for the HYSED-3D model is provided at the downstream boundary by a three-constituent model of the astronomic tide. The objective sought with this model is to simulate tides with the expected variation in tidal range observed during a typical year in Hampton Roads. Tidal range is defined as the difference in elevation between two successive tidal extremes, i.e., a high water and a low water, on any given day. It varies from day to day and from month to month in accordance with lunar and solar orbital motion. In a semidiurnal tide regime such as that of Hampton Roads, the majority of the monthly and semimonthly variation in tidal range is contributed by M_2, the principal lunar semidiurnal constituent, S_2, the principal solar semidiurnal constituent, and N_2, the larger lunar elliptic semidiurnal constituent. Numerically, the tide model is represented by the following equation:

$$h(t) = M_2 \cos(2\pi t/T_m - \phi_m) + S_2 \cos(2\pi t/T_s - \phi_s) + N_2 \cos(2\pi t/T_n - \phi_n)$$

where

t = time (hours)
M_2, S_2, N_2 = constituent amplitudes (meters)
ϕ_m, ϕ_s, ϕ_n = constituent phase angles (radians)
T_m, T_s, T_n = constituent periods (hours)

Amplitudes for these constituents at Hampton Roads (Sewells Point) were obtained from the National Ocean Service and are shown with the corresponding constituent periods in Table 2. For the cases being evaluated, there is no requirement to model the tide for a specific date and time; hence, a specific phase angle is not required for any of the constituents. In order to simulate tides of maximum range for our tide model, we computed initial phase angles that would place

all three tidal constituents exactly in phase at the end of the model startup period (beginning of data recording period). Note that when M_2 and S_2 are in phase or nearly so, their amplitudes add together and the resulting condition is referred to as a **spring tide**. Similarly, when M_2 and N_2 are in phase or nearly so, their amplitudes add together and the resulting condition is referred to as a **perigean tide**. The combination of the two conditions yields **perigean-spring tides** of near maximum range for a given locality. Later in their respective cycles, **neap tide** results when M_2 and S_2 are completely out of phase or nearly so, and **apogean tide** results when M_2 and N_2 are completely out of phase or nearly so. The combination of these two conditions yields **apogean-neap tides** of near minimum range for a given locality. Mean range of tide for the three-constituent model is equal to twice the M_2 amplitude.

Table 2. Tide model constituent period and amplitude, Hampton Roads, VA.

Constituent	Period (hours)	Amplitude (meters)
M_2	12.421	0.342
S_2	12.000	0.063
N_2	12.658	0.076

The semimonthly progression between the extremes in tidal range devised for the model test period is shown in Figure 7.

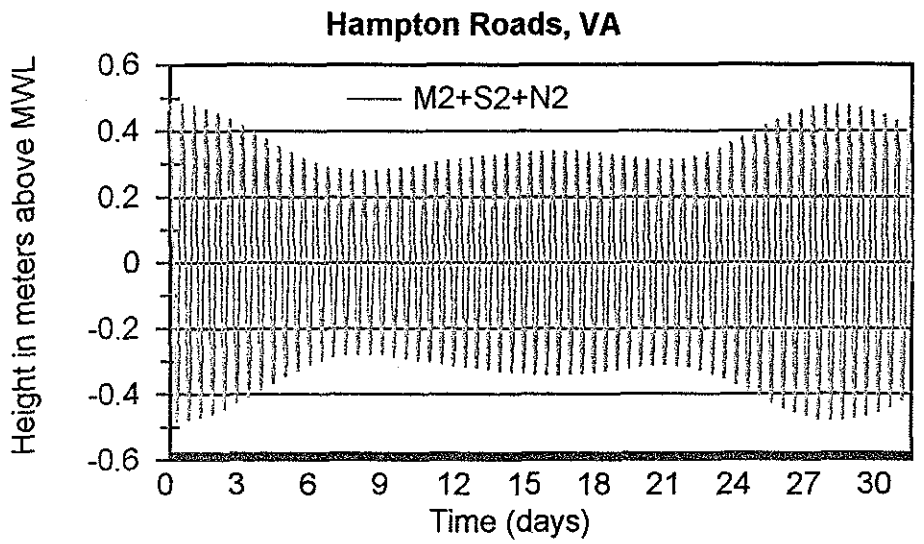

Figure 7. Three-constituent tide model producing apogean-neap tides (day 8), mean range (day 25) and perigean-spring tides (day 29).

C. Simulation of structures and their impact on flow - As indicated in the previous section, the VIMS HYSED-3D model set up in the James River is a fine-scale numerical model. One of the main advantages of using a fine-scale numerical model in the present project is its capability to incorporate structures from different design plans and simulate their effects on the host water body. The tunnel island, for example, can be resolved by the current grid scale and therefore, its effect on the water body can be simulated directly. Obviously, even with the use of fine grid spacing of 370 m, it still does not permit investigation of all the near-field effects from the structure, such as scouring at the base of the pilings. But it does allow the cumulative effect of the local processes to be parameterized at the scale of the cell size and used for studying its far-field effect. Those local processes include the constriction of flows by the spatial distribution of the pier in a cell, the impedance of flow by the collective drag forces from the individual pilings, and the corresponding turbulence mixing induced by the flow-structure interaction. Using adequate parameterization procedures, the effects of the structure on tidal fronts, eddy systems, and other far-field phenomena can then be properly investigated.

Two kinds of structures considered in this project are: 1) tunnel islands whose dimensions cover more than one grid cell (i.e., close to 740 m in length and slightly less than 370 m in width); 2) cylindrical pilings of approximately 137 cm (54 in) in diameter standing vertically or near vertically. Based on the design drawings, the spacing between the individual pilings is more or less at regular intervals under the bridge. Both the pilings and the tunnel island extend from the water surface all the way to the bottom. Since the dimensions of the designed tunnel island are comparable to the grid resolution, it can either be treated as a 'thin wall' boundary if the shape is slender or as a land cell if it occupies most of the grid cell. Cells can be masked, depending on the position and orientation of the island, either in the west face, the south face, or both faces of a cell so that no flow is allowed to pass through the boundary. The resultant flow is thus forced to deviate and follow another path around the island boundary inserted by this procedure. The piling dimension designed, on the hand, is smaller than the grid resolution (i.e., a sub-grid scale), and thus needs to be parameterized.

To parameterize the piling effect, first the porosity defined as the water fraction of the piling area in a cross-section is introduced into the constant x, y, z plane. These values are estimated from the actual designed plan. For example, in the application of the plan of Alternative 9, the design calls for a predominantly north-south oriented bridge piling with 70 feet (21 m) intervals and 10 feet (3 m) intervals in the cross-section direction. The porosities, once determined, are then incorporated into the mass balance control volume formulations. The continuity equation is thus given as:

$$\frac{\partial}{\partial t}(\phi_z \zeta) + \frac{\partial}{\partial x}(\phi_x H u) + \frac{\partial}{\partial y_e}(\phi_y H v) + \frac{\partial}{\partial z}(\phi_z w) = 0$$

where ζ is the water surface elevation; H is the local depth of the water column; u, v, w are the horizontal and vertical velocities; ϕ_x, ϕ_y, ϕ_z are porosity in x, y and z planes, respectively. The typical values of ϕ_x, ϕ_y are estimated as 0.93, 0.96 and ϕ_z in the z

direction as 0.99. The mass conservation equation for a dissolved or suspended material with concentration C is:

$$\frac{\partial}{\partial t}(\phi_z C)+\frac{\partial}{\partial x}(\phi_x HuC)+\frac{\partial}{\partial y}(\phi_y HvC)+\frac{\partial}{\partial z}(\phi_z wC)=\frac{\partial}{\partial z}\left(\phi_z H^{-1}k_z\frac{\partial}{\partial z}C\right)+(\phi_z S_c)$$

where k_z is the eddy diffusivity; S_c is the source or sink term. The second step for the parameterization is to modify the momentum and the turbulence equation to include the flow-structure interaction. A resistance term was incorporated into the momentum equation as a result of the boundary shear stress introduced at and around the piling. The x- momentum equation is:

$$\frac{\partial}{\partial t}(\phi_z Hu)+\frac{\partial}{\partial x}(\phi_x Huu)+\frac{\partial}{\partial y}(\phi_y Hvu)+\frac{\partial}{\partial z}(\phi_z wu)-\mathrm{f}\,\phi_z\,\mathrm{H}\,\mathrm{v}$$

$$=-\phi_z H\frac{\partial}{\partial x}(\mathrm{g}\zeta+\mathrm{p})+\frac{\partial}{\partial z}\left(\phi_z H^{-1}N_z\frac{\partial u}{\partial z}\right)-\mathrm{c_p}\frac{\mathrm{B_p}}{\mathrm{L_p^2}}\mathrm{H}\left(u^2+\mathrm{v}^2\right)^{0.5}u$$

where the terms on the left represent the inertial terms and the Coriolis force terms, and those on the right, the pressure gradient term, the vertical shear stress term and lastly the resistance term due to the piling. The N_z represents eddy viscosity, c_p the drag coefficient, B_p the projected piling width and L_p the separation length scale for the piling density. The resistance term is applied throughout the water column as opposed to the bottom shear stress, which is applied only at the bottom as a bottom boundary condition. The y–momentum equation (not shown) can be derived similarly.

The accompanied turbulence production and dissipation associated with the momentum resistance are also incorporated into the turbulence equations. The turbulence formulation used is the standard Mellor-Yamada turbulence closure scheme, as extended by Galperin et. al. (1988) and Blumberg et. al. (1992). The modifications were made to include an additional term for the turbulence energy production and dissipation induced by the bridge piling. The term which corresponding to the resistance term in the momentum equation is:

$$2\,\mathrm{c_p}\frac{\mathrm{B_p}}{\mathrm{L_p^2}}\mathrm{H}\left(u^2+\mathrm{v}^2\right)^{1.5}$$

where $c_p, B_p, \mathrm{L_p}$ are as defined in the momentum equation. The term essentially includes the effect of the turbulence flow at and around the piling as a result of the flow and the piling interaction.

d. Sedimentation Model – The HYSED-3D model presently uses two approaches to investigate sedimentation effects. The first approach evaluates the hydrodynamic conditions under which bottom sedimentation can occur; the second determines whether sediment of a given particle size can be transported in suspension from a known source area to sites in the model domain with conditions conducive to deposition.

The basis for the first approach is the model-generated prediction of bottom shear stress at discrete time intervals in each of the basal cells within a selected sub-region of the model grid. After continuing this calculation over many tidal cycles, the **sedimentation potential** is determined as the percent of total time that bottom shear stress falls below a critical value permitting sediment of a given particle size to deposit. The potential for each cell is computed and its distribution is then mapped over the selected bottom region. The sedimentation potential is defined irrespective of the availability of any sediment to be deposited from suspension. It merely serves to delineate those areas that are conducive to deposition as well as those that are not. More importantly, it pin-points areas subject to change in sedimentation potential as a result of change in hydrodynamic conditions.

In the second approach, simulations are made treating sediment particles as discrete objects that are assigned a particular settling velocity according to their nominal grain size. The particles are released for a given time at a given rate in one or more cells representing a sediment source. This type of simulation is analogous to a tracer experiment in which a small portion of the total sediment particle population is 'tagged' or labeled according to known source areas and subsequently detected at various deposition sites. The particles are transported partially coupled to the fluid; i.e., with non-zero settling velocity equivalent to a negative buoyancy relative to the fluid. When these particles enter a basal cell during a period in which bottom shear stress is below the critical value (about 0.1 pascals), they are removed from the active cell layer and counted as deposited particles. A particle deposition density (mass per unit area) is then determined at the end of a run of 67 tidal cycles following particle release. This approach does not simulate sedimentation *per se* (i.e., by a rate of deposition) but is an extension of the sedimentation potential weighted by particle availability from a defined source area.

e. Model Verification for Tide and Current – Hydrodynamic simulations produced by the HYSED-3D model for the James River have been verified principally through comparison with field observations of tide and current. Least squares harmonic analysis of predicted and observed time series of tidal height show very good agreement in terms of the amplitude and phase of seven of the principal tidal constituents. Tidal height curves 'synthesized' with these constituents permit a visual comparison of the predicted and observed **astronomic tide** (tide of celestial origin without meteorological or hydrological input). Examples of astronomic tidal height comparisons are shown in Figures 8 and 9. Expected error based on these comparisons is approximately 5-8 minutes for the times and 3-4 cm for the heights of the simulated highs and lows. Comparison of predicted and observed tidal currents is not as straightforward as tidal height comparisons since the direction as well as the speed of the current must be considered. We follow the convention in which horizontal current vectors are resolved into u,v orthogonal components, initially projected onto east-west and north-south axes and presented as a

dual time series in u and v. Most estuarine flows are channeled to a greater or lesser extent and it is convenient to rotate the reference axes until one series, u, contains the maximum possible variance. After this is done, the new reference axis of maximum variance is usually found to be aligned parallel to the channel axis and the u component alone is compared in that event. By convention, the upstream flow is termed flood current (u positive) and the downstream flow is termed ebb current (u negative). Examples of flood and ebb currents compared in the surface and bottom layers of the water column near Newport News Point are shown in Figures 10 and 11.

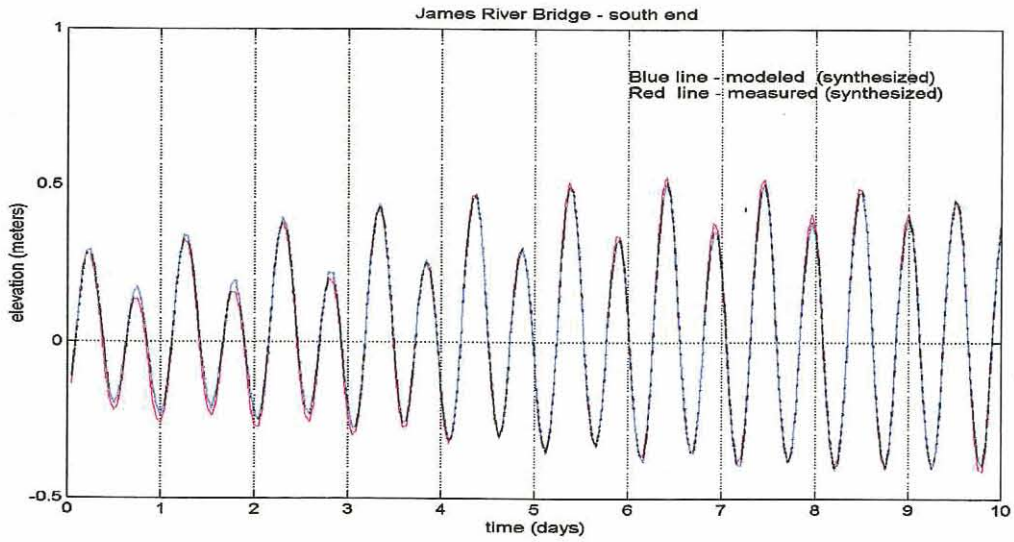

Figure 8. Astronomic tide verification, James River Bridge.

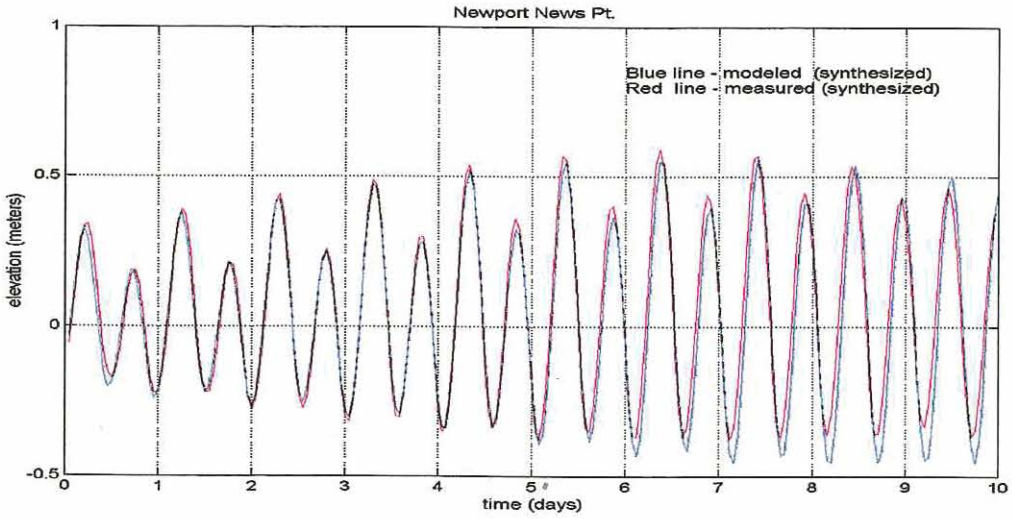

Figure 9. Astronomic tide verification, Newport News Point.

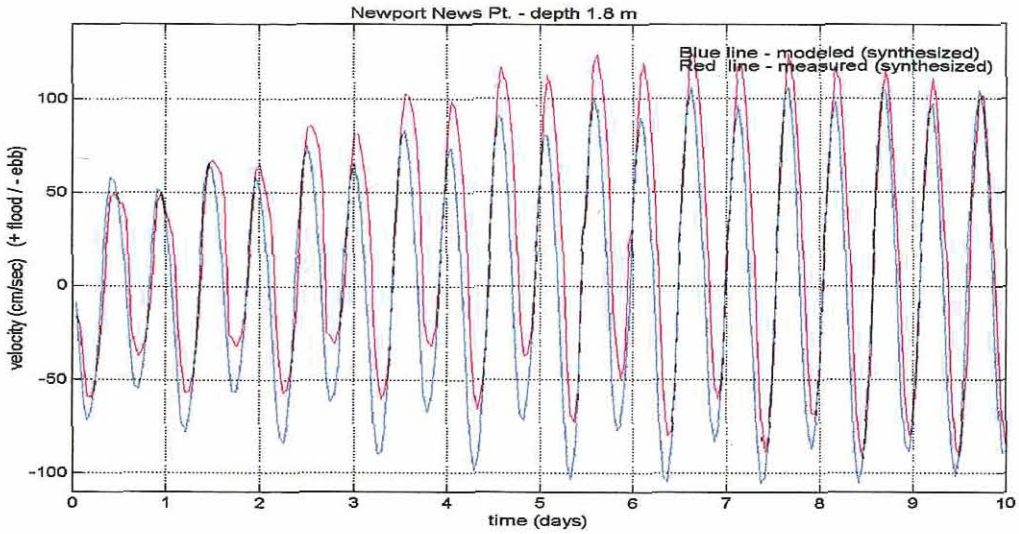

Figure 10. Astronomic Surface Current Verification,
1 km South of Newport News Point.

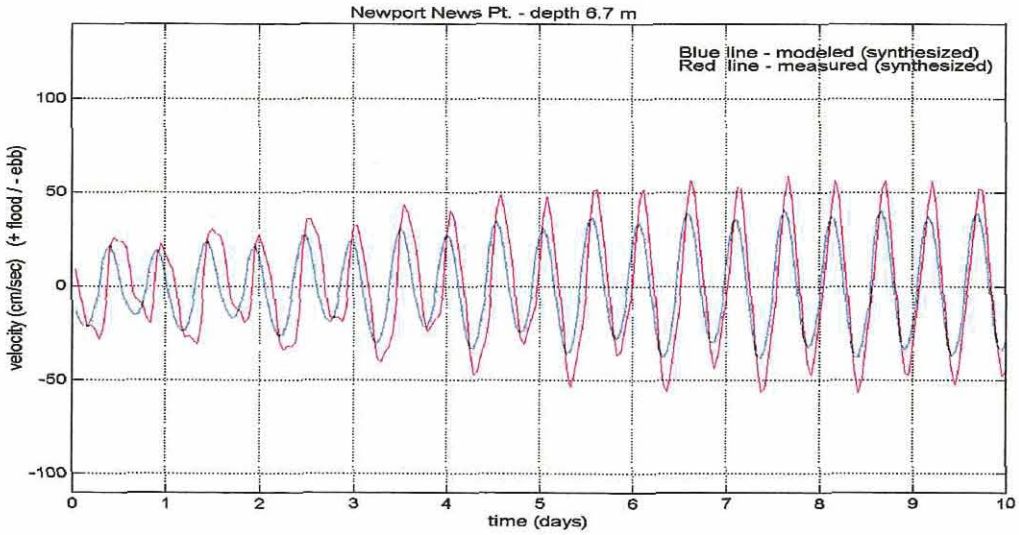

Figure 11. Astronomic Bottom Current Verification,
1 km South of Newport News Point.

Astronomic tidal currents are no more difficult to predict than astronomic tidal heights in the deterministic sense. Tidal currents, however, tend to demonstrate greater spatial variability (in three dimensions) in their parameters of speed and direction. This is particularly true where bottom topography and shoreline configuration is complex as it is within the major bend of the lower James River below Newport News Point. The

comparisons shown in Figures 10 and 11 may be judged reasonable in view of this fact and the fact that the model's point of current prediction and the point of current observation are often not the same. On the other hand, both tidal and non-tidal (tidally averaged) water flows are fundamentally important because of their ability to transport dissolved and suspended particulate material and a closer examination of the probable error associated with predicted tidal current is clearly warranted.

To gain insight into the error in tidal current predictions, we compared two simple cosine waves representing hypothetical flood and ebb currents, one predicted and one measured. For the measured wave, let the amplitude and phase equal 100 cm and zero, respectively, while allowing the amplitude and phase of the predicted (test) wave to vary. Both cosine waves are assigned a period of 12.42 hours and two time series of simultaneous current values are calculated at short intervals over that time. The accuracy of current predictions may then be estimated from variation about the 1:1 reference line of perfect agreement in a plot of predicted versus measured current speed. An example is presented in Figure 12 with the test wave amplitude unreduced at 100 cm but with a phase 'lag' of 20 minutes (the time equivalent of the phase angle in radians for a 12.42-hour wave period). The lag may be thought of as a 20-minute error in predicting the time of maximum current.

The standard error of estimate (RMS error) for the hypothetical example shown in Figure 12 is 11.9 cm/s. Figure 13 illustrates an RMS error of 13.4 cm/s for the same test wave with its amplitude reduced by 10% (from 100 cm to 90 cm). Aside from the general magnitude of the expected error, Figures 12 and 13 illustrate that the error source (the amplitude and/or phase lag difference) may be inferred from the form of departure of data points from the 1:1 line of perfect fit. More specifically, a clockwise rotation of the data point 'ellipse' axis relative to the 1:1 line indicates that the current amplitude is under-predicted and vice-versa. For real currents in general, and surface currents in particular, amplitude comparison errors increase with the directional variability of the current.

Actual current data from the surface and bottom layers of the main river channel at the James River Bridge are presented in Figures 14 and 15, respectively. The flow components compared are those in the direction parallel to the channel axis. For error estimation purposes, this is an optimal comparison because of the relative straightness of the river channel and uniformity of flow at this site. RMS error in predicted surface currents due to phase lag is about 6.7 cm/s, increasing to about 9.9 cm/s due to a combination of phase lag and amplitude difference. RMS error in predicted bottom currents due to phase lag is about 4.2 cm/s, increasing only slightly to about 5.1 cm/s when the amplitude difference is added. These results support the generalization that channel "steering" greatly restricts the directional variability of the bottom current. When compared with the test waves, they suggest amplitude estimation error of less than 10% with a phase estimation error of less than 20 minutes.

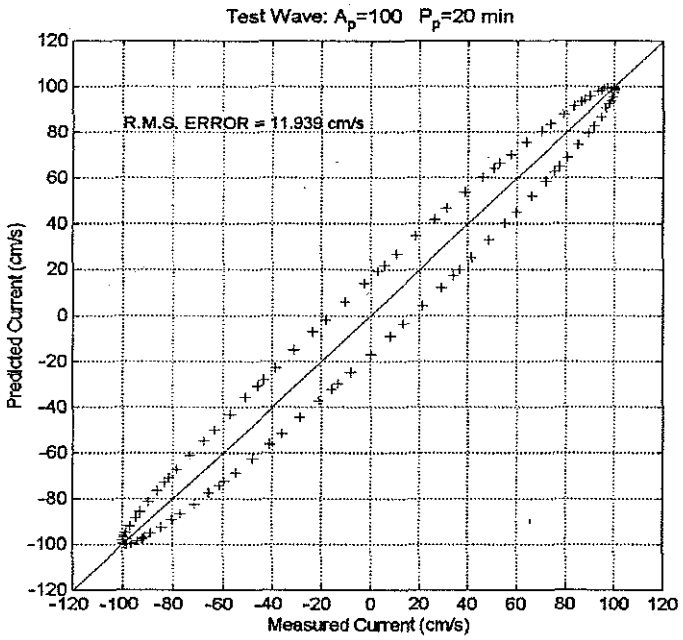

Figure 12. Predicted versus measured current, test example with 20 minute phase lag.

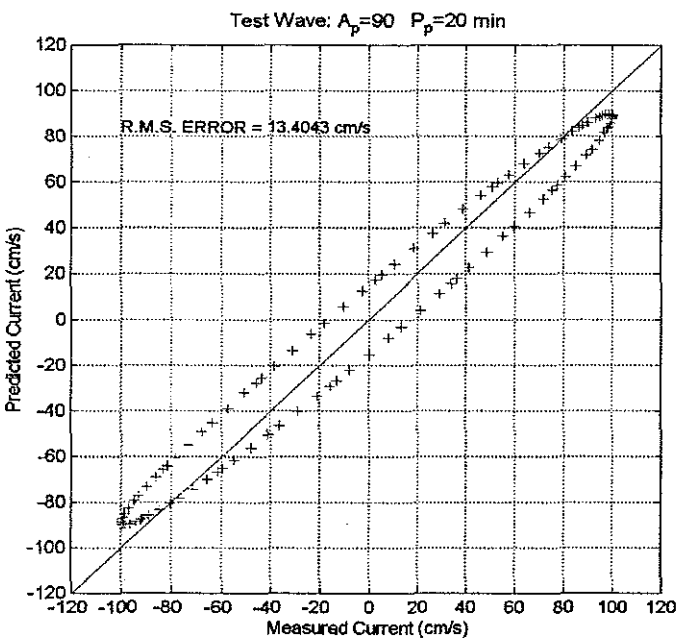

Figure 13. Predicted versus measured current, test example with 20 minute phase lag and 10 % amplitude reduction.

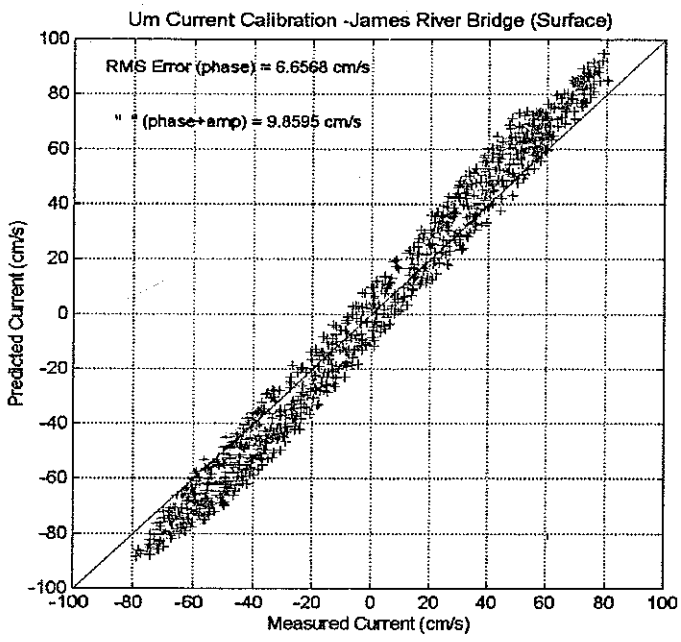

Figure 14. Predicted versus measured surface current, James River Bridge.

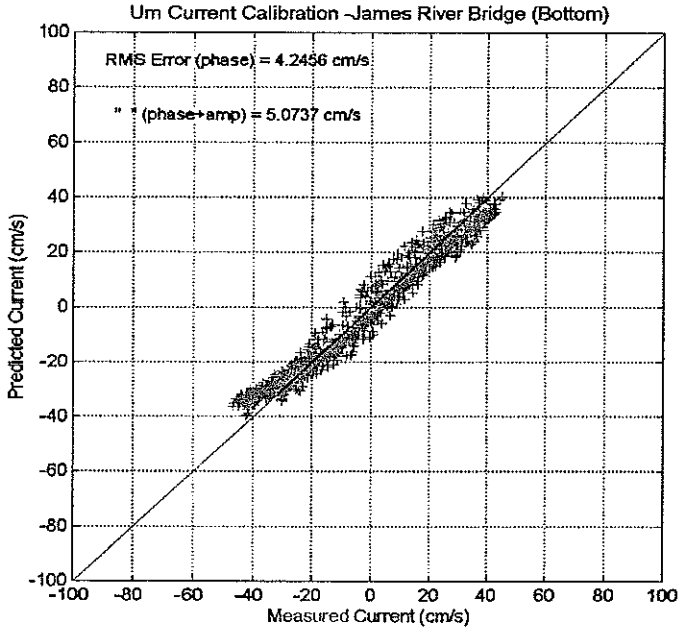

Figure 15. Predicted versus measured bottom current, James River Bridge.

III. RESULTS

a. Simulation Comparisons: Tidal Heights – Simulated time series of tidal heights were computed at the center of selected cell stations (crossed circles) as shown in Figure 16. Using the boundary conditions described in Section II.b. for the generation of simulation results, twelve standard runs were made covering the three river inflow conditions and the four test cases (Base Case and three alternative crossing designs). As noted in Section II.b., each run covered a period of 33 days in which output was selected for apogean-neap tides (day 8), mean range tides (day 25) and perigean-spring tides (day 29).

None of the above runs produced evidence of significant change in tidal height, tidal range, or tidal phase in any of the three base comparisons: (1) Base Case versus Alternative 1; (2) Base Case versus Alternative 2; and (3) Base Case versus Alternative 9. An example of the type of comparison obtained with the runs described above is given in Figure 17. The curves shown (solid line and dots) match well within the accuracy limits expected for the model when computing height differences (about 3 cm) . A tabulation of high and low water tidal heights and their difference (tidal range) for the first half of day 25 (mean tidal range) is presented in Table 3.

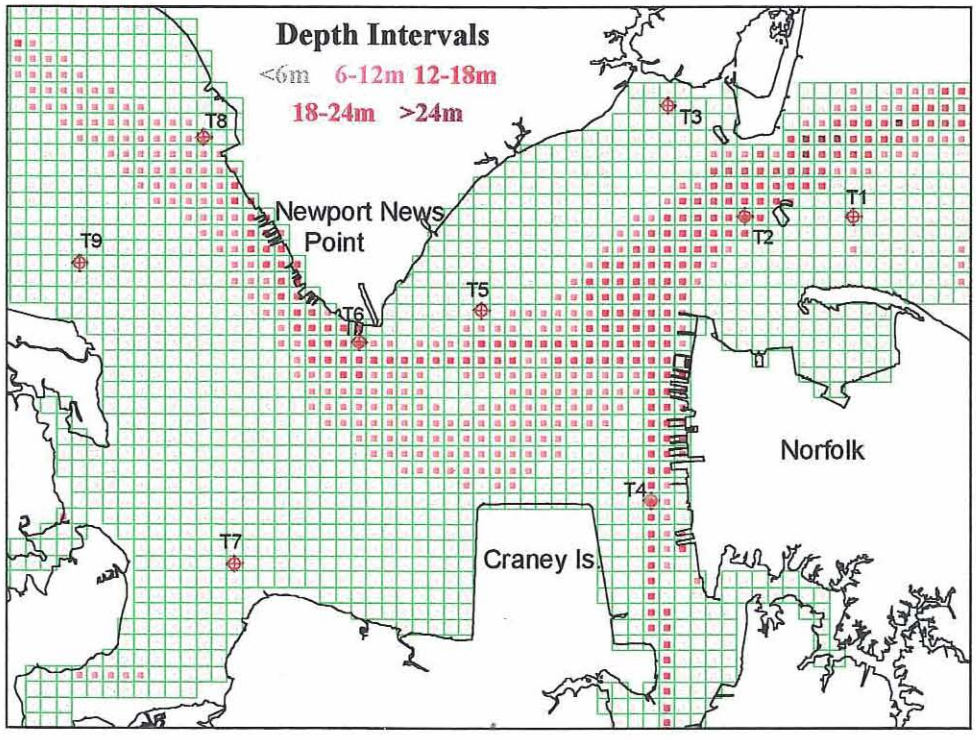

Figure 16. Location of tide simulation stations, T1 – T9. Color dots indicate depth interval in meters. Grid interval is 370 meters east-west and north-south.

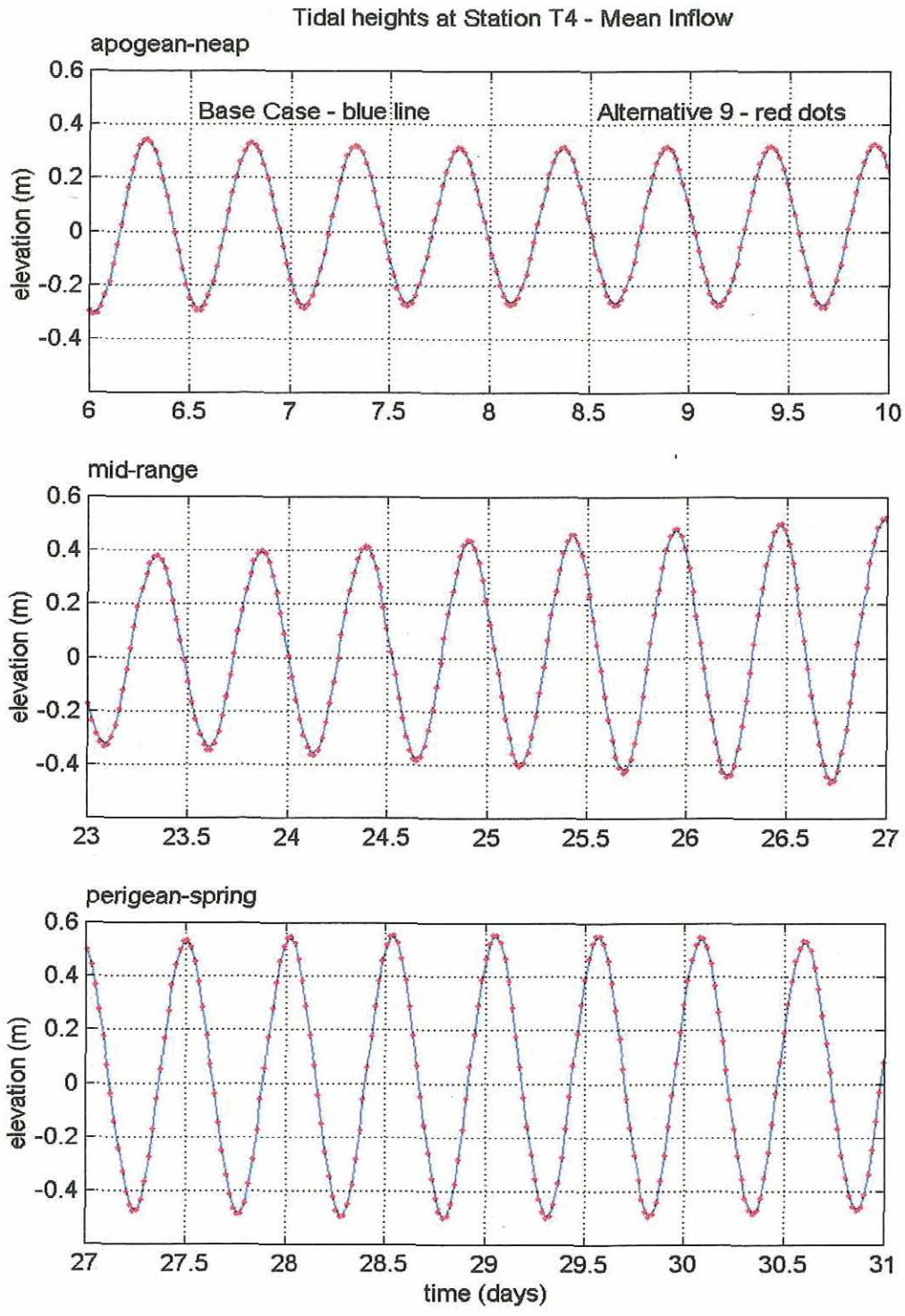

Figure 17. Simulated tide comparison at Station T4, Base Case versus Alternative 9, mean river inflow condition.

Table 3. Model predictions of high water (HW), low water (LW), and tidal range (RN) in centimeters on model day 25 (mean range) at tide simulation Stations T1 through T9, lower James River.

	Inflow	Base Case			Alt 1			Alt 2			Alt 9		
		HW	LW	RN	HW	LW	RN	HW	LW	RN	HW	LW	RN
T1	HI	42.0	-42.0	84.0	42.1	-42.0	84.1	42.1	-42.0	84.2	42.8	-42.7	85.5
	MED	40.6	-42.9	83.5	40.6	-42.9	83.4	40.6	-42.8	83.4	41.1	-43.3	84.5
	LO	40.9	-43.7	84.6	40.9	-43.7	84.6	40.9	-43.7	84.7	41.4	-44.1	85.5
T2	HI	42.4	-38.8	81.3	42.4	-38.7	81.1	42.5	-38.7	81.2	43.1	-39.4	82.4
	MED	40.3	-40.0	80.4	40.3	-40.0	80.3	40.3	-40.0	80.3	40.9	-40.6	81.5
	LO	40.2	-41.4	81.6	40.2	-41.3	81.5	40.2	-41.4	81.5	40.5	-41.8	82.4
T3	HI	44.4	-40.2	84.5	44.5	-40.3	84.8	44.6	-40.3	84.8	45.0	-40.8	85.9
	MED	42.1	-41.1	83.2	42.1	-41.2	83.3	42.2	-41.2	83.3	42.5	-41.6	84.1
	LO	42.1	-42.3	84.4	42.0	-42.3	84.4	42.0	-42.3	84.4	42.4	-42.6	85.0
T4	HI	46.2	-38.5	84.8	46.3	-38.5	84.8	46.3	-38.9	85.2	46.9	-40.1	87.0
	MED	43.4	-39.6	83.0	43.3	-39.6	82.9	43.4	-39.9	83.3	43.9	-40.6	84.5
	LO	42.9	-41.3	84.2	42.9	-41.2	84.0	42.9	-41.3	84.2	43.3	-41.6	84.9
T5	HI	46.1	-42.6	88.7	46.1	-42.5	88.6	46.2	-42.5	88.7	46.8	-42.9	89.7
	MED	43.4	-42.8	86.2	43.4	-42.8	86.2	43.4	-42.8	86.1	43.8	-43.0	86.8
	LO	42.7	-43.2	85.9	42.7	-43.2	85.8	42.7	-43.2	85.8	43.0	-43.4	86.4
T6	HI	46.2	-40.7	86.9	46.2	-40.6	86.8	46.3	-40.7	86.9	46.2	-39.7	85.9
	MED	42.5	-40.8	83.3	42.5	-40.7	83.2	42.5	-40.8	83.2	41.9	-40.0	81.9
	LO	41.4	-41.0	82.4	41.3	-41.0	82.4	41.3	-41.0	82.3	40.5	-40.7	81.2
T7	HI	47.7	-38.5	86.2	47.7	-38.4	86.1	47.7	-38.5	86.1	47.6	-37.8	85.4
	MED	44.2	-38.6	82.8	44.2	-38.6	82.8	44.3	-38.6	82.8	43.9	-37.9	81.8
	LO	42.9	-39.5	82.4	42.8	-39.5	82.3	42.8	-39.5	82.3	42.5	-38.9	81.4
T8	HI	46.4	-39.0	85.5	46.5	-39.0	85.4	46.5	-39.0	85.4	46.5	-38.2	84.7
	MED	42.6	-38.8	81.4	42.6	-38.7	81.3	42.6	-38.7	81.3	42.6	-38.1	80.7
	LO	40.1	-38.3	78.5	40.1	-38.3	78.4	40.1	-38.3	78.4	40.1	-37.7	77.8
T9	HI	46.1	-37.7	83.8	46.1	-37.6	83.8	46.2	-37.6	83.8	46.1	-37.0	83.1
	MED	42.1	-37.3	79.4	42.1	-37.3	79.3	42.1	-37.3	79.4	42.0	-36.7	78.6
	LO	39.4	-36.9	76.3	39.3	-36.9	76.3	39.4	-36.9	76.2	39.2	-36.3	75.6

b. Simulation Comparisons: Tidal Currents - Simulated time series of tidal currents were computed at the center of selected cell stations (red arrows) as shown in Figure 18. The same series of standard runs were made as described in Section III.a. for tidal heights. The time series are flood and ebb representations of the horizontal component of flow having maximum variance, usually the component parallel to the local bottom contours or channel axis. The directional heading of the flood component (always positive upstream) is referenced on each of the time series graphs presented below.

Note that HYSED-3D tidal current simulations may contain a **nontidal or residual component**. The residual appears as a non-zero result from tidal averaging of the time series data over one or more tidal cycles.

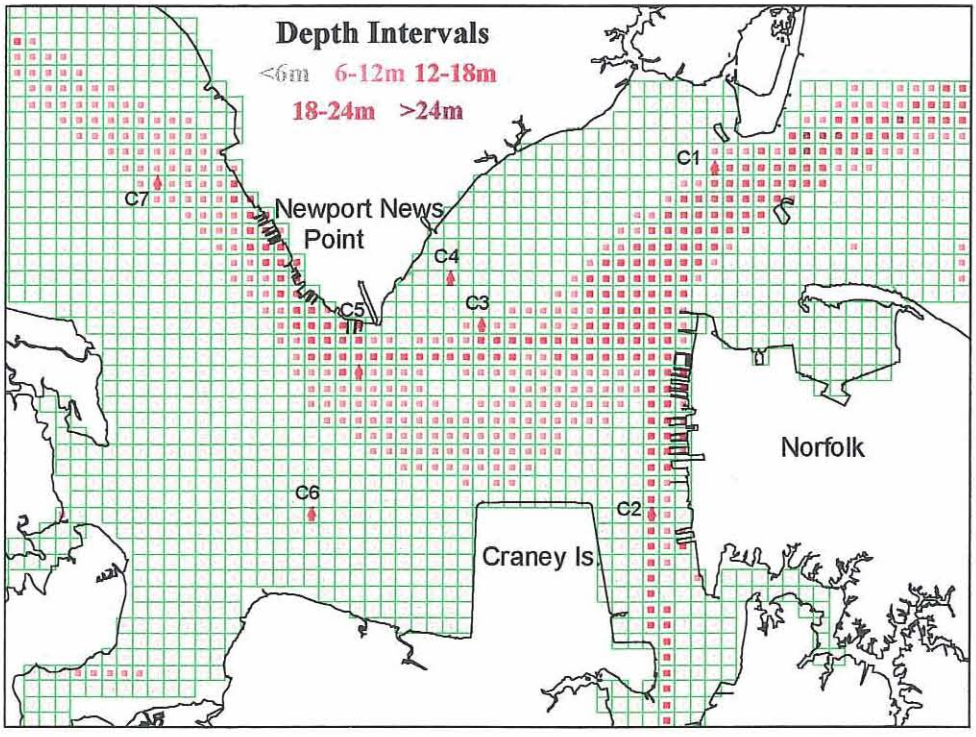

Figure 18. Location of tidal current simulation Stations, C1 – C7. Color dots indicate depth interval in meters. Grid interval is 370 meters east-west and north-south.

Most of the simulated tidal current comparisons show very little change. However, a few relatively minor changes were noted at certain stations for certain test case comparisons. Examples for each test case are presented below.

1. Base Case – Alternative 1: Little, if any, change is apparent for most of the conditions examined for this case. A slight change in form of the surface current curve appears in tides of mean range in combination with low river inflow as shown in Figure 19.

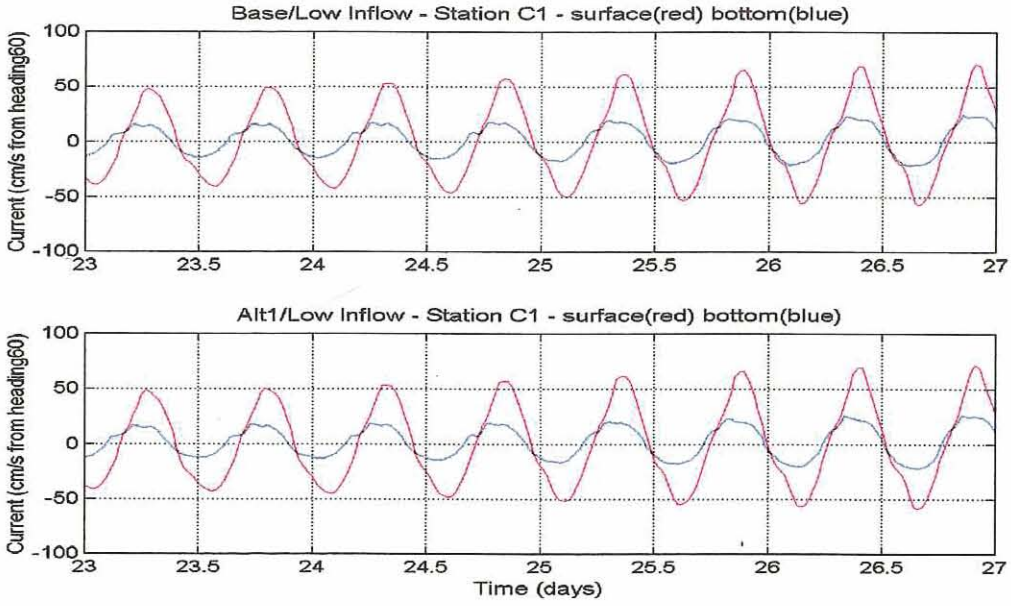

Figure 19. Simulation comparison of tidal current at Station C1, Base Case and Alternative 1; mean tidal range and low river inflow.

2. Base Case – Alternative 2: Minor changes are noted at Stations C1 and C2 in this comparison. A very slight change in curve form for the surface current occurs at Station C1 as illustrated in Figure 20. The change in surface current form at Station C2 at the Elizabeth River Entrance (Figure 21) is more pronounced, particularly in the flood segment for Alternative 2 which has a sharper peak with a delay in the time of maximum flood compared to the Base Case. Changes also occur in the form of the bottom current.

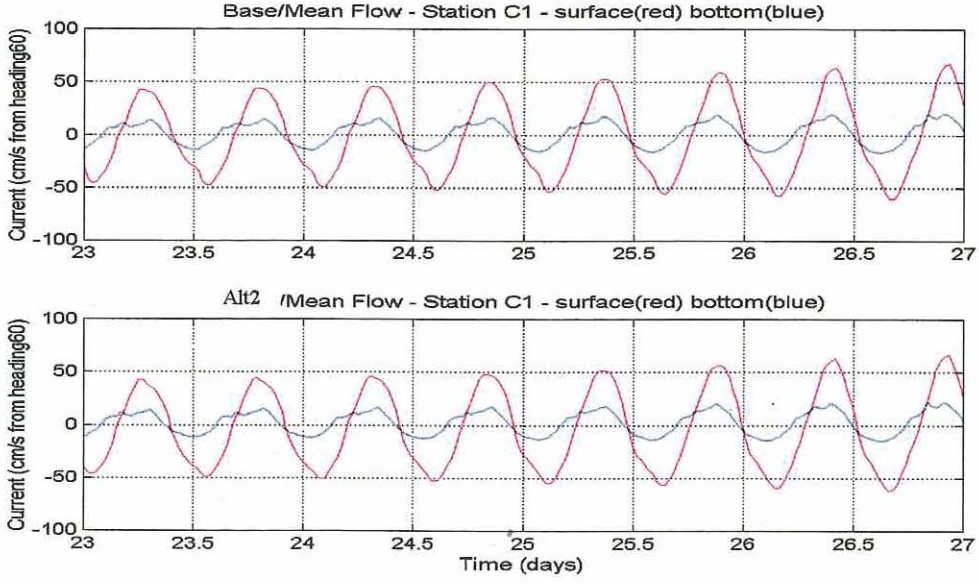

Figure 20. Simulation comparison of tidal current at Station C1, Base Case and Alternative 2; mean tidal range and mean river inflow.

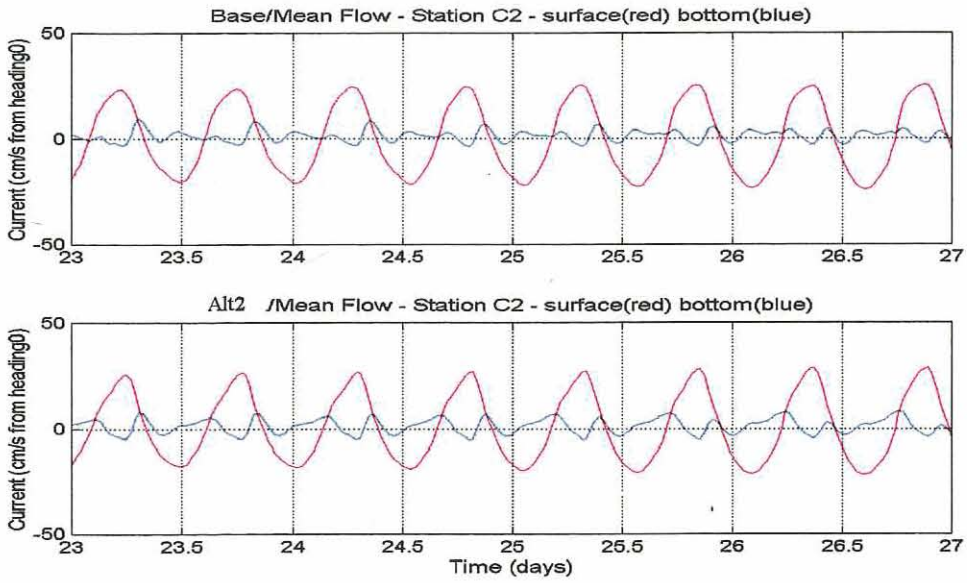

Figure 21. Simulation comparison of tidal current at Station C2, Base Case and Alternative 2; mean tidal range and mean river inflow.

3. Base Case – Alternative 9: Simulations for Alternative 9 produce notable changes in current at Stations C2, C3, and C5. For Station C2 at the entrance to the Elizabeth River, the change is similar to that just described for Alternative 2 but with flood current peaks that appear even sharper and more asymmetric (flood maxima exceeding ebb maxima) for Alternative 9 during both mean river inflow (Figure 22) and high river inflow (Figure 23). The bottom current is small but highly variable at Station C2 and, therefore, difficult to interpret. In general, model simulations seem to predict a small increase in peak flood bottom current at Station C2 due to the effects of Alternative 9.

Station C3 in the main Newport News navigation channel and Station C5 just below Newport News Point show pronounced changes in surface current, but not bottom current, as a result of Alternative 9. The Base Case time series curves for Station C3 show a pronounced surface current asymmetry (peak ebb greater than peak flood) with an enhanced ebb current residual that appears noticeably stronger in the runs for Alternative 9 (Figure 24). Surface currents at Station C5 show a small downstream residual initially that is enhanced after Alternative 9 is added. The current range (gross difference between flood and ebb current maxima) is reduced at Station C5 (Figure 25) but not at Station C3 (Figure 24). The range reduction at Station C5 is the result of a change in current direction relative to the channel axis and not a reduction in current magnitude.

Downstream surface current residuals are consistent with classical two-layer estuarine circulation models, provided there is evidence of a counterbalancing upstream bottom current residual. The bottom currents shown in Figures 24 and 25 do, in fact, appear to have residuals directed upstream but, unlike the surface currents, they show only a slight degree of change as a result of Alternative 9. This pattern of change suggests possible enhancement of an eddy (non-tidal) motion in the surface current.

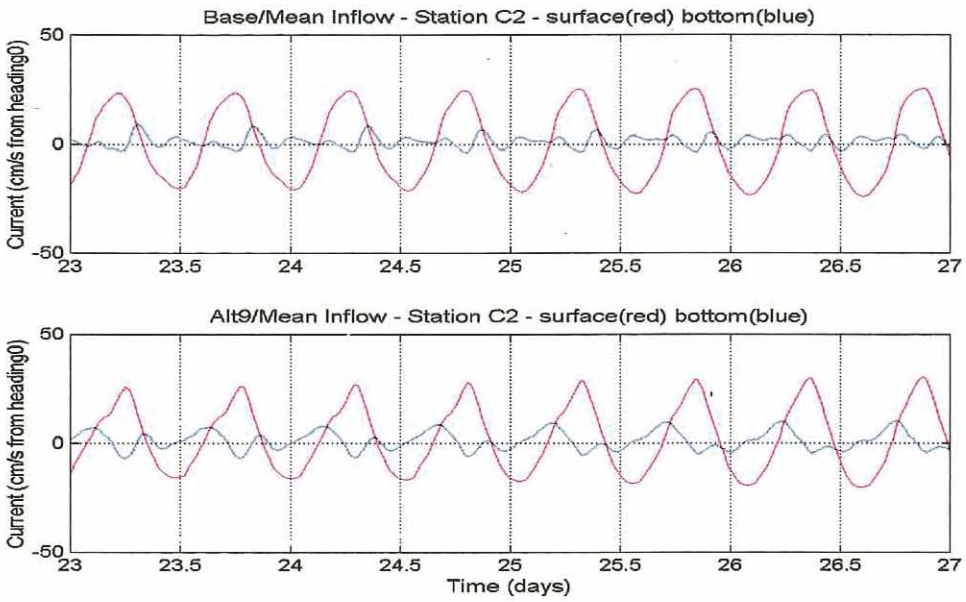

Figure 22. Simulation comparison of tidal current at Station C2, Base Case and Alternative 9; mean tidal range and mean river inflow.

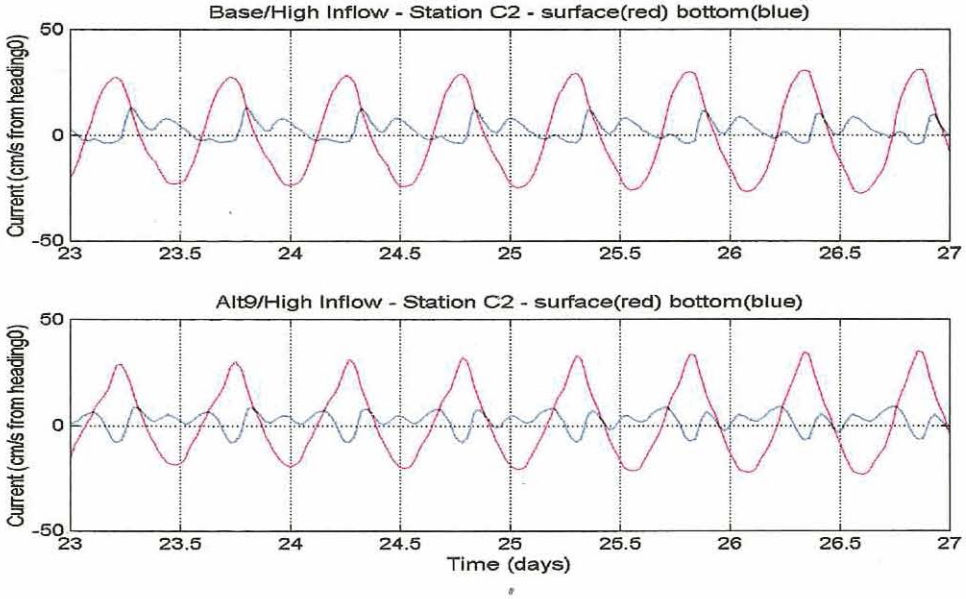

Figure 23. Simulation comparison of tidal current at Station C2, Base Case and Alternative 9; mean tidal range and high river inflow.

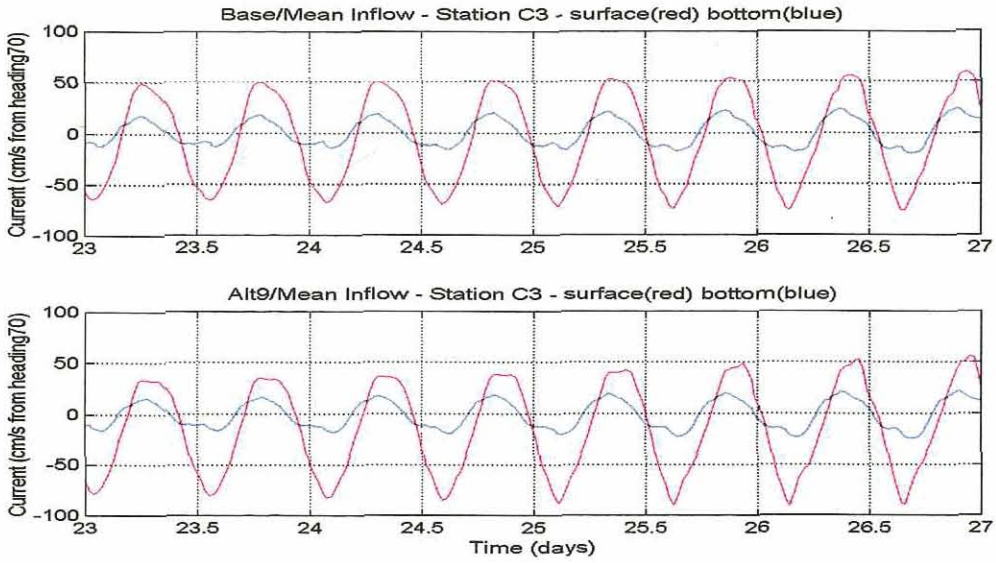

Figure 24. Simulation comparison of tidal current at Station C3, Base Case and Alternative 9; mean tidal range and mean river inflow.

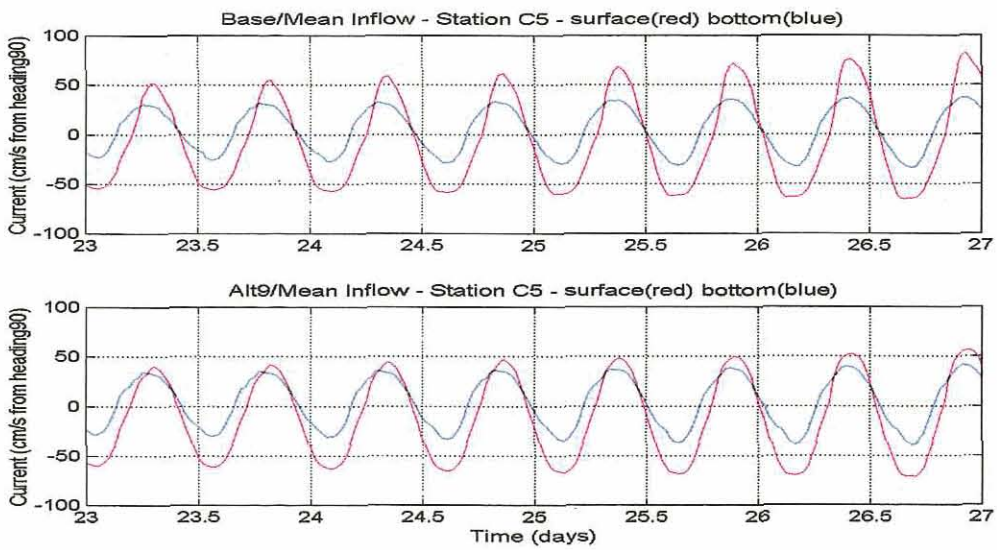

Figure 25. Simulation comparison of tidal current at Station C5, Base Case and Alternative 9; mean tidal range and mean river inflow.

c. Simulation Comparisons: Composite Mapping of Current and Salinity – Spatial distributions of model simulated tidal current and salinity in Hampton Roads are illustrated using computer visualization and color mapping as shown in Appendix A. The plan view maps in Appendix A use vector 'arrows' of varying length to depict the instantaneous speed and direction of the horizontal current and a color scale to depict instantaneous salinity in parts per thousand (ppt). Maps are presented in a 6-panel layout representing, from left to right, Base Case, Alternative 2, and Alternative 9 results. Alternative 1 produced model results indistinquishable from the Base Case at the scales shown and is not included. Currents and salinity for the surface and bottom layers are shown in the top and bottom panels, respectively. The current 'arrows' show the major current pathways during maximum flood and ebb. In general, changes in either the magnitude or direction of the current are small with only a few exceptions noted locally. Attention in these figures also is focused on spatial salinity changes using the added detail that color maps impart.

1. Low River Inflow - Figures A1 through A4 depict elevated salinity ranging between 20 ppt and 30 ppt in overall response to the low river inflow condition. A comparison of the panels in Figure A1 (apogean-neap tides) with those in Figure A2 (perigean-spring tides) shows the typical decrease in **stratification** (higher salinity, higher density water overlain by lower salinity, lower density water) that occurs with a higher tidal range and stronger vertical mixing.

Comparing the Base Case to Alternative 2 during maximum flood, a small salinity difference of about 2-3 ppt is noticeable in a two- to three grid cell area just above the northeast corner of Craney Island (upper and lower middle panels, Figure A1). This reflects a local increase in turbulent mixing in the vicinity of the single tunnel island and bridge 'loop' placed on the west side of the Elizabeth River entrance in Alternative 2 (Figure 4). The effect of local mixing is to reduce local stratification; i.e., to produce a relative increase in salinity in the surface layer and a relative decrease in salinity in the adjoining bottom layer. Comparing the Base Case to Alternative 9, the decrease in stratification is slightly more pronounced over a wider area just to the north of Craney Island, reflecting the increased mixing induced by pilings under the east-west bridges added there (see Figure 5).

Alternative 9 also adds two more tunnel islands immediately west of the existing I-664 tunnel islands and adds more bridge structure in a 'crossover' zone just below the present south tunnel island on I-664 (Figure 5). Figure A1 (upper right panel) displays an anomalous reduction in surface salinity (by about 1-2 ppt) during maximum flood in a narrow strip extending eastward from the Alternate 9 west tunnel islands below Newport News and over the region known as Middle Ground Shoal (Figure 2). This change may be related to local flow diversion caused by the added islands or by frontal activity. Further discussion of the Newport News frontal system is presented in Section III.e.

A further salinity change connected with Alternative 9 appears during maximum ebb in the form of a broad band of increased surface salinities extending east of the 'crossover' zone from I-664 (upper right panel, Figure A3). This increase also is believed to be due to vertical mixing with the added salt coming from the bottom layer near the bridge structure (lower right panel, Figure A3).

2. Mean River Inflow – Overall salinities decrease to the 10 to 20 ppt range in Hampton Roads in the model results for mean river inflow. The mixing effects noted above for Alternatives 2 and 9 along the east-west bridge structure north of Craney Island are still apparent at maximum flood during mean river inflow (Figure A5). However, the anomalous decrease in surface salinity previously described as a narrow band extending over Middle Ground Shoal during maximum flood is not evident. The salinity distributions for maximum ebb show the previously described changes related to mixing within the 'crossover' zone of Alternative 9 (Figure A7).

3. High River Inflow – During high river inflow overall salinity is predicted to range between 5 and 16 ppt within Hampton Roads. At maximum flood, surface and bottom mixing is evident in the region north of Craney Island as noted before (Figure A9). At maximum ebb, mixing is again evident in the region east of the Alternative 9 'crossover' zone (Figure A11).

Organized patterns of spatial change in the current field occurred only in the surface current simulated for Alternative 9 during maximum flood at apogean-neap tide. Tidal range is then near its minimum and vertical stratification is near its maximum. An area of minimum flow and an eddy-like feature appears at these times near the center of the main Newport News Channel. This feature is shown in the center of the upper right panel in Figures A1, A5, and A9 representing each of the three river inflow conditions tested.

d. Simulation Comparisons: Tidal Prism and Residual Current - Specific information is required for certain parts of the lower James River system considered to be problem areas. Problem areas include the Elizabeth River, a **semi-enclosed tidal basin** whose branching waterways have long been adversely affected by industrial and domestic pollutants, causing it to be designated one of three Chesapeake Bay Regions of Concern (ROC) by the Chesapeake Executive Council. Among the kinds of information needed to evaluate the response of a tidal basin system to modifications by structures in or near its entrance region is the change in tidal prism and residual current as simulated through a transect cross-section at the entrance. Transect 1 has been developed for this purpose.

Transect 1 was placed at the entrance to the Elizabeth River where it enables simulation of current flow entering and leaving the Elizabeth River basin normal to the cross-section (Figure B1). There are no other entrances admitting estuarine water and no measurable upstream sources of freshwater inflow are included in the simulation. Among the possible effects that could occur as a result of emplacement of new structure is a change in the **tidal prism**, the volume of water entering or leaving the basin over a half tidal cycle. A reduction in tidal prism implies a reduction in the flushing ability of the basin. Another

measure of importance in terms of dissolved or suspended material transport in and out of the basin is the **residual (non-tidal) current** flowing through its entrance cross-section.

1. Tidal prism – Tidal prism estimates were obtained from time-integrated volumes of model simulated tidal discharge. Time series of tidal discharge (m^3/s) were produced at half-hour intervals as the summed product of current speed (m/s) and cross-sectional area (m^2) calculated by cells (6) and by layers (6) in subsections of Transect 1. The results for the tested cases and conditions are presented in Table 4. Because there are no freshwater sources assigned to the Elizabeth River, model-generated net volumes (Q net) should be zero. Q net, expressed as a percentage of Q mean under the % change column in Table 4, therefore serves as an error estimate on tidal prism calculations. Except for the high inflow condition, the error is less than 3%. The second number given under the % change column compares the tidal prism estimate (Q mean) for each of the alternative test cases against the base case. Except for Alternative 9 under the high inflow condition, the compared values differ by less than 3%. The model simulations therefore provide no measurable evidence of a reduction in tidal prism for the Elizabeth River basin.

Table 4. Discharge volumes (Q), in units of 10^6 m^3, passing through Transect 1.

Base Case	Low Inflow	Percent Change	Mean Inflow	Percent Change	High Inflow	Percent Change
Q flood	18.4949		17.5492		18.1150	
Q ebb	-18.5584		-18.0786		-18.7169	
Q net	-0.0635	-0.34%	-0.5294	-2.97%	-0.6019	-3.27%
Q mean	18.5267	0.00%	17.8139	0.00%	18.4160	0.00%
Alternative 1	Low Inflow		Mean Inflow		High Inflow	
Q flood	18.5073		17.5690		18.1178	
Q ebb	-18.5539		-18.0684		-18.7163	
Q net	-0.0466	-0.25%	-0.4994	-2.80%	-0.5985	-3.25%
Q mean	18.5306	0.02%	17.8187	0.03%	18.4171	0.01%
Alternative 2	Low Inflow		Mean Inflow		High Inflow	
Q flood	18.5690		17.7283		18.2212	
Q ebb	-18.5952		-18.1478		-18.8026	
Q net	-0.0262	-0.14%	-0.4195	-2.34%	-0.5814	-3.14%
Q mean	18.5821	0.30%	17.9381	0.70%	18.5119	0.52%
Alternative 9	Low Inflow		Mean Inflow		High Inflow	
Q flood	18.6588		18.1167		18.7323	
Q ebb	-18.7810		-18.4982		-19.2132	
Q net	-0.1222	-0.65%	-0.3815	-2.08%	-0.4809	-2.53%
Q mean	18.7199	1.04%	18.3075	2.77%	18.9728	3.02%

2. Residual Current – As defined in this report, the residual current is simply the measured or predicted current averaged over a tidal cycle at a fixed point in the water column. A tidal current appearing as simple periodic motion averages to zero so the residual current is sometimes referred to as the non-tidal current; i.e., a steady or quasi-steady flow that is superimposed on the tidal current. It is usually much smaller in magnitude than the tidal current. Classical, two-layer models of estuarine circulation call for residual currents directed seaward at the surface and landward at the bottom, with a layer of zero-net motion in between. In some estuaries, a circular horizontal current or eddy produces a residual current field with speed and direction dependent on horizontal position relative to the center of the eddy. Transport of water-borne materials then becomes more complex than conventional estuarine models would suggest. Recent studies show that high particle concentrations can develop locally within eddy systems through a trapping effect (Hood et al., 1999).

Examples of eddy motion outlined by model-generated residual currents can be seen in plan view in Figures B2 and B3, Appendix B. Figure B2 shows a large eddy system on Hampton Flats that has been recognized for many years. Figure B3 displays a smaller eddy at the mouth of the Elizabeth River that has not, to our knowledge, been previously observed.

Within the Hampton Roads area, a large counter-clockwise eddy appears in the residual surface current at the southwest end of Hampton Flats (Figure B2). Characteristically, eddy development is greatest during apogean-neap tides. Eddy motion is not readily apparent in the bottom layer during any phase of the tide. During perigean-spring tides, the surface eddy becomes weaker and shifts to the east away from Hampton Flats. Comparing the Base Case with Alternative 2, a very slight amount of change can be seen in the Hampton Flats eddy. The change is more apparent, however, in the comparison for Alternative 9. In the latter comparison, the Hampton Flats eddy becomes less organized due to a strengthening of the ebb residual current in the adjacent Newport News Channel. The strengthening of the ebb residual current in the Newport News Channel was also noted in simulated current time series for the Base Case and Alternative 9 (Figure 24).

A clockwise eddy appears at the entrance to the Elizabeth River with a diameter approximately equal to the width of Transect 1 (Figure B3). Noting the strong eastward component of the residual current immediately north of Craney Island during apogean-neap tides, this plan-view display suggests that the eddy is a simple vortex generated in the lee of Craney Island's northeast corner. During perigean-spring tides, the residual current above Craney Island is directed more to the northeast and the surface eddy at the river entrance disappears. Likewise, the structures associated with Alternatives 2 and 9 appear to inhibit the eastward residual current across the top of Craney Island, resulting in a reduction of the eddy motion in the entrance. To examine this process in more detail, plots of the simulated residual current through Transect 1 were developed as described in the following paragraph.

The model's three-dimensional grid divides Transect 1 into 36 rectangles formed by its intersection with six horizontal grid cells and six vertical layers (Figure 26). Currents normal to the transect are obtained at the center of each rectangle. Due to the use of

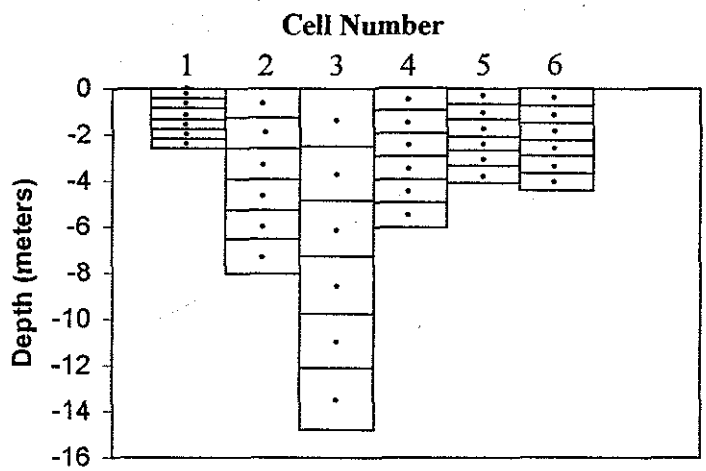

Figure 26. Cross-section, Transect 1, consisting of 6 horizontal cells and 6 vertical layers. Residual currents normal to the cross-section are computed at the center of each layer (view looking upstream).

sigma coordinates, the spatial coordinates of the current array remain fixed relative to the water column (i.e., as a fixed percentage of the time-varying depth) and facilitate the calculation of residual current in the same spatial frame. Using color mapping, the interpolated residual current is displayed across the face of the transect as shown in Figures B4 through B6 in Appendix B. Also included in each figure is the **residual water** (m^3) passing upstream or downstream through the cross-section over a tidal period (12.42 h). Residual water is calculated by multiplying residual current by tidal period and rectangle area for each of the 36 points, then summing according to sign (positive upstream, negative downstream). Similar to the tidal discharge volumes, residual water volumes passing through a cross-section into, or out of, an enclosed basin should be equal after allowing for computational errors. It is the change in these volumes that may warrant concern. Results for each test case under apogean-neap and mean river inflow conditions are discussed below.

Base Case - The base case illustrated in Figure B4 (upper panel) shows a strong and relatively concentrated residual current outflow (color blue) from the Elizabeth River on the shallow west side of the transect (right side of the channel looking upstream). This outflow is matched by inflow elsewhere in the transect with the strongest residual inflow (color red) moving upstream in the bottom layer of the main channel. The residual water volumes average 6.9 $x10^6$ m^3 and differ by approximately 5% of the average.

Alternative 1 – As illustrated in Figure B5 (lower panel), residual currents for Alternative 1 show a nearly identical distribution compared to the Base Case. The residual water volumes are slightly greater for Alternative 1 and again differ by about 5% of the average.

Alternative 2 – Alternative 2 (Figure B6, lower panel) shows a distinct weakening of the outflow (negative residual current) on the west side of Transect 1, with some shifting of the outflow into the mid-depth region of the channel and across to its steep east wall.

Residual water volumes are reduced to an average of about 4.2 x10^6 m^3 or about 39% less compared to the Base Case.

Alternative 9 – Alternative 9 (Figure B7, lower panel) also shows a general weakening and eastward redistribution of the negative residual current on the west side of Transect 1, although the pattern differs slightly from that of Alternative 2. Residual water volumes are reduced to an average of about 4.5 x10^6 m^3 or about 35% less compared to the Base Case.

e. Simulation Comparisons: Position and Form of Newport News Tidal Front – Further evaluation of potential change in the hydrodynamics of the lower James River system is guided by prior knowledge of specific estuarine processes. One process found to be of considerable importance in the lower James is the three-dimensional circulation that exists in association with a **tidal front system** located just below Newport News Point (Figure B8). Described as a tidally-induced salinity front, this system develops during the early flood stage of each tide as higher salinity (higher density) bay water flows westward across Hampton Flats and converges with lower salinity (lower density) river water still ebbing to the southeast in the main channel. Because of the difference in density, bay water is subducted beneath river water at the front and travels upstream in the bottom layer of the channel (Kuo et al., 1988; 1990). This unique mechanism has been associated with enhanced upstream transport and higher rates of larval recruitment of seed oysters in the middle James compared to other estuaries (Ruzecki and Hargis, 1988).

Figure B9 presents a pair of cross-sections for Transect 2 comparing instantaneous current and salinity results for the Base Case and Alternative 9 during early flood for mean inflow and mean tidal range. Alternatives 1 and 2, as expected, show no difference in this region.The distribution of salinity is shown by a color map in Figure B9 and the direction and magnitude of the horizontal current, flowing parallel to the plane of the transect, is indicated by arrows. The computational frame is similar to that shown in Figure 26 except that the instantaneous velocity component parallel to the transect is being shown in lieu of residual velocity normal to the transect. The shallow area shown on the right (northeast) side of the transect is the western edge of Hampton Flats adjoining the main channel.

For the Base Case, the front shown in the upper panel of Figure B9 is located mostly within the middle cell (longest column) representing the deep channel. Its position is indicated both by a salinity change (from 17 ppt to 14 ppt at the surface) and an abrupt change in surface flow direction at points of current convergence. The zone of convergence is not static but moves from east to west as the flood stage advances toward maximum current strength. For Alternative 9, the front shown for the same tidal hour as the other cases (lower panel of Figure B9) remains operative but is displaced to the east, with surface water of 14-15 ppt showing the largest displacement. One half-hour later the front for Alternative 9 appears similar to the other cases, indicating that westward frontal advancement has been delayed relative to these cases, most likely in response to an increase in the ebb residual current.

Additional model runs were made for the low river inflow and high river inflow conditions. The front does not appear as sharply defined under the low inflow condition but is clearly apparent during high inflow. Figures B10 and B11 show the frontal interfaces at successive half-hour intervals as red lines drawn through current convergence points. The results show no substantive change in the position of the tidal front but a slight change of form is noted in the surface layer for Alternative 9 compared to the Base Case. As previously indicated in Section III.b.3, surface currents are modified by Alternative 9.

f. Simulation Comparisons: Longitudinal Salinity Distribution - Transect 3 (Figure B8) was configured to show the longitudinal cross-section of the salinity field following the main channel axis of the James River. This was done to address the question of possible change of the limit of salt intrusion, upstream or downstream, as a result of construction in Alternatives 1, 2, or 9. In performing model comparison tests for this purpose, extremes in river inflow assume primary importance and temporal salinity variations are commonly examined at intervals longer than a tidal period. Field observations of the longitudinal variation in salinity and other water properties in estuaries have traditionally been done during slack water periods (slack before ebb or slack before flood). We follow the same convention in our model comparisons.

Figure B12 shows the instantaneous salinity distribution at **slack before ebb** in cross sections extending from the mouth of the James to a point 30 km upstream. For the low inflow condition, salinities are predicted to vary from 26-30 ppt at the mouth to 20-22 ppt at the upstream limit of the transect. During high inflow conditions, the salinity limits are predicted to range from 20-22 ppt at the mouth to 5 ppt or less upstream. Very little change is noted for any of the alternatives with the possible exception of Alternative 9 during high inflow. Fixing the limit of salt intrusion at 10-12 ppt, it is noted that this limit in the bottom water moves approximately 2 km downstream in response to Alternative 9. No other change is apparent from these tests.

Figure B13 shows the instantaneous salinity distribution at **slack before flood** in cross sections extending from the mouth of the James to a point 30 km upstream. Coming at the end of an ebb, the overall salinity field is displaced seaward, as expected, compared to slack before ebb. Again, among the transects shown, only those of Alternative 9 exhibit any degree of apparent change. During high inflow, the Alternative 9 transect shows a thicker surface layer of brackish to fresh water (5 ppt or less) in the zone extending from 11 to 18 km from the mouth of the James. No other change is apparent from these tests.

g: Simulation Comparisons: Sedimentation – For the effect on sedimentation, we adopted two approaches: (1) the study of sedimentation potential and (2) the tracking of sediments released from upstream into the system. Sedimentation potential was determined by the percentage of time during which bottom stress falls below critical bottom stress. We chose 1.0 pascal as the critical stress, a value observed by Maa et al. (1995) for Chesapeake Bay sediments. Nichols (1972) presented data showing the location of a turbidity maximum upstream of the study area. We simulated the fate of suspended sediment from a hypothetical source based on his data. We selected 3 size

classes with different settling velocities—very fine sand (w_{sf}~ 1.0 cm/s), coarse silt (w_{sf}~ 0.1 cm/s), and medium silt (w_{sf}~ 0.01 cm/s). Initially no bottom sediment in the system was assumed. For each size class, sediments were released for 2 tidal cycles from the surface along the James River Bridge at the rate of 2 kg/s. After 67 tidal cycle runs, total bottom sediment accumulation amounts (kg/m^2) were determined in each cell.

1.Sedimentation potential – Figure C1 shows existing data for bottom sediments in the James River (Nichols et al., 1991), depicting coarser sandy bottom sediments in the channel and northern flank in Hampton Flats and finer muddy bottom sediments in the southern flank near Craney Island. Figure C2 shows the calculated sedimentation potential for the Base Case. As can be seen, its distribution is consistent with coarser sediments along the northern flank and finer sediments along the southern flank of the lower James. This again suggests the sedimentation potential is a reasonable proxy for bottom sediment distribution. In addition, pier effects reported by Fang et al. (1972) in a previous physical model study evidence decreased sedimentation potential in the zone surrounding the existing I-664 bridge pilings north of Portsmouth. This is born out in figure C2.

The results for both Alternative 1 and Alternative 2 show little change except in three limited areas. Areas showing a slight increase in sedimentation potential include the northeast corner of Hampton Flats (Alternative 1) and the northeast end of Craney Island Flats, a shoal northeast of Craney Island (Alternative 2). Decreased sedimentation potential occurs in a limited zone surrounding the tunnel island west of the Elizabeth River entrance (Alternative 2). Runs for Alternative 9 illustrate a more definitive decrease in sedimentation potential along the immediate route for the bridge pilings north of Craney Island (Figure C3). Runs for Alternative 9 also forecast a broad decrease in deposition potential within the Elizabeth River entrance. Changing freshwater inflow conditions produced similar results with sedimentation potential further increasing at the northeast corner of Craney Island Flats during high river inflow (Figure C4 and Figure C5).

2. Tracking sediment released from upstream – Figure C6 shows the grain size effect on particle settling velocity. Coarser sediments (very fine sand in this study) were deposited almost immediately in the area of release (the line source coinciding with the James River Bridge). Coarse silt also did not penetrate very far toward the region of interest. Thus, we chose to use medium silt in our study of the proposed construction effects. For the mean freshwater inflow condition, there is little change in the sedimentation pattern except for a limited area of increased sedimentation of medium silt in the Northeast corner of Hampton Flats for Alternatives 1 and 2 (Figure C7). For Alternative 9, increased deposition of medium silt was observed along the bridge pilings north of Craney Island.

Little change was noted for the condition of low river inflow compared to mean river inflow (Figure C8). High river inflow, however, produced more dramatic results. A higher level of particle settling is indicated throughout Hampton Roads in runs with high freshwater inflow (Figure C9). Events of this type would seem to influence sedimentation

from an upstream source to a much greater degree than any one of the three alternatives tested.

IV. Summary and Conclusions

A three-dimensional hydrodynamic and sedimentation model, HYSED-3D, was used to simulate the tide, current, and salinity fields of the James River in Virginia. In addition to these physical properties, the model also was used to simulate sedimentation in the lower James River as part of a study to assess the environmental effects of bridge-tunnel construction in a planned crossing of Hampton Roads. The design infrastructure for three separate highway crossings, designated as Alternatives 1, 2, and 9, was tested using a fine-scale computational grid representing the existing waterways of the lower James River and the Elizabeth River, a tributary basin located just inside the entrance to the James River. The model was required to simulate the full range of hydrodynamic and hydrologic conditions expected for the prototype system, including tides of maximum and minimum range as well as extremes in freshwater inflow expected for the headwaters of the James River. In each test, model-simulated properties were compared between the existing highway crossing structure (Base Case) and that of either Alternative 1, 2, or 9 (simulation comparisons). The results were analyzed to determine the response to the design structures added to the Base Case under the test conditions specified. Several points may be made in conclusion:

1. Tidal Heights - No discernable change in simulated tidal heights was noted at any of the nine tide stations selected for comparison of the Base Case with Alternatives 1, 2 and 9 (Figures 16 and 17; Table 3). None of the comparisons evidenced any structure-induced change in tidal height related to variations in tidal range or river inflow. Changes in the times and heights of high and low water were consistently less than the expected accuracy limits of the model (5–10 minutes and 3-4 cm, respectively).

2. Tidal Currents - Changes in tidal current time histories were apparent at four of the seven current stations selected for comparisons in Hampton Roads (Figure 18). Station C1 at the entrance to the James River evidenced a slight difference in simulated currents for the Base Case and Alternatives 1 and 2 for most combinations of tidal range and river inflow. This change was manifest only in the form of the surface current curve with no discernable difference in either the time or speed of the flood and ebb current maxima (Figures 19 and 20). Station C2 at the entrance to the Elizabeth River demonstrated a more noticeable change in the surface current time histories for Alternatives 2 and 9 during all nine combinations of tidal range and river inflow. In addition to changes in curve form (sharper peaks; e.g., Figure 21), there are small differences in the strength of the current maxima (stronger flood and weaker ebb; e.g., Figures 22 and 23) . Such differences suggest a residual current when the duration of flood and ebb are approximately equal as they are in these figures. Bottom currents at Station C2 were weaker and more variable than surface current. Although they suggest a change for Alternatives 2 and 9, they are more difficult to characterize in terms of a consistent and recognizable pattern of change.

Surface currents at Stations C3 (Newport News Channel) and C5 (Newport News Point) show distinct changes in current maxima when comparing Alternative 9 to the Base Case. Bottom currents appear unaffected at either station. From Figure 24, under the mean tidal range and mean river inflow conditions, it is apparent that the surface current at Station C3 possesses an ebb residual which is strengthened by Alternative 9 while the current range (gross difference in current extremes) remains constant. At Station C5 near the Newport News tunnel islands required for Alternative 9, the current range at mean tide (120 cm/s) decreases by approximately 12 cm/s (10%) while the ebb current residual again increases by a slight amount (Figure 25). These observations suggest a change in the direction of the surface current or a current divergence at Station C5 which would produce a reduction in current range in the direction aligned with the channel axis. Changes at Station C3 consist of a change in the residual current only.

Spatial change in instantaneous surface and bottom currents (shown in plan view in Appendix A) is quite small and limited to a few highly local changes in current speed and/or direction (e.g., in the vicinity of the bridge tunnels for Alternative 9). The only organized change in flow patterns noted was limited to a small, eddy-like feature appearing in the surface current near the Newport News Channel in response to Alternative 9. This feature was apparent only during maximum flood and apogean-neap tide (e.g., Figure A9, upper-right panel). It is not unusual to see organized fields of motion (eddies) developing in the residual current over Hampton Flats during times of maximum stratification.

3. Tidal Prism, Residual Current – Determination of the tidal prism (volume of flood or ebb flow entering or leaving an enclosed region) was deemed important for the Elizabeth River, a tidal basin with only a single seaward entrance and no significant freshwater inflow. A reduction in tidal prism is normally associated with a reduction in the flushing ability of a tidal basin. Simulation comparisons of the flow through Transect 1 (Table 4) showed no evidence of a reduction in tidal prism for the Elizabeth River under any of the conditions tested.

The observation of a change in the current history at Station C2 underscored the necessity of examining the residual current and its possible influence on circulation within the entrance and perhaps other parts of the Elizabeth River. Residual currents associated with horizontal eddy systems have the potential to lower flushing rates and impede particle movement by a convergence or 'trapping' effect (Hood et al., 1999). For this reason the model-simulated residual currents were examined in plan and profile view and the residual water volumes passing through Transect 1 at the Elizabeth River entrance were calculated. The model results indicate that eddy motion decreases and residual water volumes passing through the transect are reduced as a result of Alternatives 2 and 9. This happens primarily during apogean-neap tides when eddy development is most pronounced. This finding suggests that residual circulation may be affected, at least within the Elizabeth River entrance region. Model grid resolution presently is not adequate to provide definitive answers on circulation throughout the interior region. Apart from further modeling studies specific to the Elizabeth River, detailed

measurements of the actual residual current in the field are needed to verify the simulation results.

4. Salinity – Changes in salinity observed through the test simulations conducted in this study were primarily limited to regions with measurable salinity stratification and enhanced vertical mixing as occurs in the vicinity of bridge pilings such as those specified for Alternatives 2 and 9. As expected, surface salinities increased and bottom salinities decreased in these regions as a result of turbulence-induced vertical mixing. The mixing is most intense during perigean-spring tides and least intense during apogean-neap tides.

Near Newport News Point, surface water from upstream areas of the James generally encounters saltier water entering from Chesapeake Bay and may override it in frontal systems. Some variation in the position of the frontal interface and the distribution of low salinity surface water is predicted as a result of Alternative 9 (e.g., Figure A7). Little change is expected, however, in the salinity field at depth. Simulated salinity profiles along Transect 3 (Figures B11 and B12) suggest little or no longitudinal change in the limit of salt intrusion in the James River as a result of any of the alternatives tested. Of course the longitudinal salinity distribution undergoes considerable change after a change in any of the three river inflow conditions and this effect greatly outweights that of any other condition tested.

5. Sedimentation – A previous investigation on the effects of I-664 construction relative to sedimentation in the Lower James River predicted only minor changes except for a possible reduction in shoaling within the Newport News Channel (Heltzel, 1988). The present investigation has little to add in terms of expected changes in sedimentation, or sedimentation potential, as a result of any of the alternatives examined. In response to Alternative 1, a minor increase in sedimentation potential was noted near shore at the northeast end of Hampton Flats. For Alternatives 2 and 9, a decrease in sedimentation potential is indicated in the vicinity of bridge structures north of Craney Island due to increased bottom tubulence. The HYSED-3D model generally predicts that areas of high sedimentation potential are located predominately along the south shore of the James with very little sedimentation potential along the north shore. This result is consistent with the observed grain size characteristics of the bottom sediments (Nichols et al., 1991). The sediments are consistently finer grained along the south shore and within the Elizabeth River entrance.

Simulated release of tagged (labeled) sediment particles with characteristic grain sizes and settling velocities indicate that only medium silt (15.6 – 31.3 μm) and finer grained sediment has the capability of reaching the lower James from known source regions upstream under mean freshwater inflow conditions. However, considerably more of this sediment and some coarser-grained material as well can be expected to reach the lower James during the tested condition of high river inflow. The change that occurs between extremes in the river inflow condition strongly outweighs the change due to structures added for any of the alternatives.

V. References

Blumberg, A. F., B. Galperin, and D. J. O'Connor, 1992. Modeling vertical structure of open channel flows. *Journal of Hydraulic Engineering,* 118: 1119-1134.

Blumberg, A. F. and G.M. Mellor, 1987. A description of a three-dimensional coastal ocean circulation model, p.1-19. In N.S. Heaps (ed.), *Three-Dimensional Coastal Ocean Models,* Coastal and Estuarine Science, American Geophysical Union.

Fang, C.S., B.J. Neilson, A.Y. Kuo, R.J. Byrne, and C.S. Welch, 1972. Physical and geological studies of the proposed bridge-tunnel crossing of Hampton Roads near Craney Island. *Special Report in Applied Marine Science and Ocean Engineering No.24,* Virginia Institute of Marine Science, Gloucester Point, VA, pp.199-241.

Galperin, B., L. H. Kantha, D. Hassid, and A. Rosati, 1988. A quasi-equilibrium turbulent energy model for geophysical flows. *Journal of Atmospheric Science,* 45: 55-62.

Hamrick, J. M., 1996. User's manual for the environmental fluid dynamics computer code. *Special Report in Applied Marine Science and Ocean Engineering No. 331,* Virginia Institute of Marine Science, Gloucester Point, VA, 223p.

Heltzel, S. B., 1988. I-664 bridge-tunnel study, Virginia sedimentation and circulation investigation. *Technical Report HL-88-25,* U.S. Army Corps of Engineers, Waterways Experiment Station, Vicksburg, MS. 40p.

Hood, R.R., H.V. Wang, J.E. Purcell, E.D. Houde, and L.W. Harding, 1999. Modeling particles and pelagic organisms in Chesapeake Bay: convergent features control plankton distributions. *Journal of Geophysical Research,* 104:1223-1243.

Johnson, B.H., K.W. Kim, R.E. Heath, B.B. Hsieh, and H.L. Butler, 1993. Validation of a three-dimensional hydrodynamic model of Chesapeake Bay. *Journal of Hydraulic Engineering,* 119: 2-20.

Kuo, A. Y., R. J. Byrne, J. M. Brubaker, and J. H. Posenau, 1988. Vertical transport across an estuary front, pp.93-109. In J. Dronkers and W. van Leussen (eds.), *Physical Processes in Estuaries.* Springer-Verlag, Berlin.

Kuo, A. Y., R. J. Byrne, P. V. Hyer, E. P. Ruzecki, and J. M. Brubaker, 1990. Practical application of theory for tidal-intrusion fronts. *Journal of Waterway, Port, Coastal, and Ocean Engineering* 116(3): 341-361.

Maa, J. P.-Y., C.-H. Lee, F.J. Chen, 1995. VIMS Sea Carousel: Bed Shear Stress Measurements. *Marine Geology,* 129 : 129-136.

Nichols, M.N., 1972. Sediments of the James River Estuary, Virginia. *Geological Society of America Memoir 133, Environmental Framework of Coastal Plain Estuaries*, pp. 169-212.

Nichols, M.N., S.C. Kim, and C.M. Brouwer, 1991. Sediment Characterization of the Chesapeake Bay and its Tributaries, Virginian Province. *NOAA National Estuarine Inventory: Supplement*. VIMS contract report, 83p.

Ruzecki, E. P., and W. J. Hargis, Jr., 1988. Interaction between circulation of the estuary of the James River and transport of oyster larvae , p. 255-278. In B. J. Neilson, A. Y. Kuo, and J. M. Brubaker (eds.), *Estuarine Circulation*. The Humana Press, Clifton, N. J.

Sisson, G. M., J. Shen, A.Y. Kuo, J. D. Boon, S.C. Kim, and W. T. Stockhausen, 1997. VIMS three-dimensional hydrodynamic-eutrophication model (HEM-3D): Application of the hydrodynamic model to the York River system. *Special Report in Applied Marine Science and Ocean Engineering No. 327*, Virginia Institute of Marine Science, Gloucester Point, VA, 64p, Appendices.

APPENDIX A

Surface and Bottom Distributions of Current and Salinity during Maximum Flood and Maximum Ebb

Shown in Plan View, Hampton Roads, VA

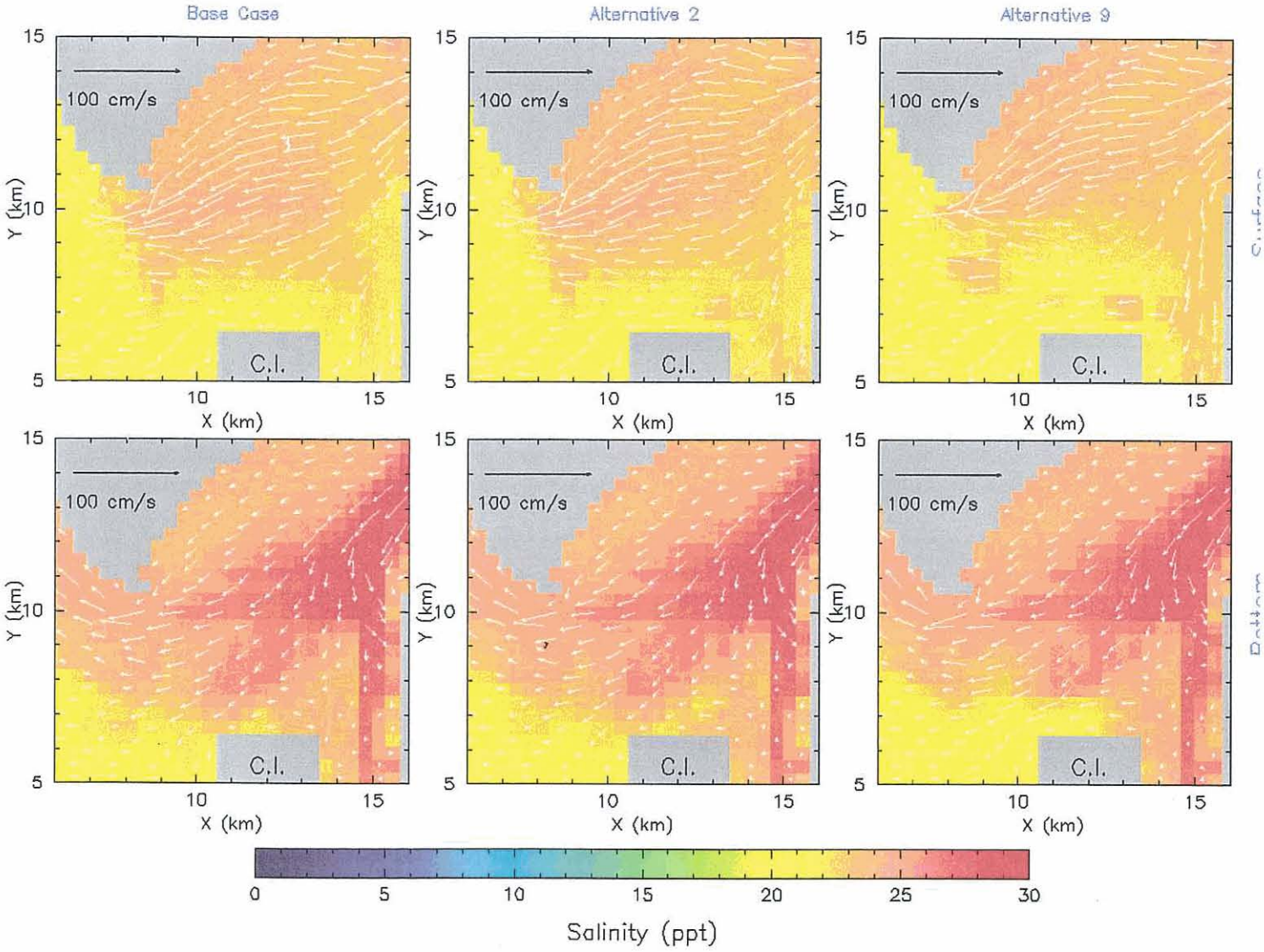

Figure A1. Current and salinity during **maximum flood**, apogean-neap tide, low river inflow.

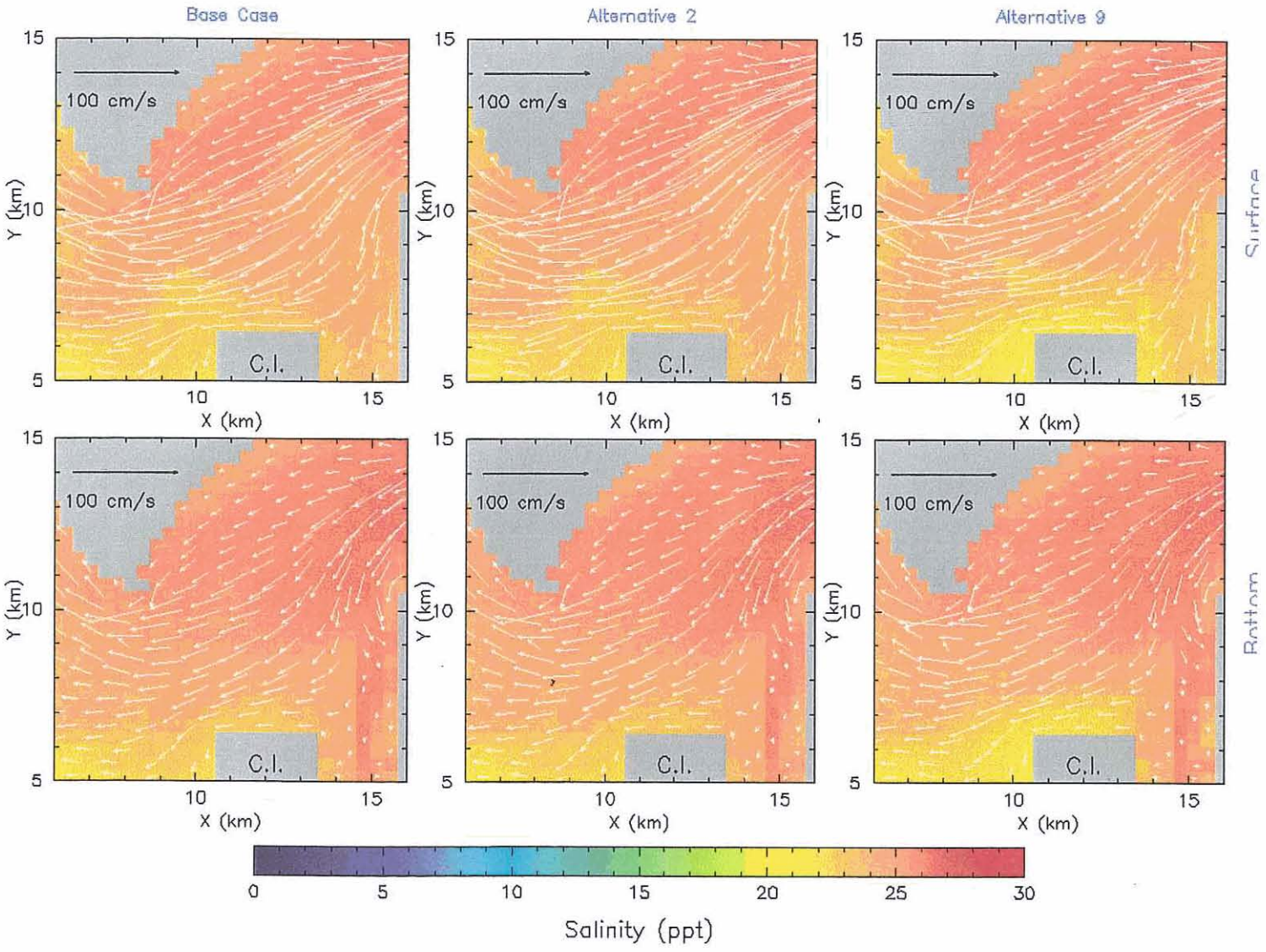

Figure A2. Current and salinity during **maximum flood**, perigean-spring tide, low river inflow.

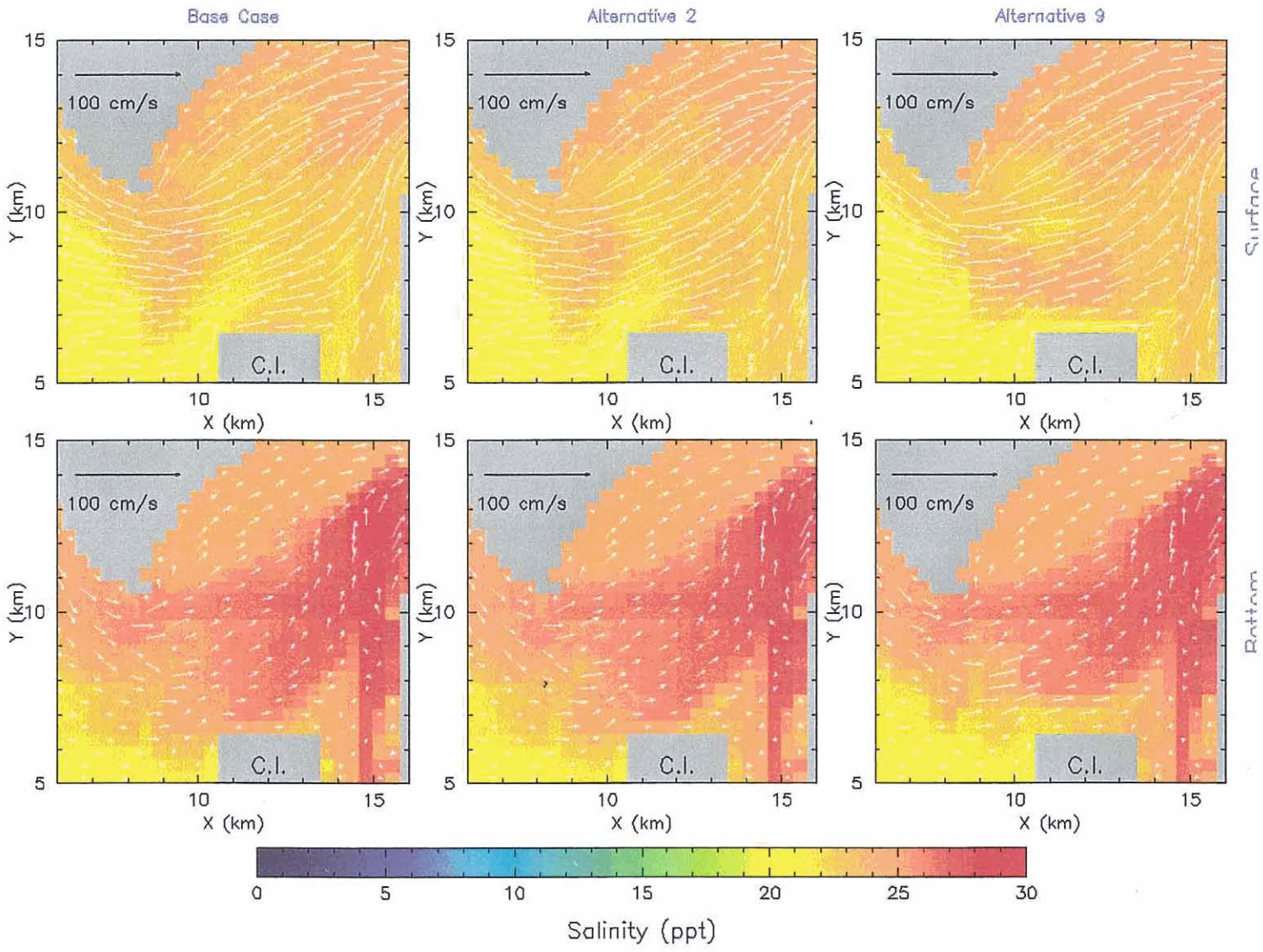

Figure A3. Current and salinity during **maximum ebb**, apogean-neap tide, low river inflow.

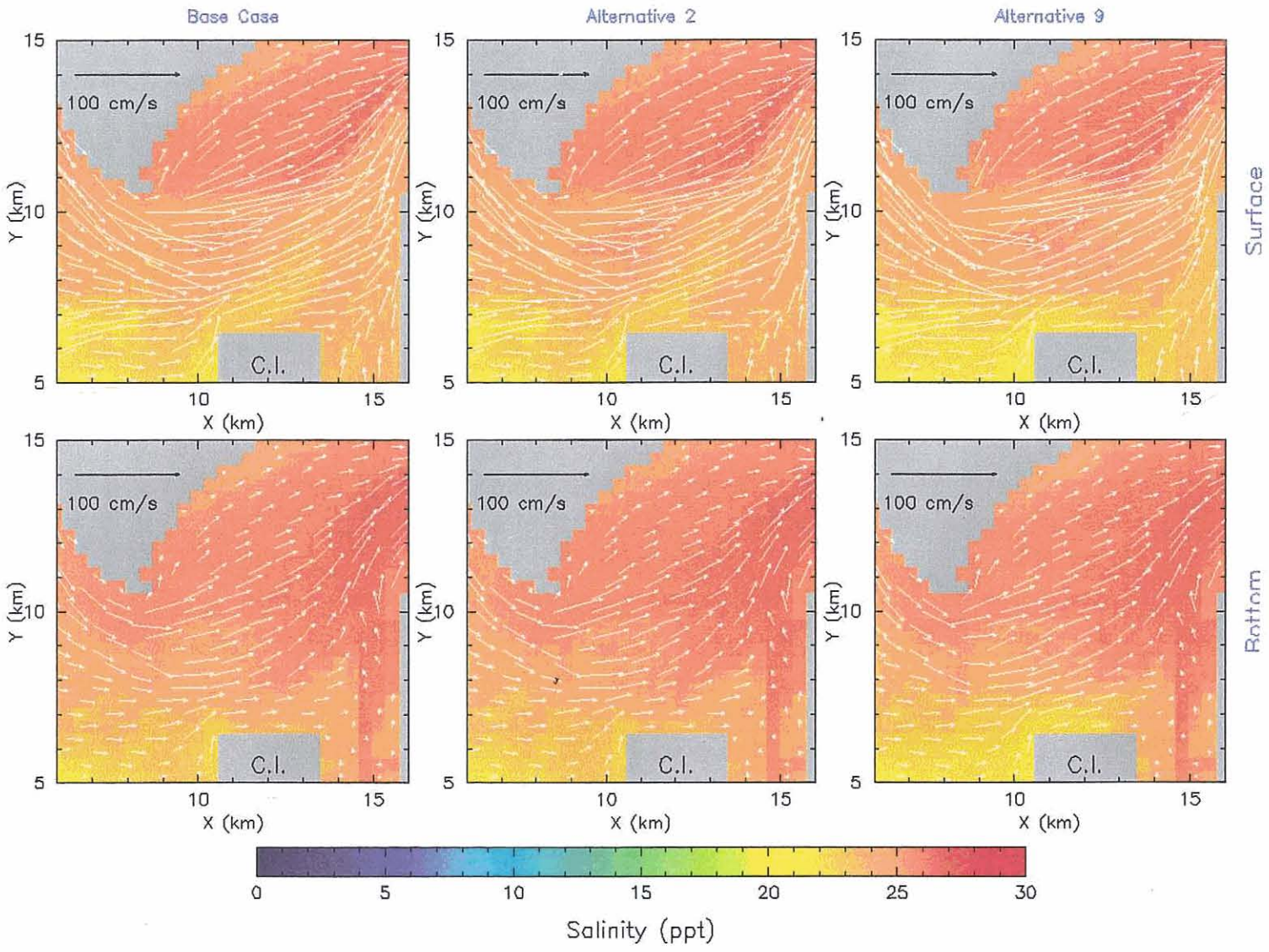

Figure A4. Current and salinity during **maximum ebb**, perigean-spring tide, low river inflow.

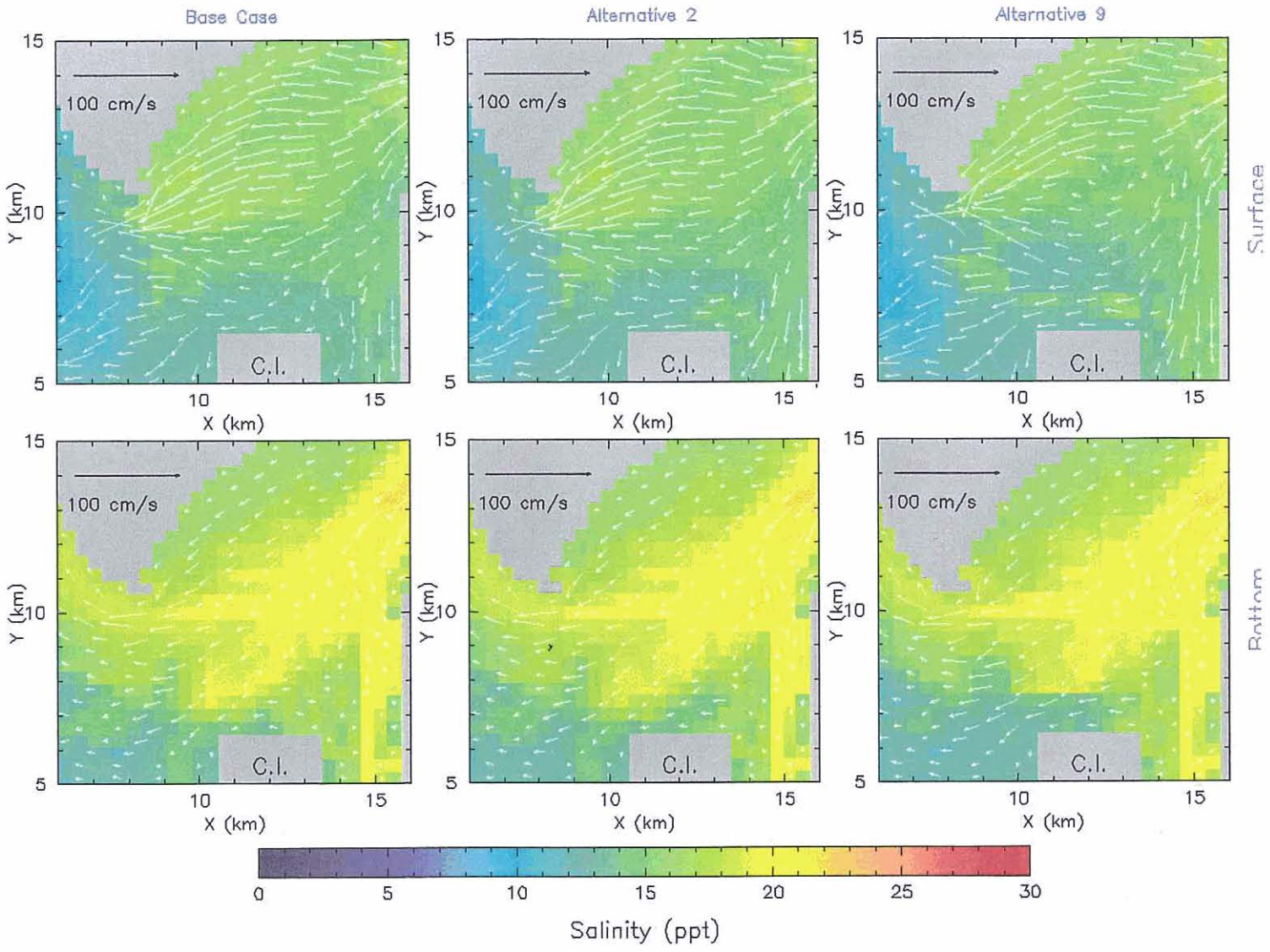

Figure A5. Current and salinity during **maximum flood**, apogean-neap tide, mean river inflow.

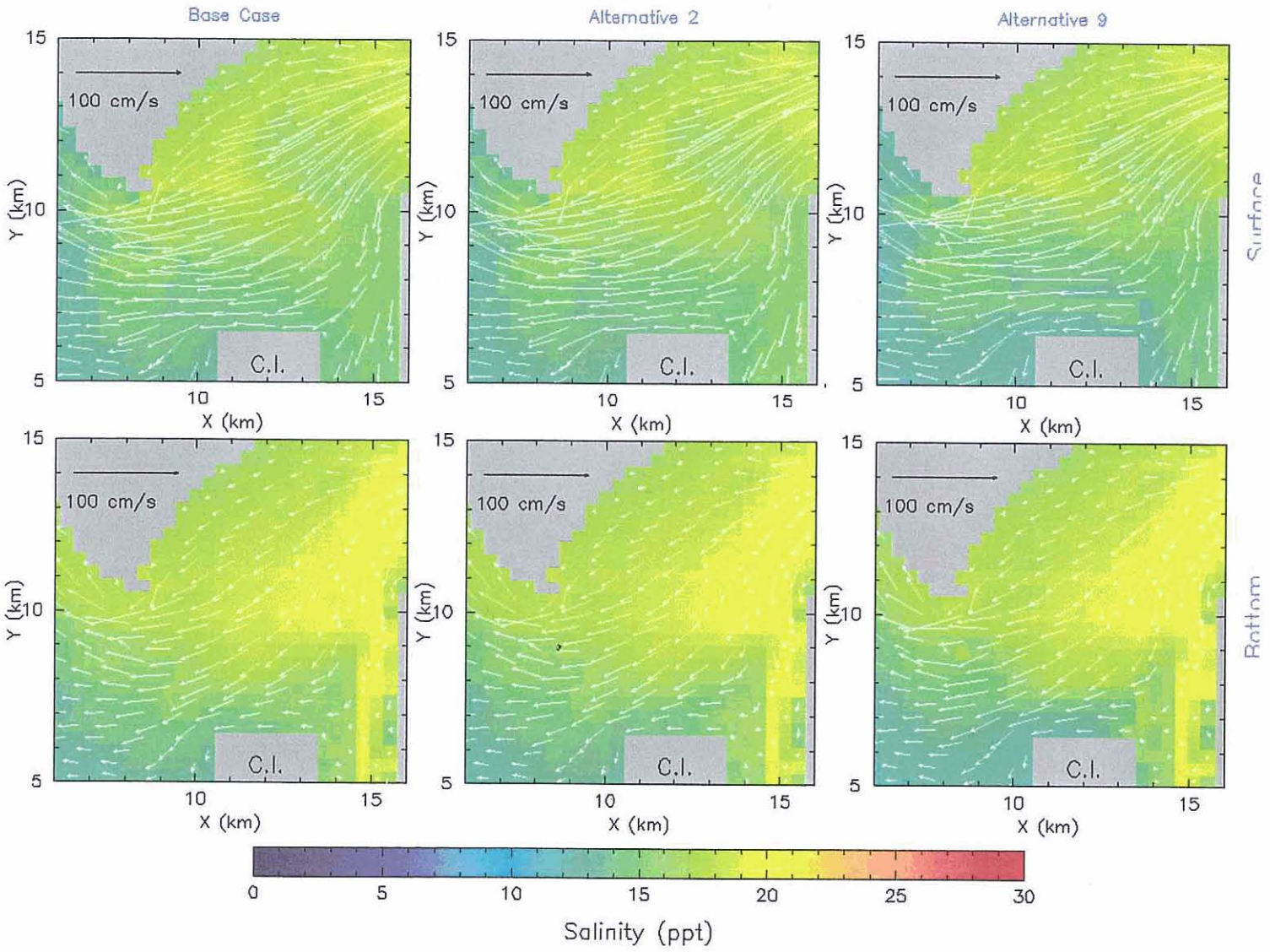

Figure A6. Current and salinity during **maximum flood**, perigean-spring tide, mean river inflow.

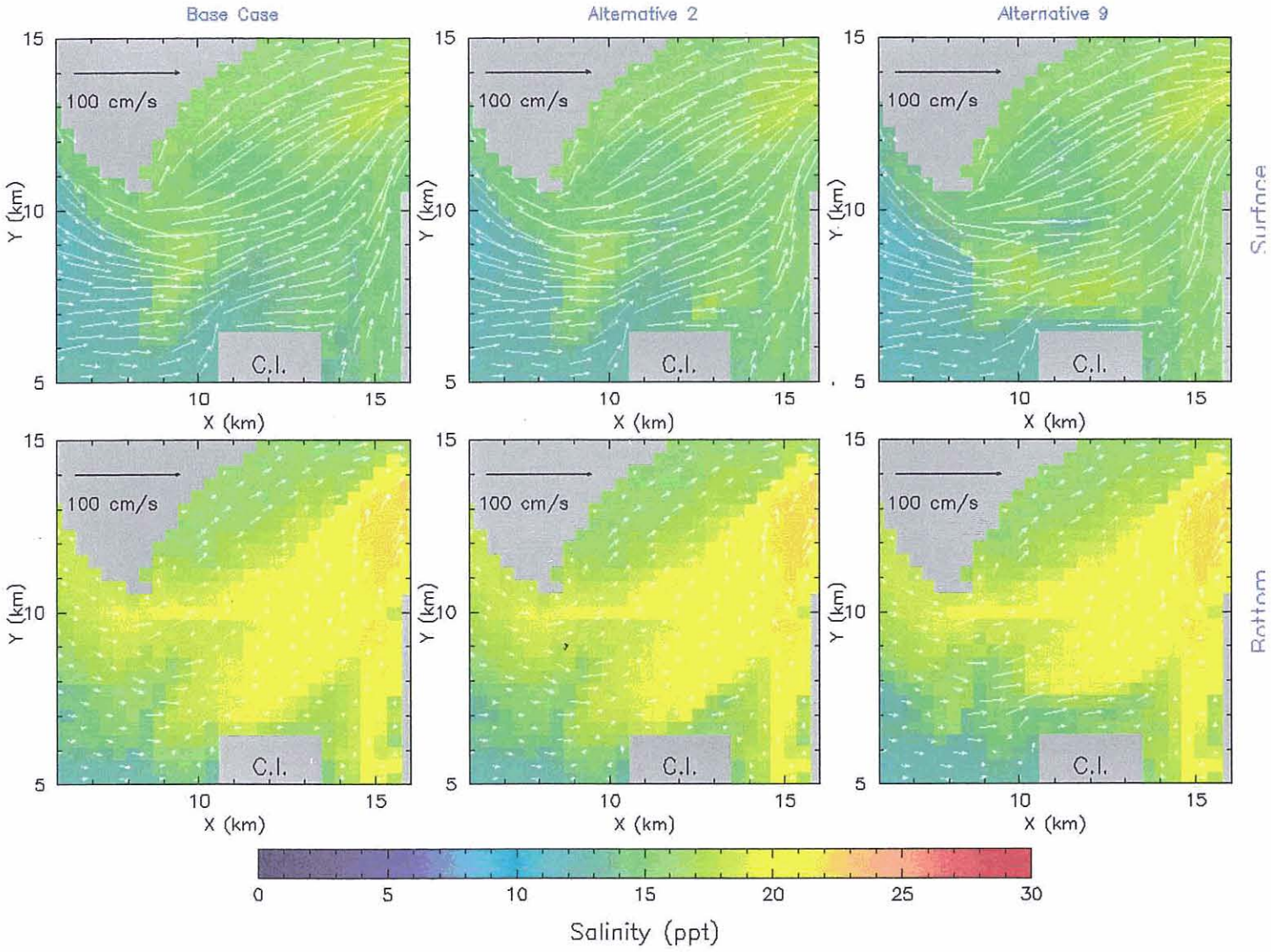

Figure A7. Current and salinity during **maximum ebb**, apogean-neap tide, mean river inflow.

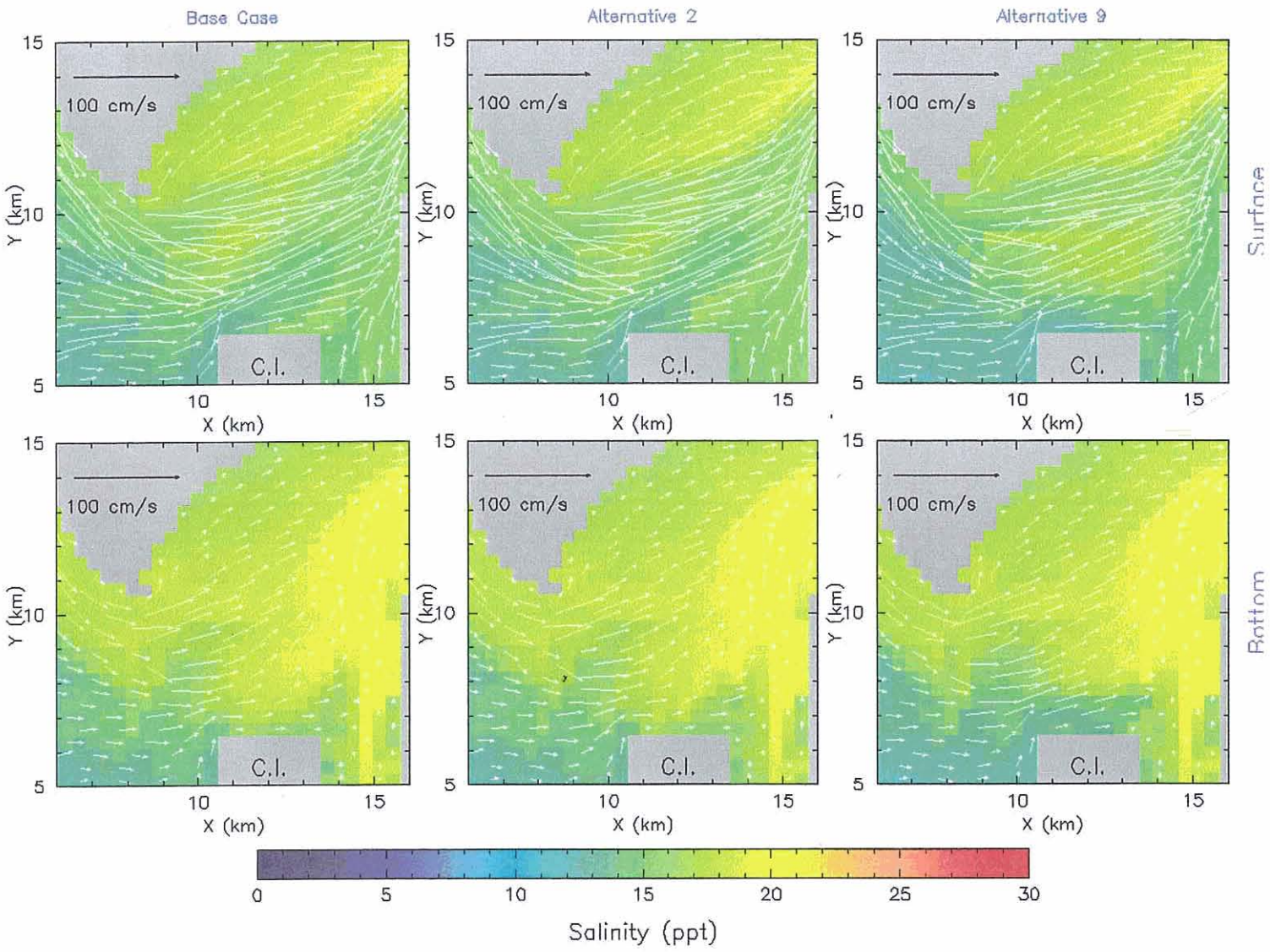

Figure A8. Current and salinity during **maximum ebb**, perigean-spring tide, mean river inflow.

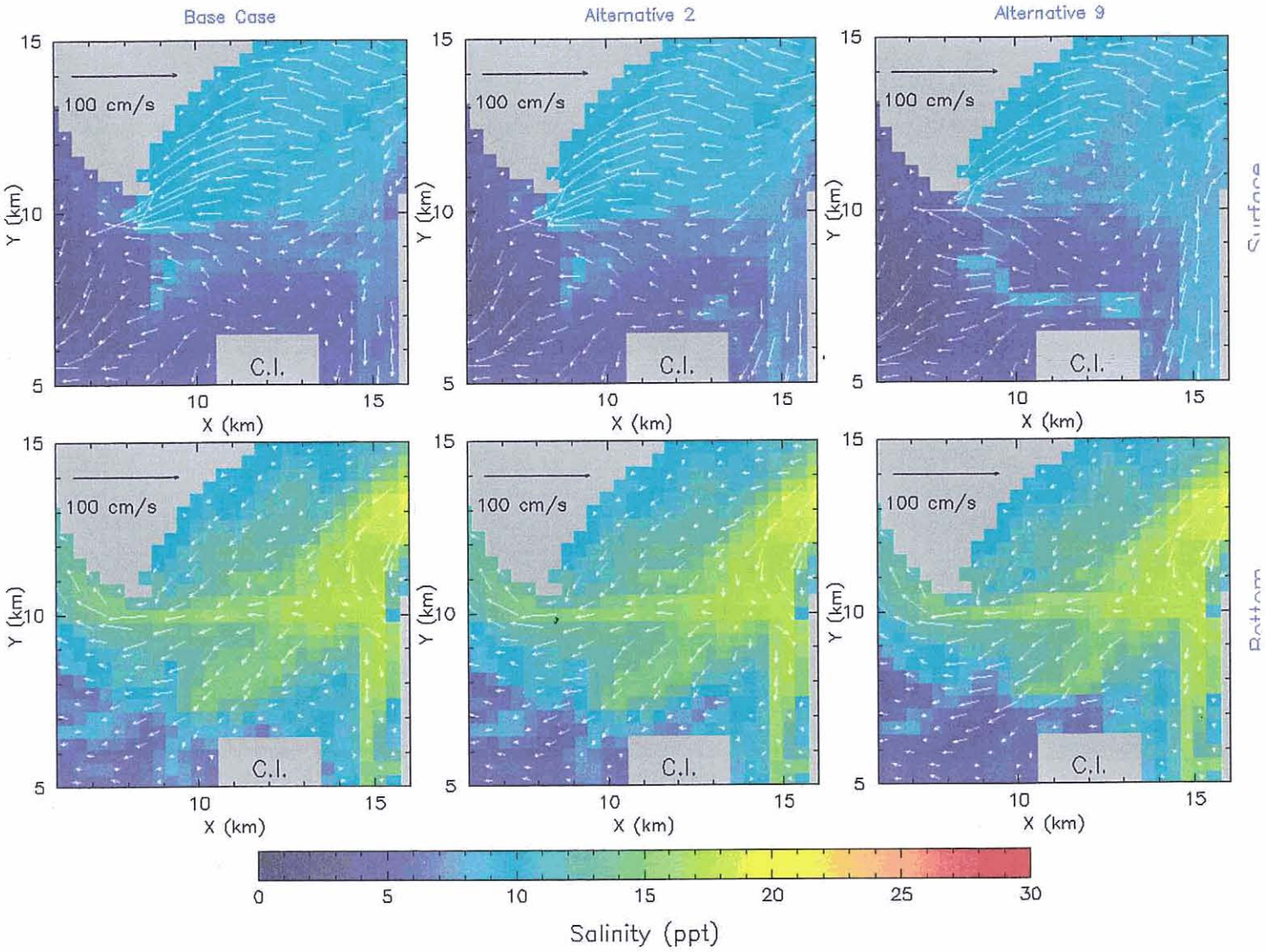

Figure A9. Current and salinity during **maximum flood**, apogean-neap tide, high river inflow.

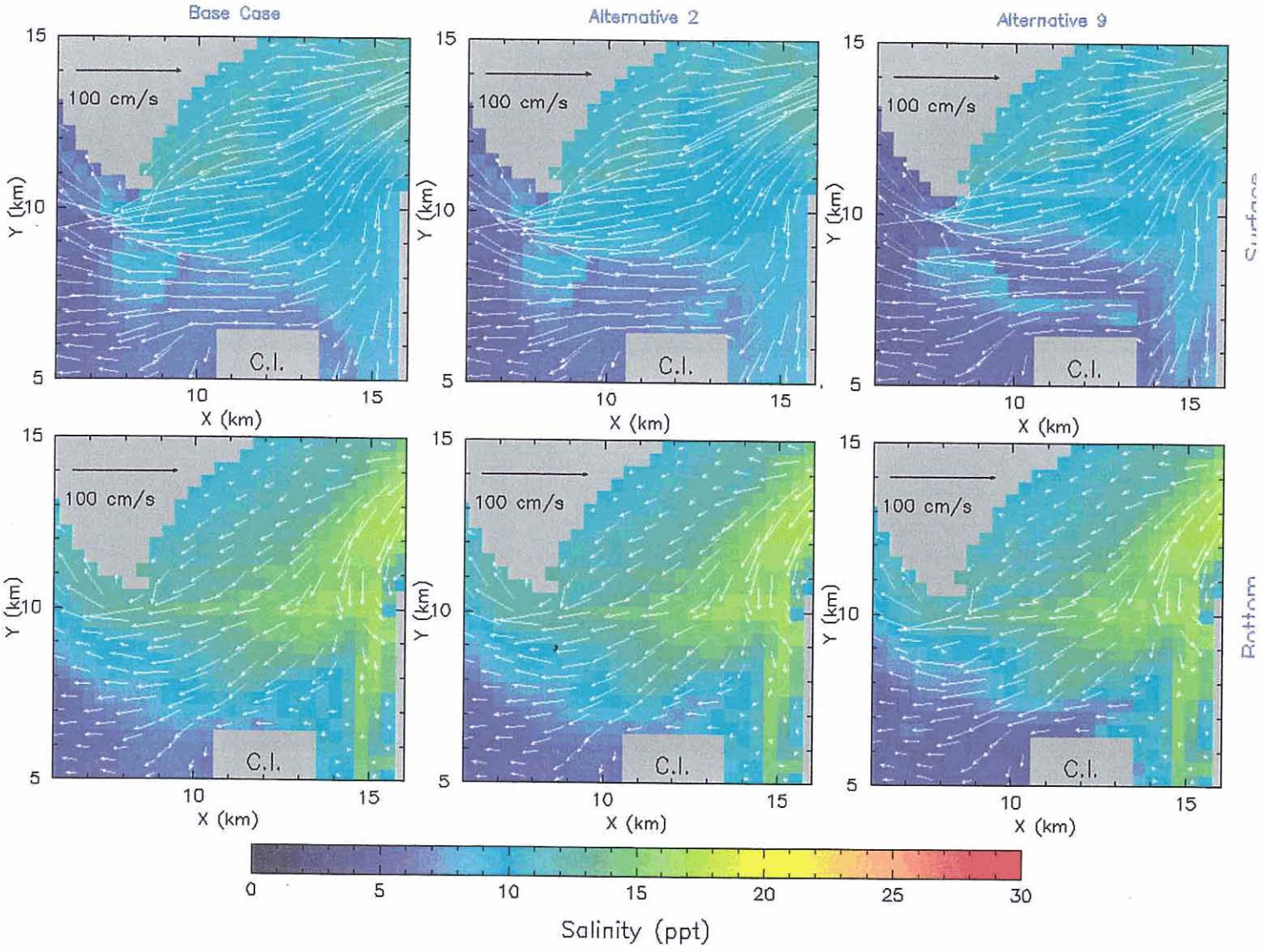

Figure A10. Current and salinity during **maximum flood**, perigean-spring tide, high river inflow.

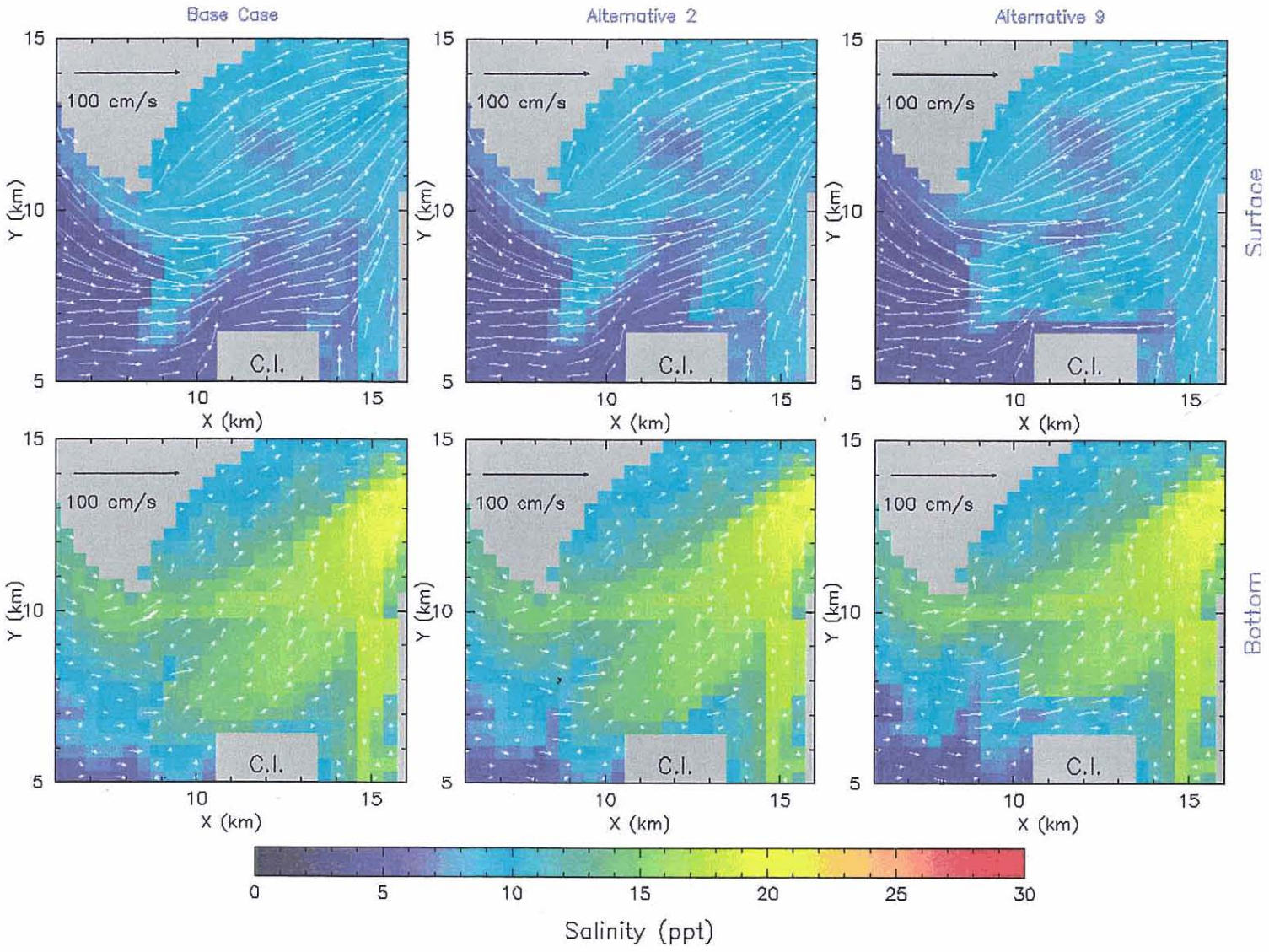

Figure A11. Current and salinity during **maximum ebb**, apogean-neap tide, high river inflow.

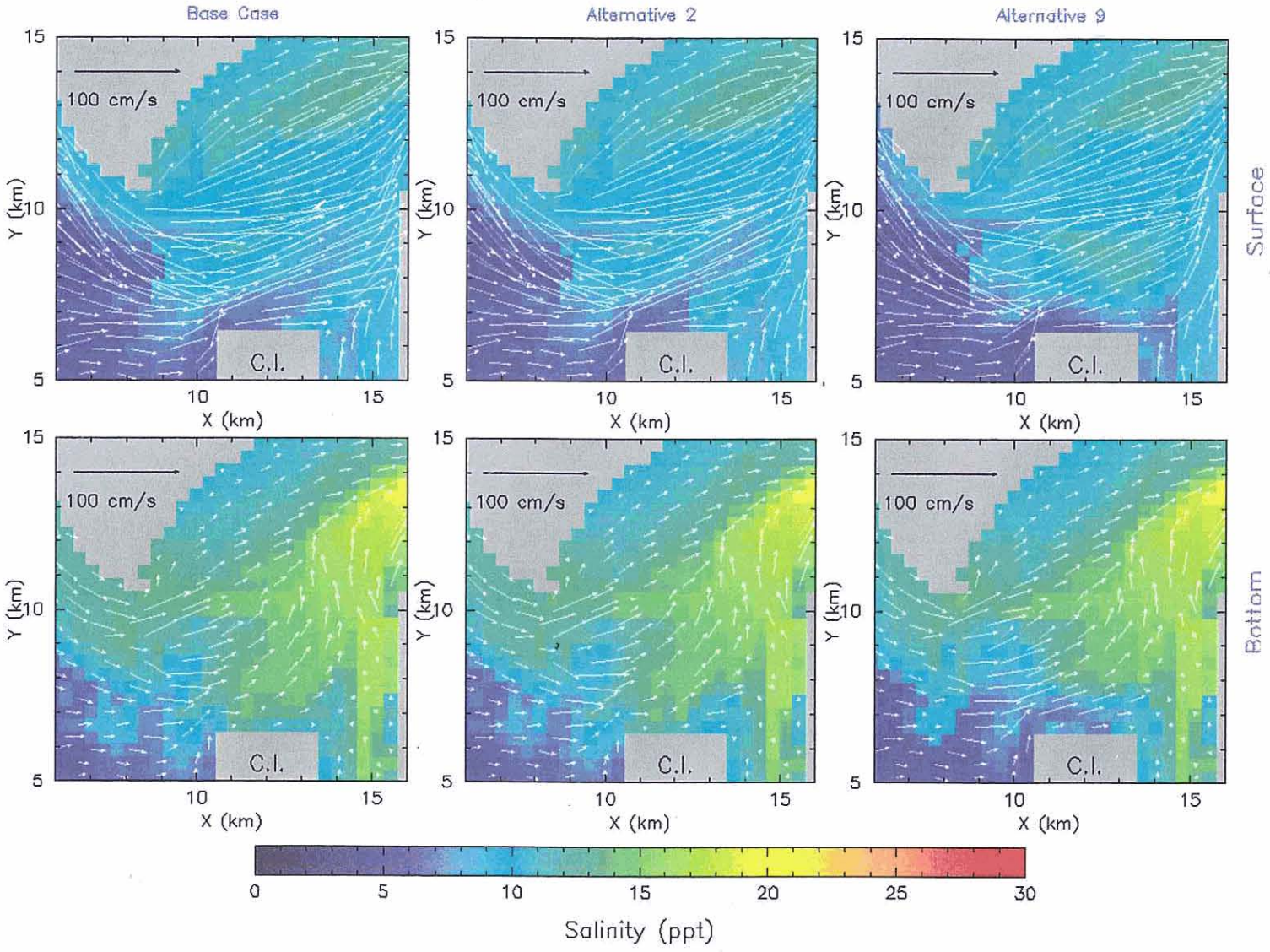

Figure A12. Current and salinity during **maximum ebb**, perigean-spring tide, high river inflow.

APPENDIX B

Non-Tidal (Residual) Currents
Position of Tidal Front

Shown in Selected Areas and Transects, Hampton Roads, VA

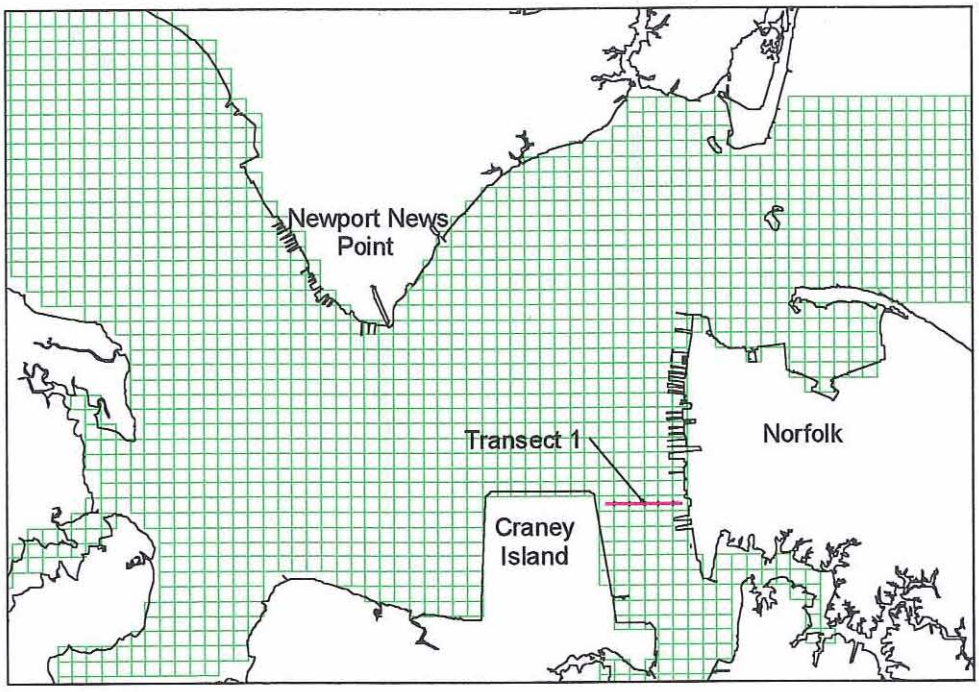

Figure B1. Map showing location of Transect 1, Hampton Roads, VA.

Note concerning model Transect 1 and surrounding area

Transect 1 is a vertical cross-section at the entrance to the Elizabeth River at the position shown above. In addition to facilitating the computation of net tidal transport and tidal prism estimates for the Elizabeth River basin, its purpose is to display the component of the model predicted residual (tidally-averaged) current flowing south (north) through the cross-section and into (out of) the basin. The residual current often appears as an "eddy" or circular current and is important as a mechanism affecting the net transport of sediments and other water-borne materials moving through an estuary. Eddy motion is apparent in the following figures which show the model predicted residual current field first in plan view (Hampton Roads, Elizabeth River entrance) and then in cross-section (Elizabeth River entrance, Transect 1).

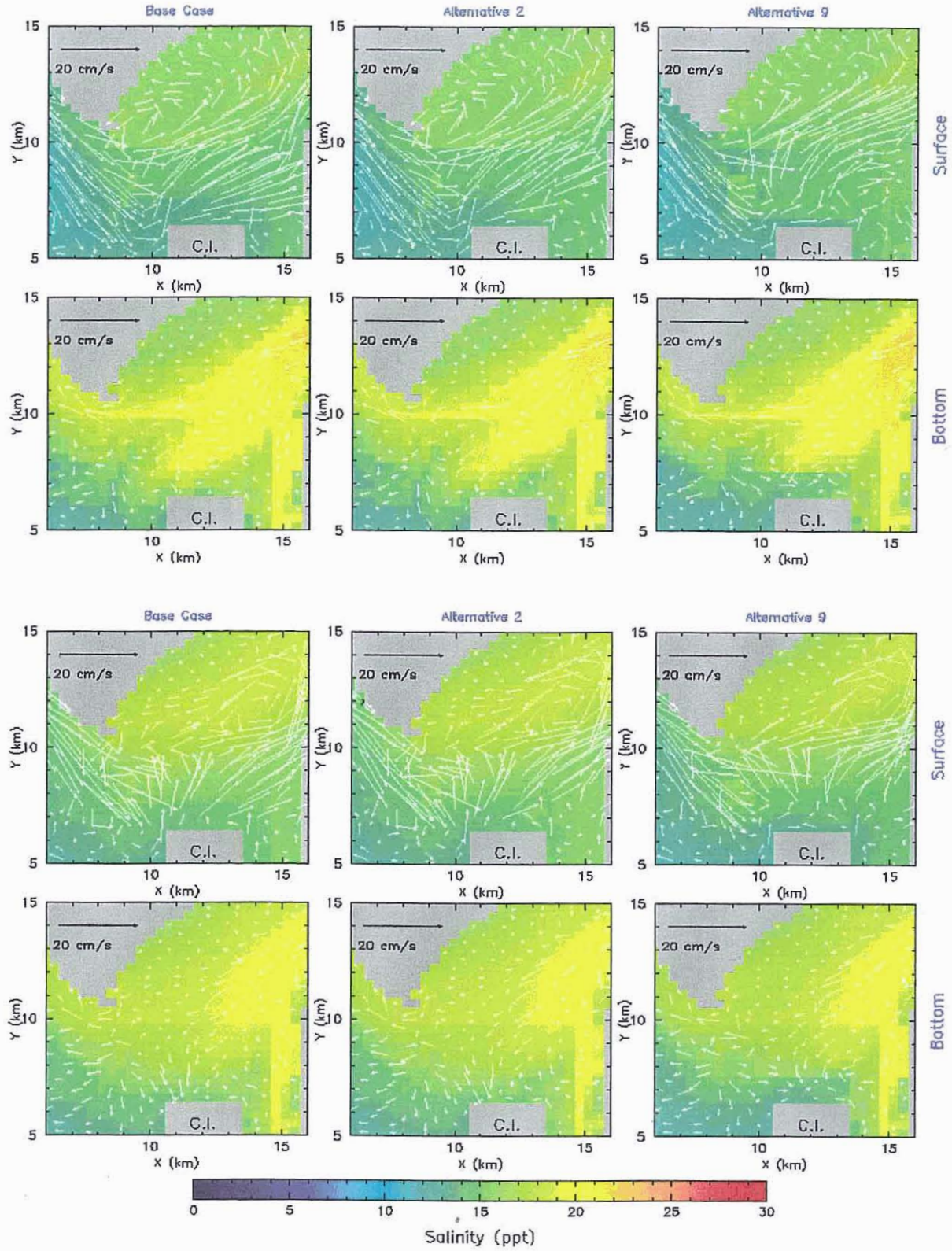

Figure B2. Tidally-averaged current and salinity: apogean-neap tide (upper 6 panels) and perigean-spring tide (lower 6 panels), simulation comparisons for **Base Case, Alternative 2, and Alternative 9, Hampton Roads, VA.**

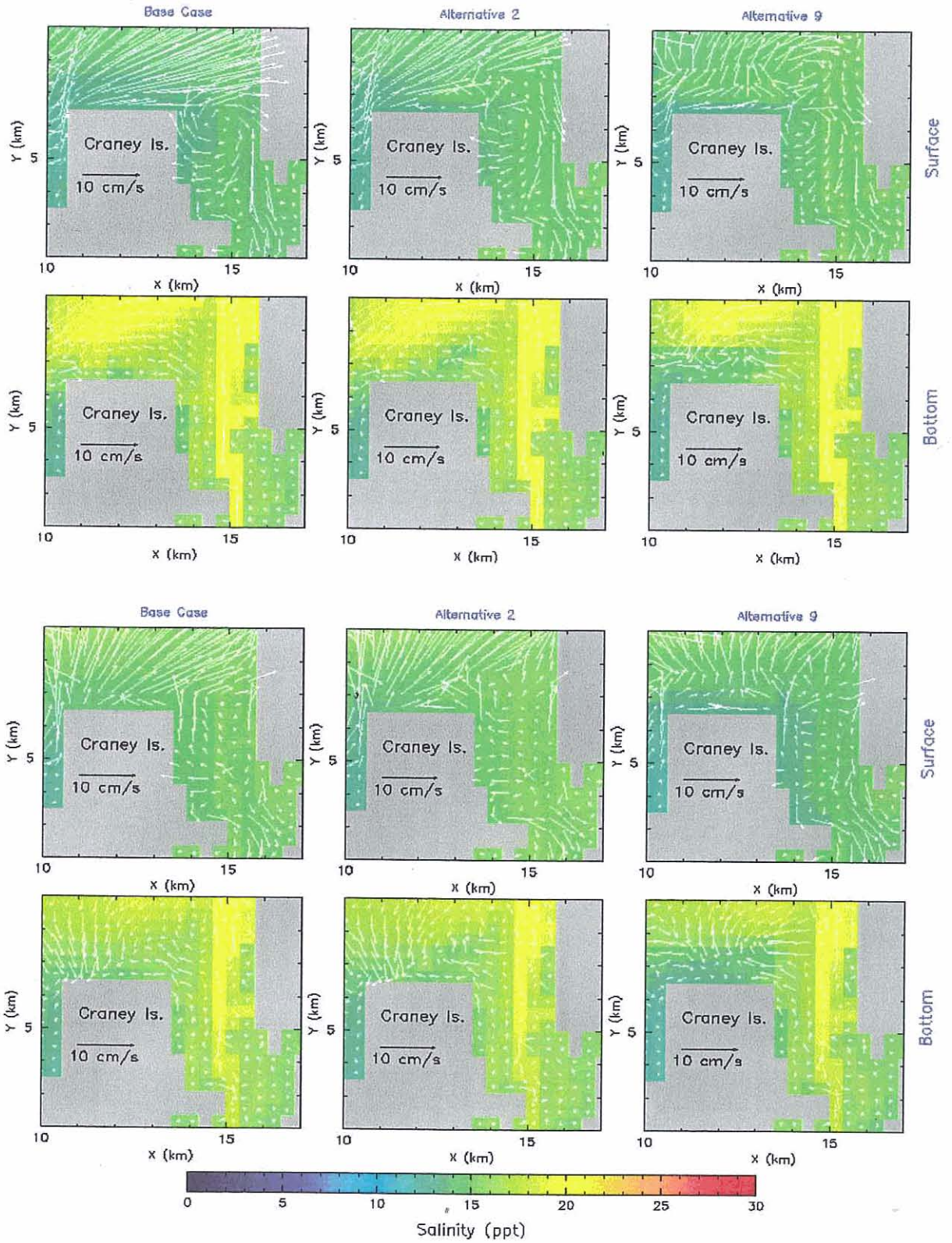

Figure B3. Tidally-averaged current and salinity: apogean-neap tide (upper 6 panels) and perigean-spring tide (lower 6 panels), simulation comparisons for **Base Case, Alternative 2, and Alternative 9, Elizabeth River entrance.**

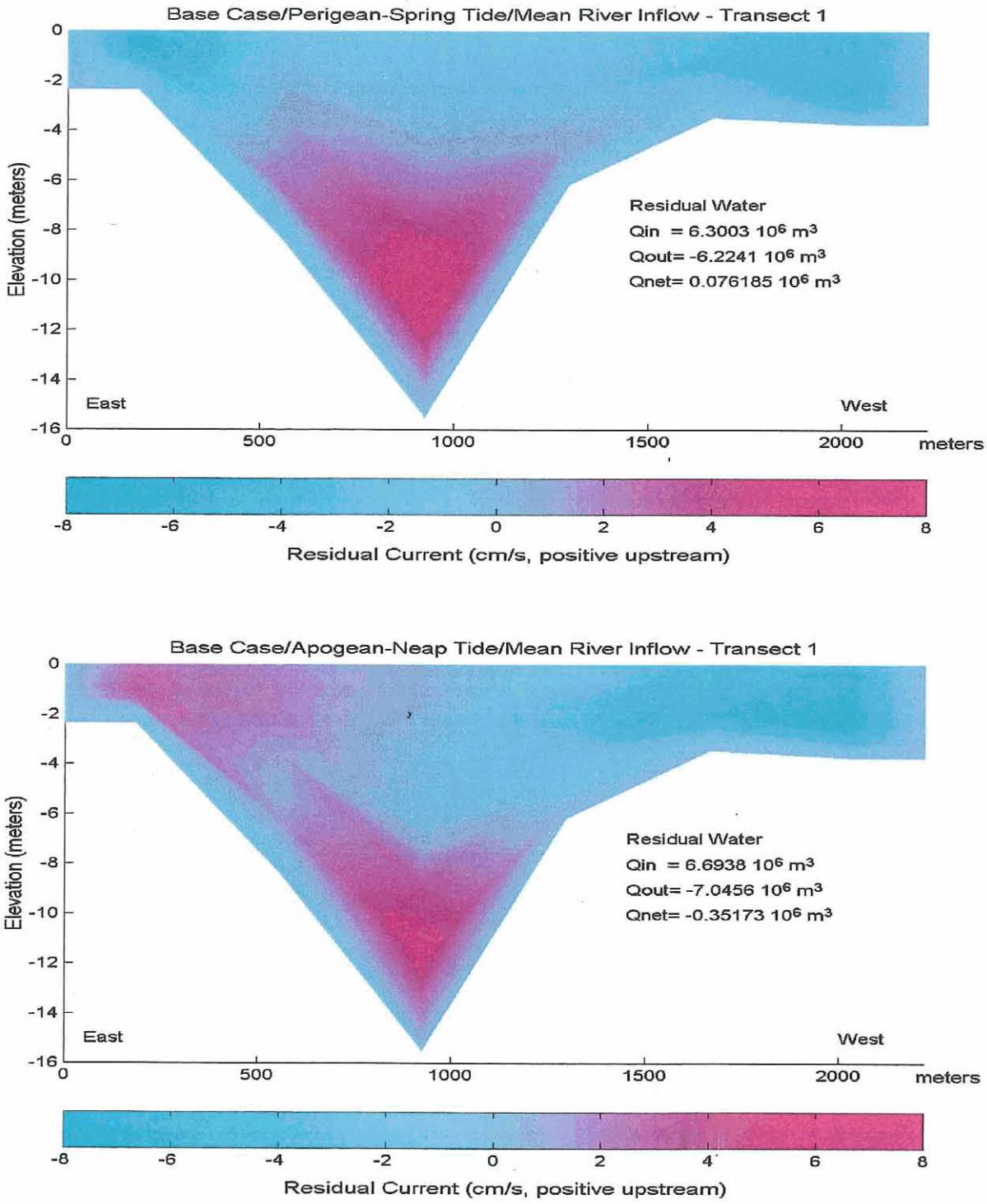

Figure B4. Residual current through Transect 1: **Base Case, Apogean-Neap Tides** (upper panel) and **Perigean-Spring Tides** (lower panel).

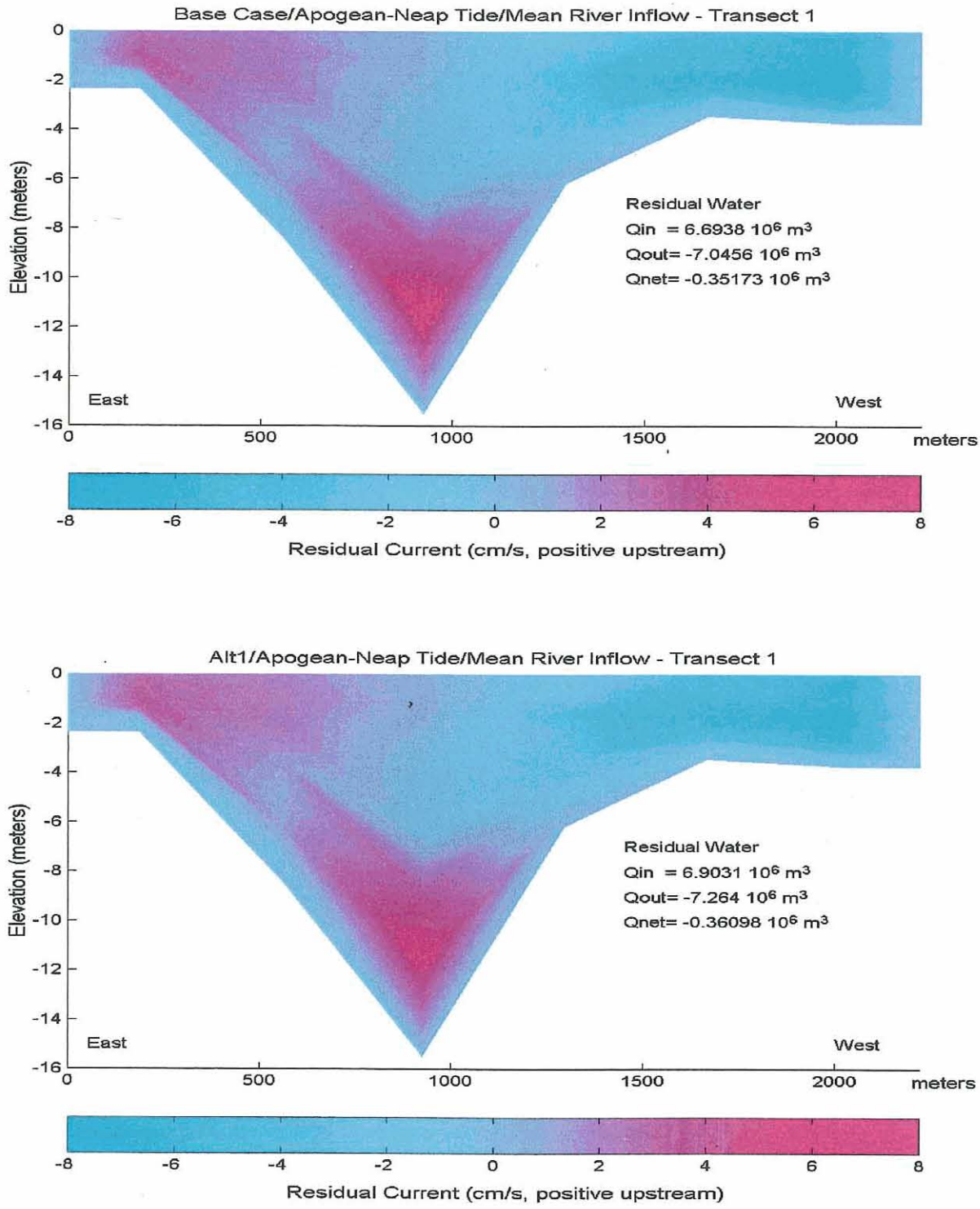

Figure B5. Residual current through Transect 1, **Base Case** and **Alternative 1**.

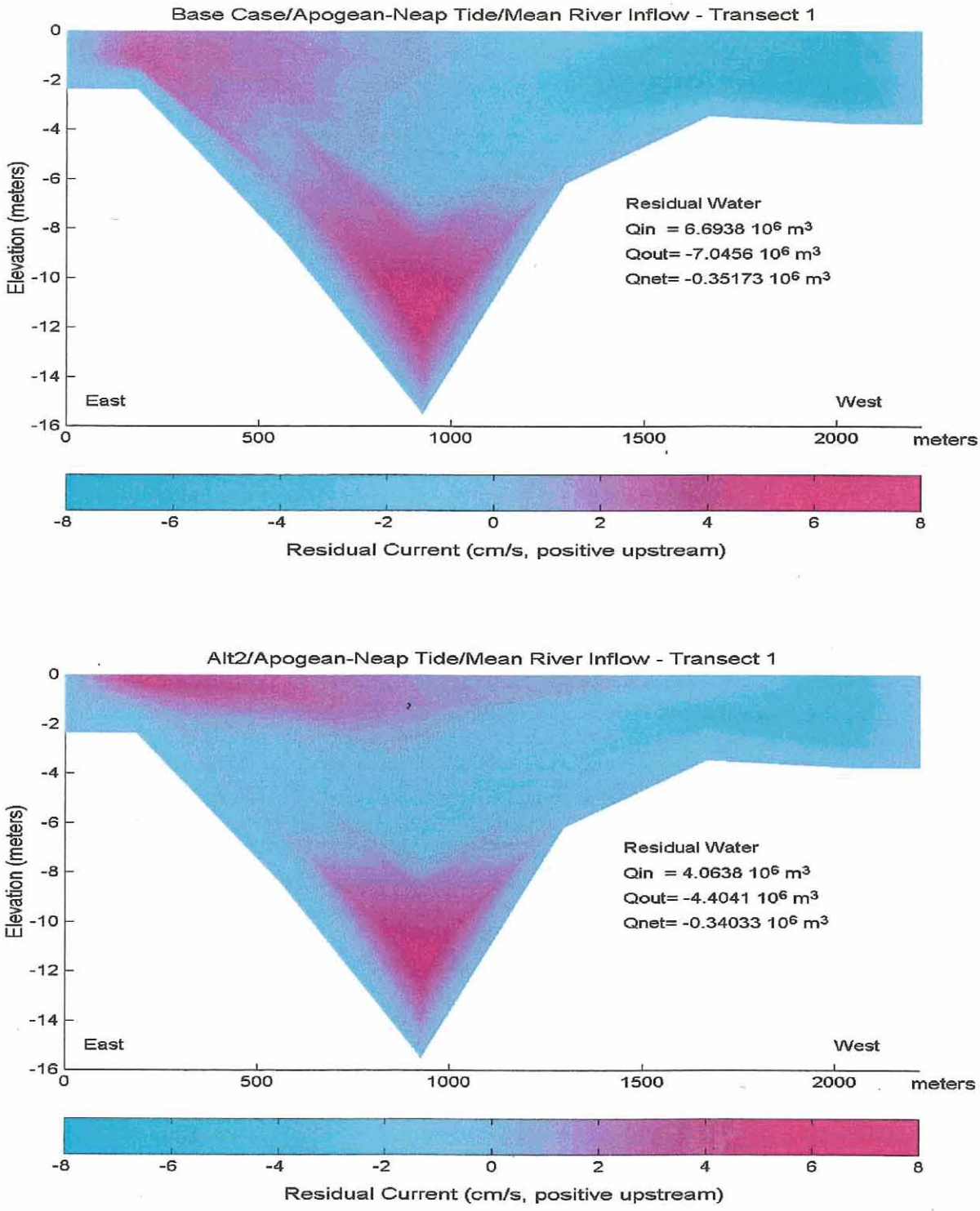

Figure B6. Residual current through Transect 1, **Base Case** and **Alternative 2**.

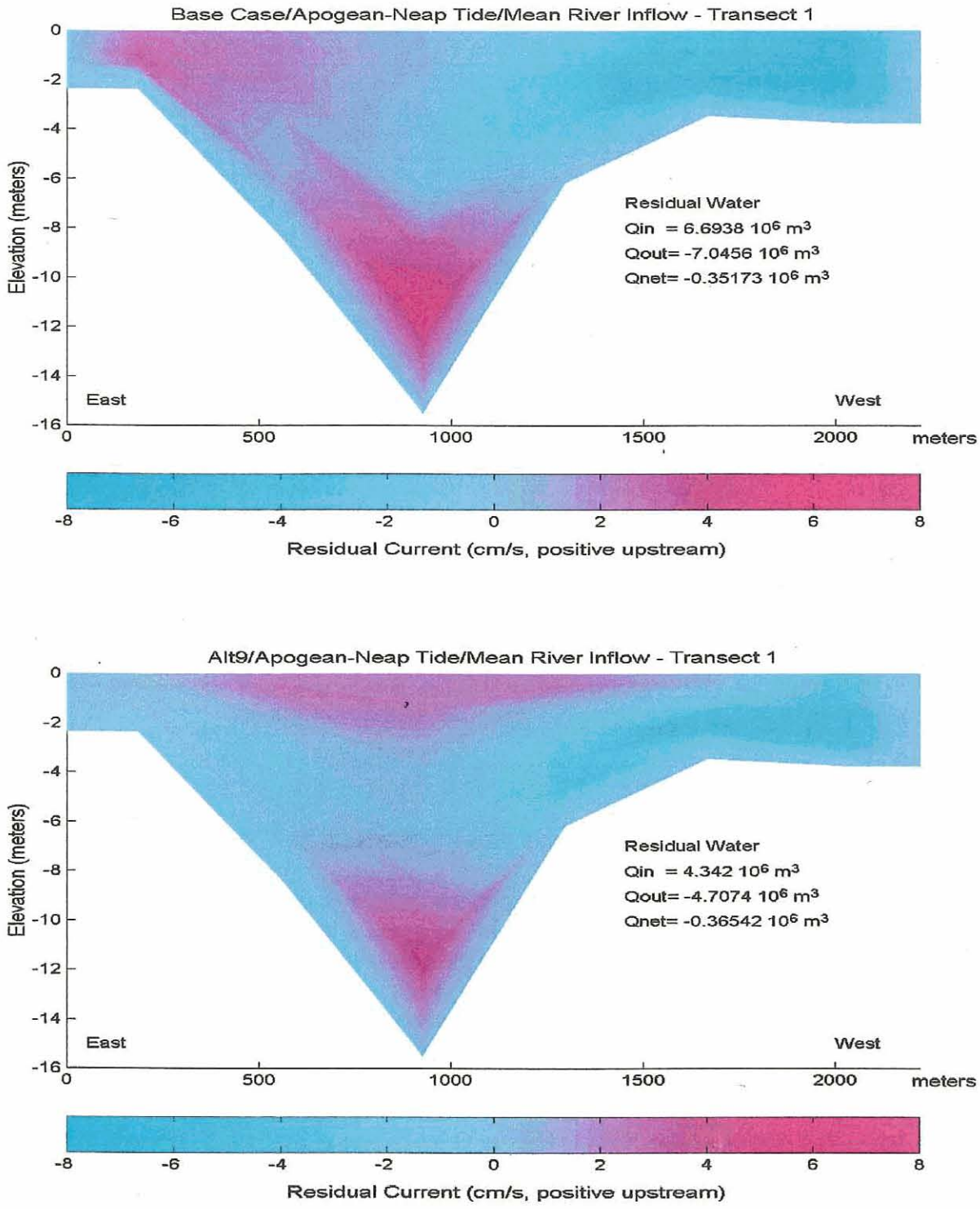

Figure B7. Residual current through Transect 1, **Base Case** and **Alternative 9**.

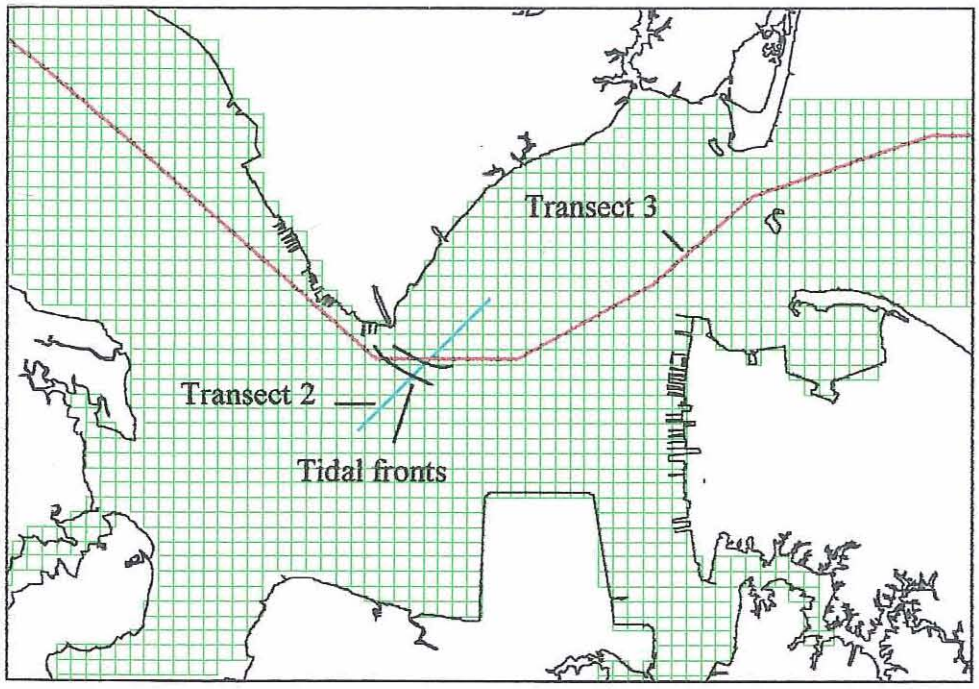

Figure B8. Location map showing Transects 2 and 3, and the surface position of an observed tidal front, Hampton Roads, VA.

Note concerning model transects 2 and 3

Transects 2 and 3 are used to display model output data in cross-section, providing a vertical 'slice' through selected areas of the model domain. The data include the component of the horizontal current flowing parallel to the face of the cross-section and the salinity within the cross-section during a specific phase of the tide. Transect 2 is oriented approximately perpendicular to a tidal front that forms south of Newport News Point during the early stages of flood current and shifts its position to the west with time. The front marks the interface between higher salinity water beginning to enter the James River across Hampton Flats and low salinity river water still exiting the James River in the main channel. Transect 3 is composed of several straight segments that follow the axis of the main channel.

Base Case

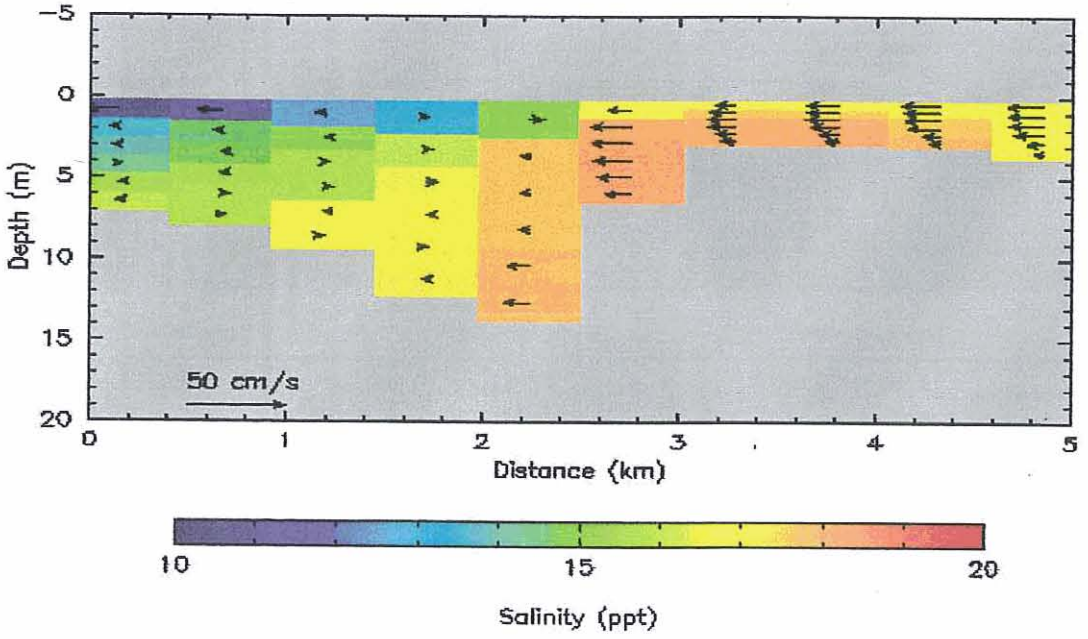

Alternative 9

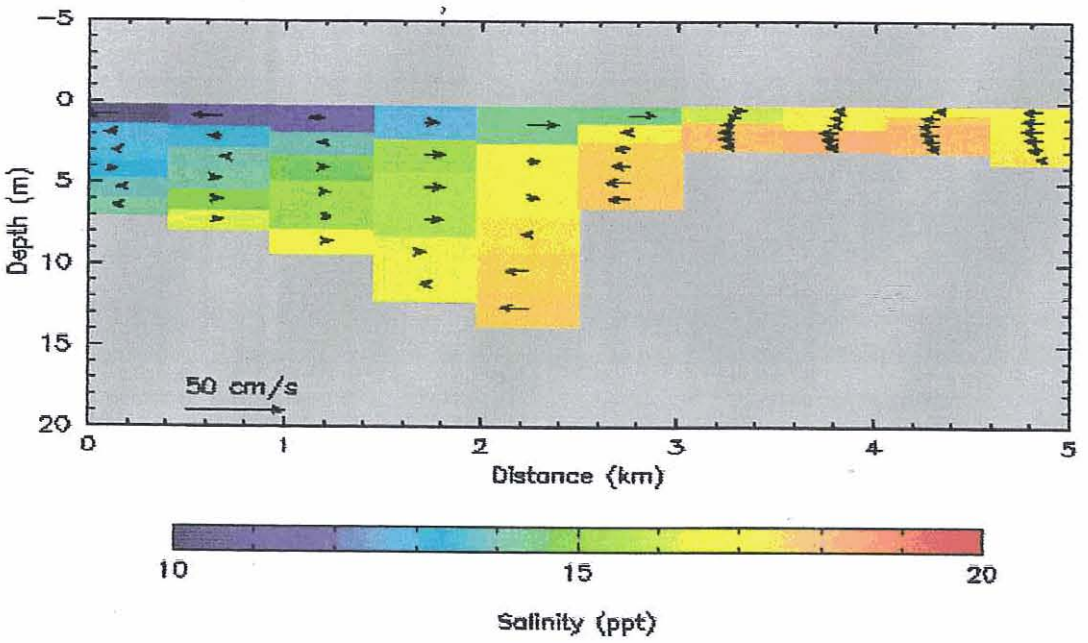

Figure B9. Current and salinity for mean tidal range, mean river inflow at Transect 2 during early flood for **Base Case** (upper panel) and **Alternative 9** (lower panel).

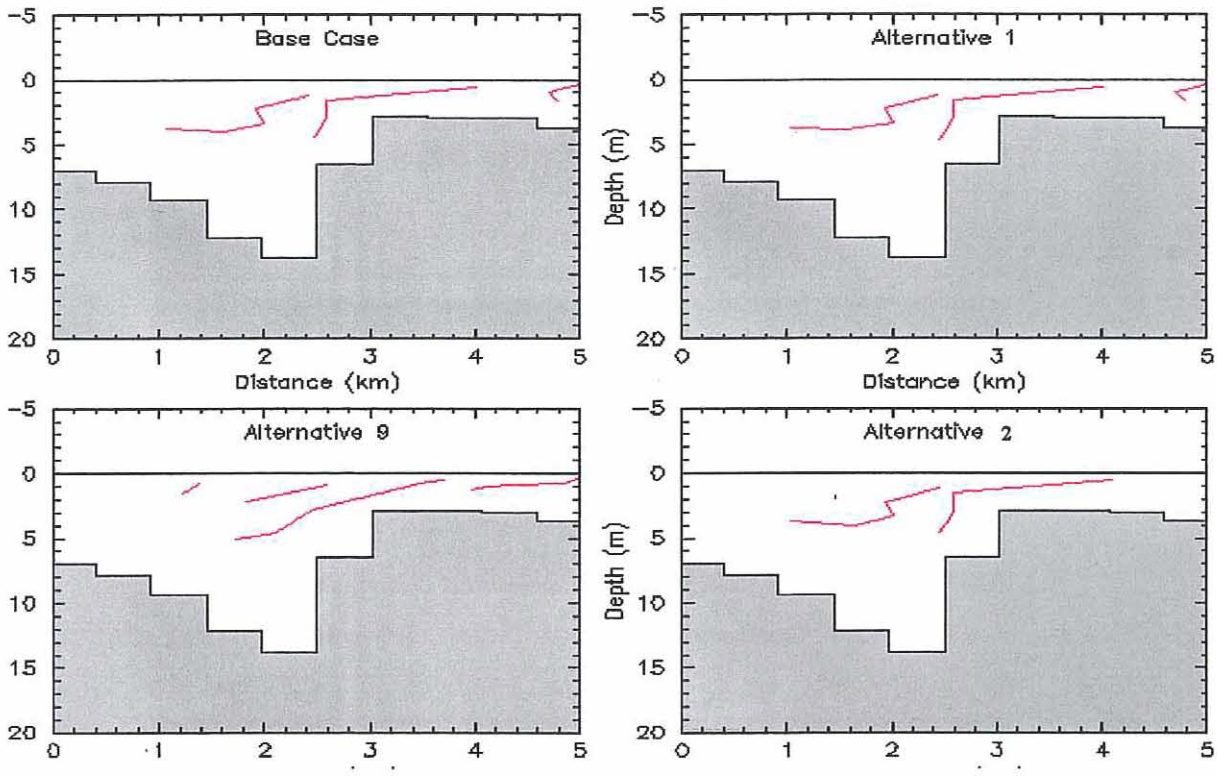

Figure B10. Transect 2, **mean river inflow**, showing frontal interface (red lines).

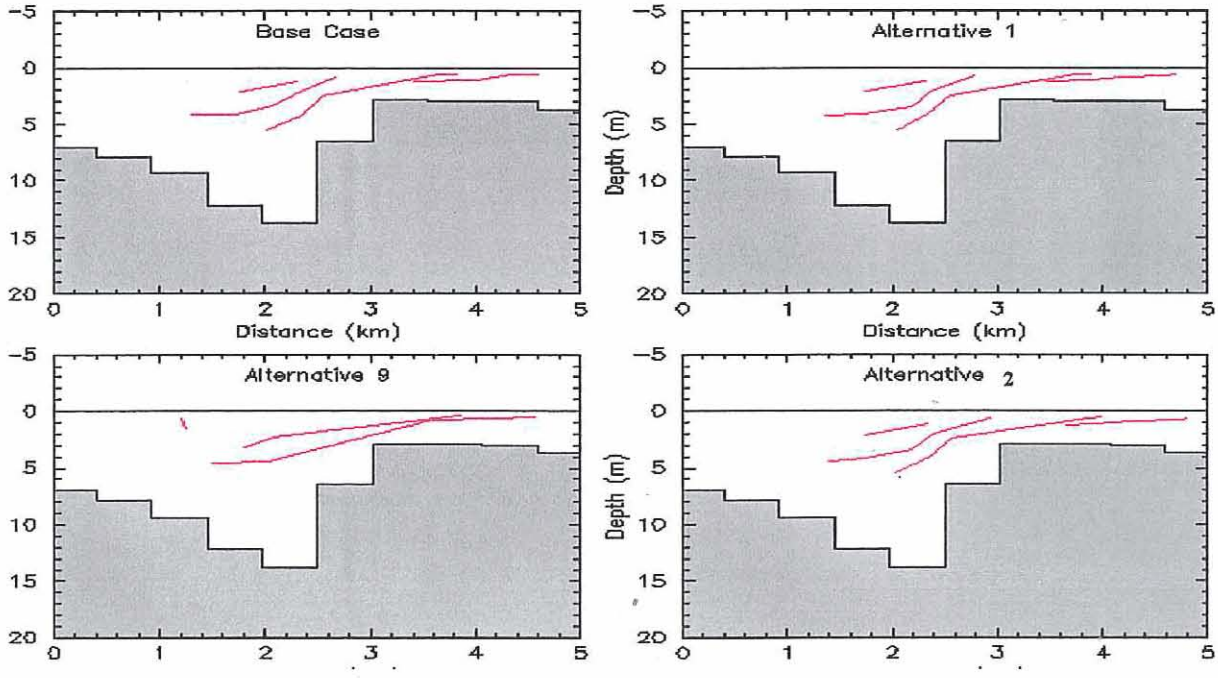

Figure B11. Transect 2, **high river inflow**, showing frontal interface (red lines).

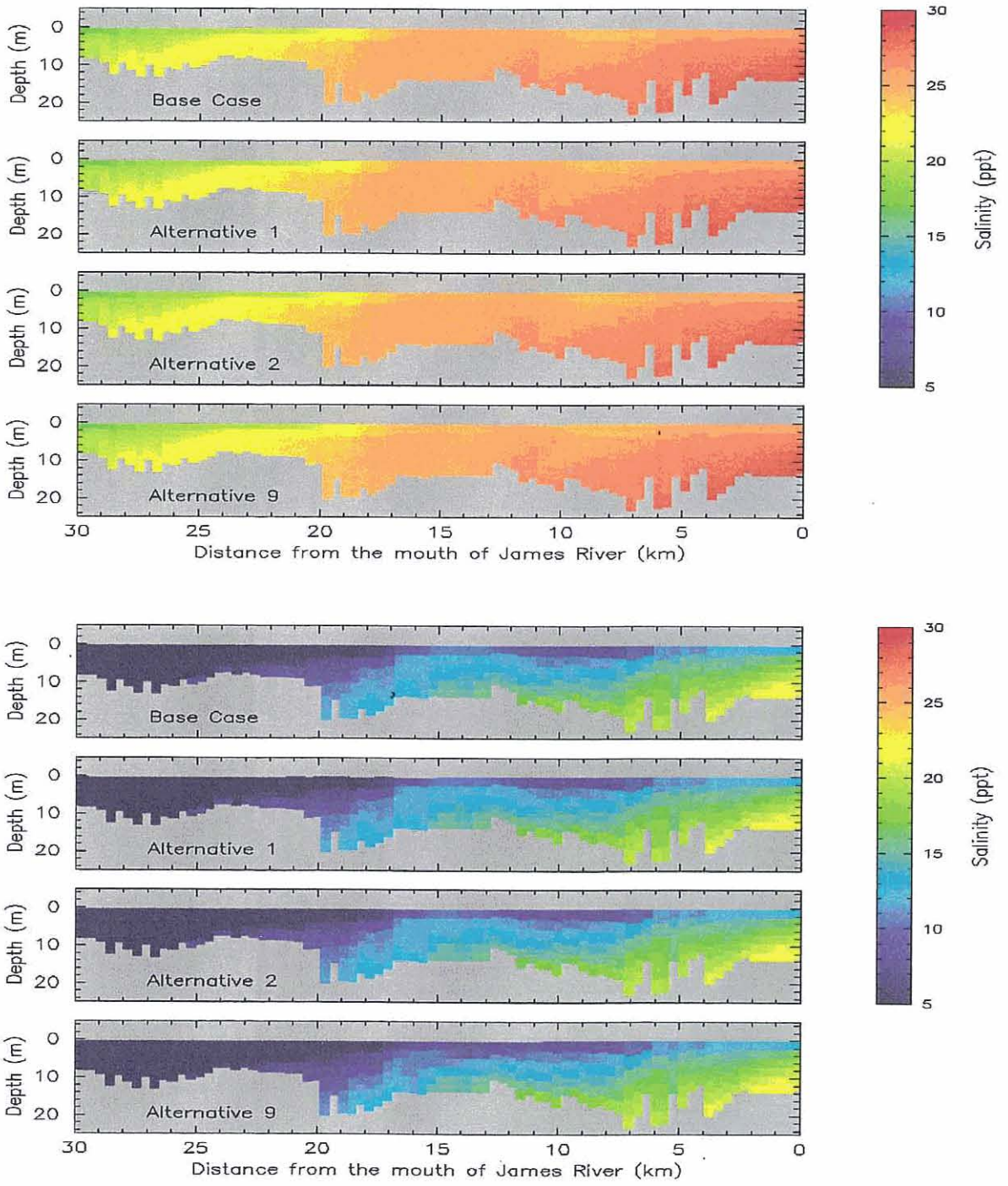

Figure B12. Salinity, slack before ebb, Transect 3, **low river inflow** (upper panels), **high river inflow** (lower panels).

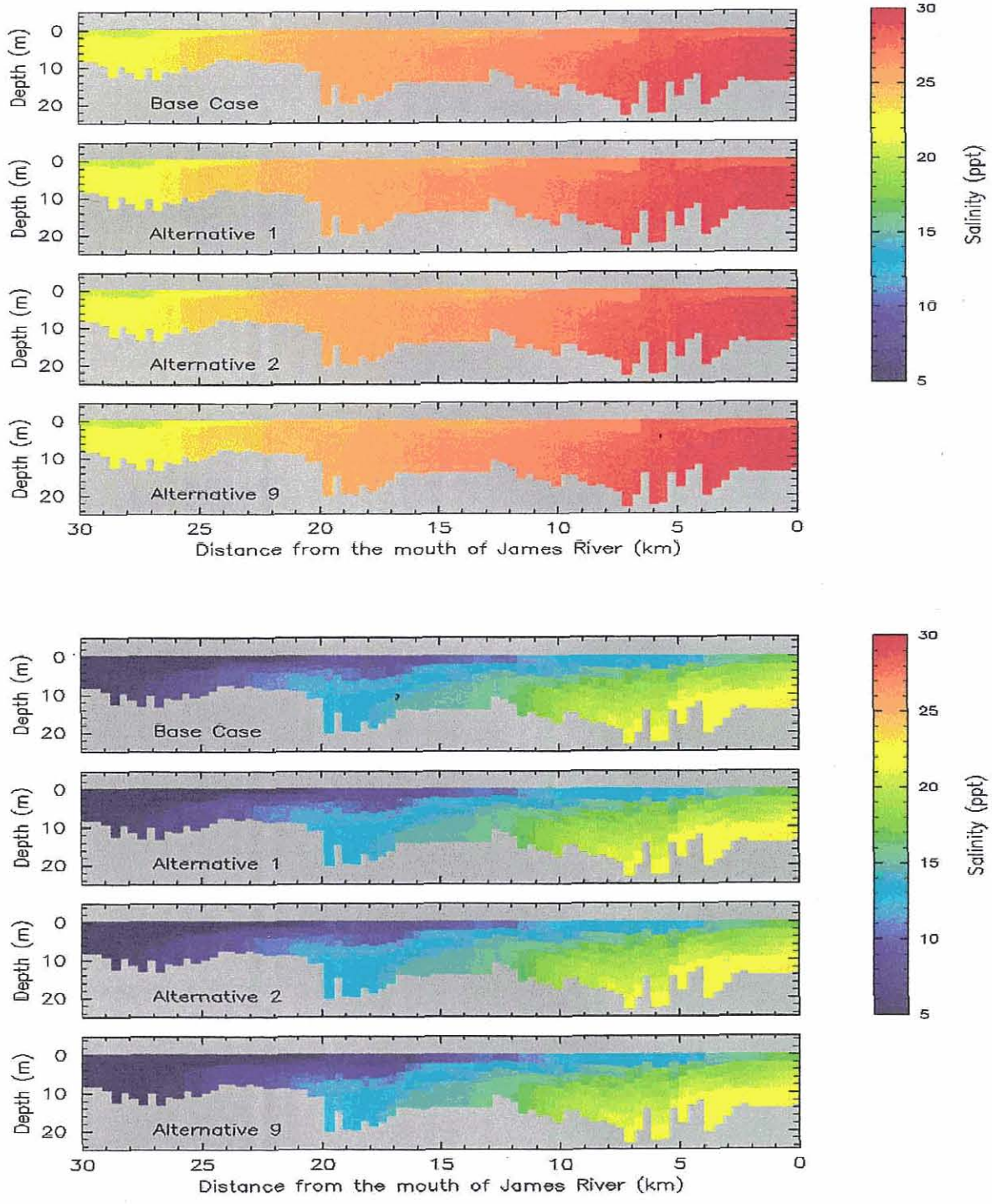

Figure B13. Salinity, slack before flood, Transect 3, **low river inflow** (upper panels), **high river inflow** (lower panels)

APPENDIX C

Sedimentation

Sedimentation Potential and Tagged Particle Deposition

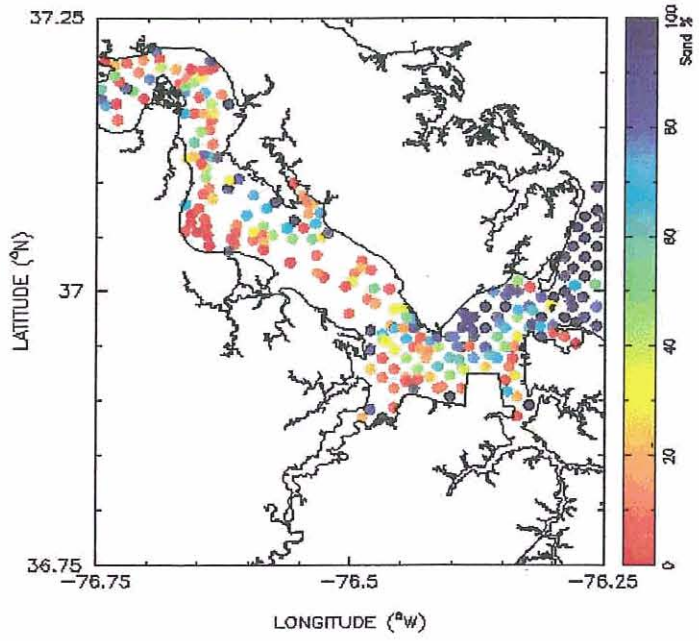

Figure C1. Bottom sediment grain size distribution (Nichols et al., 1991).

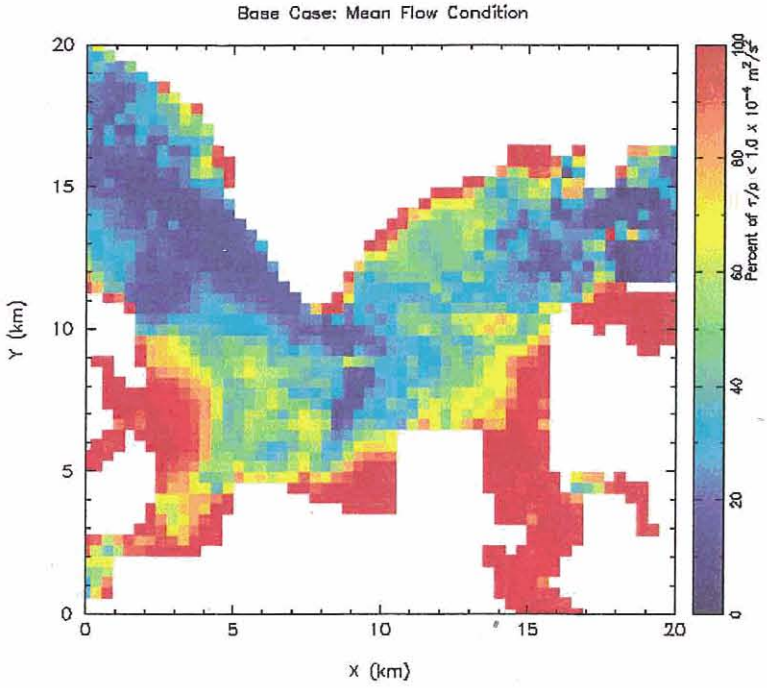

Figure C2. Sedimentation Potential: Base Case, mean river inflow.

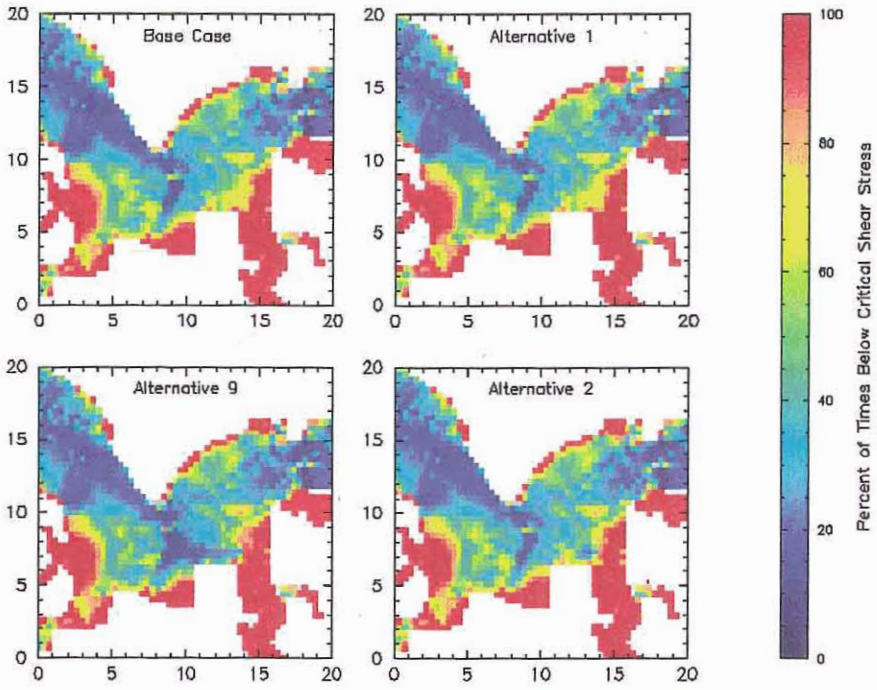

Figure C3. Sedimentation potential: Base Case, Alternative 1, 2, and 9, **mean river inflow**.

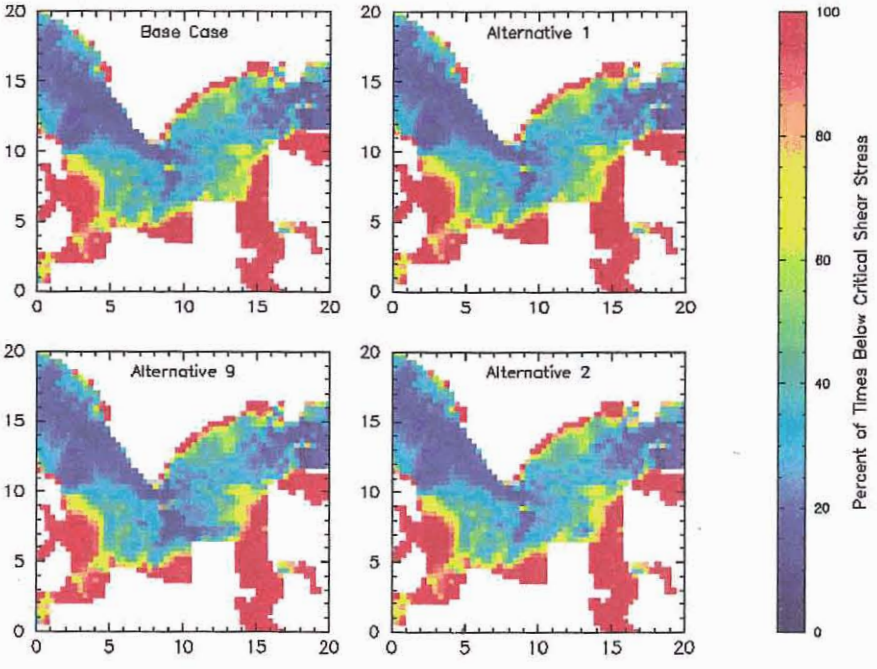

Figure C4. Sedimentation potential: Base Case, Alternative 1, 2, and 9, **low river inflow**.

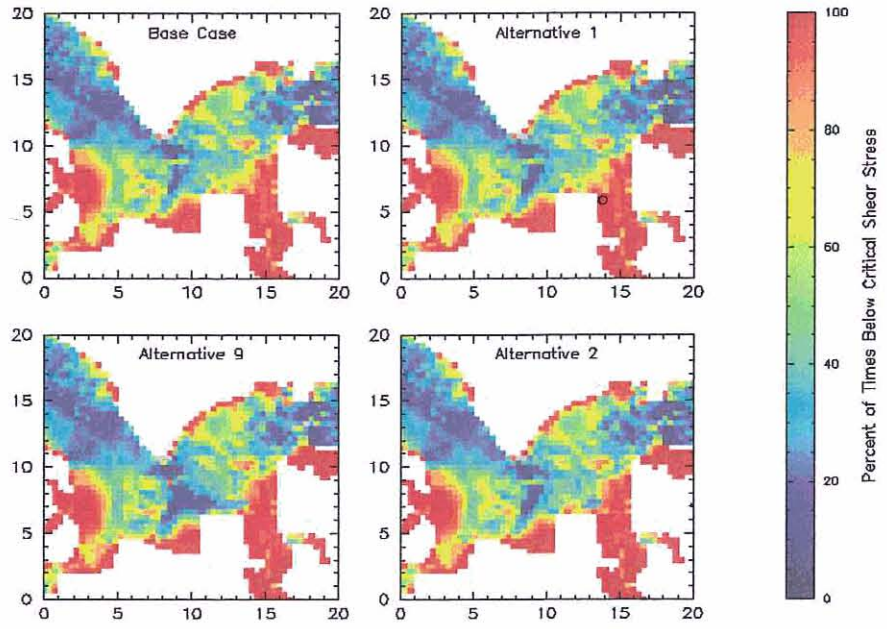

Figure C5. Sedimentation potential: Base Case, Alternative 1, 2, and 9, **high river inflow**.

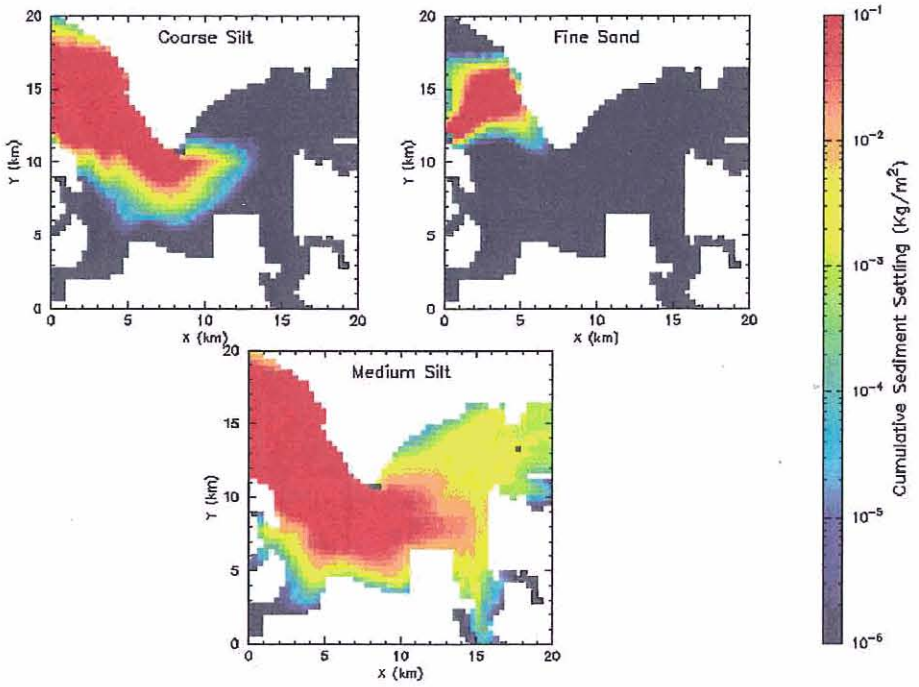

Figure C6. Sediment deposition after 67 tidal cycles: Base Case, mean river inflow.

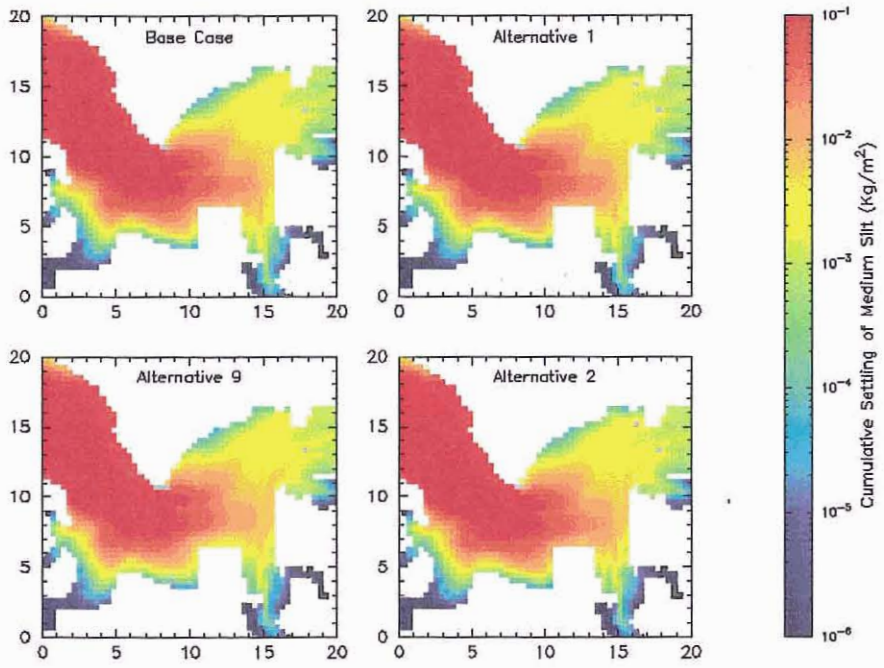

Figure C7. Medium silt deposition after 67 tidal cycles: **mean river inflow**.

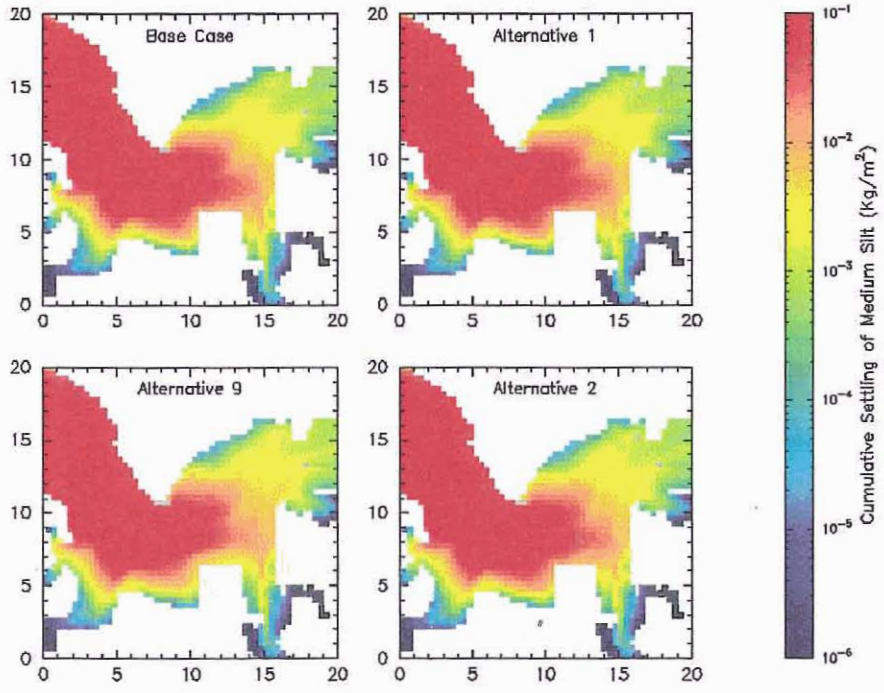

Figure C8. Medium silt deposition after 67 tidal cycles: **low river inflow**.

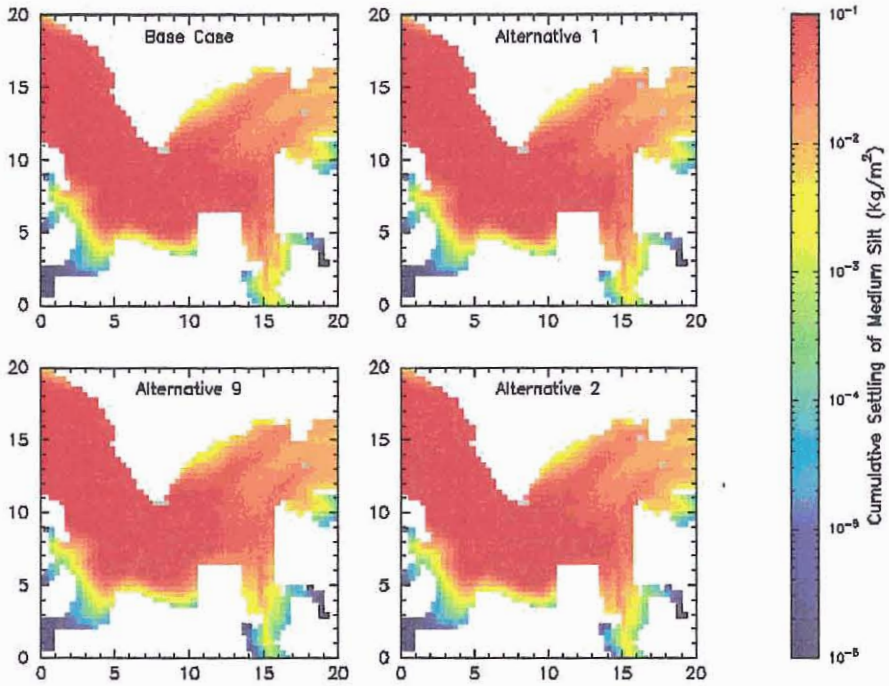

Figure C9. Medium silt deposition after 67 tidal cycles: **high river inflow.**

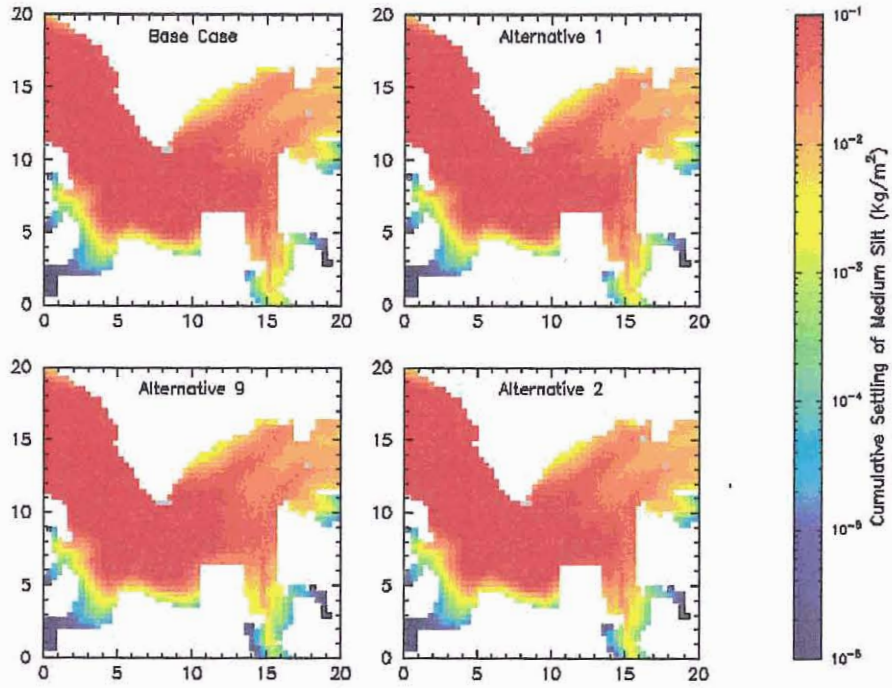

Figure C9. Medium silt deposition after 67 tidal cycles: **high river inflow**.